Treball de Fi de Màster

Enginyeria Industrial

Dynamic grasping of objects with a high-speed parallel robot

MEMÒRIA

Autor: David Llevat Pàmies
Director: Lucas Philippe Van Wunnik
Ponent: Sébastien Briot

Convocatòria: Agost 2017

Escola Tècnica Superior
d'Enginyeria Industrial de Barcelona

ÉCOLE CENTRALE DE NANTES FIRST YEAR INSTITUTION

MASTER ARIA-ROBA
"AUTOMATIQUE, ROBOTIQUE ET INFORMATIQUE APPLIQUÉE"

2016 / 2017

Master Thesis Report

Presented by

David LLEVAT PÀMIES

On 29/08/2017

Dynamic grasping of objects with a high-speed parallel robot

Jury

President:	Philippe MARTINET	Professor, LS2N, ECN
	Olivier KERMORGANT	Asst. Professor, LS2N, ECN
Supervisor(s):	Vincent BEGOC	Researcher, ICAM
	Sébastien BRIOT	CNRS Researcher at LS2N, ECN

Laboratory: Laboratoire des Sciences du Numérique de Nantes LS2N

Abstract

Underactuated grippers aim to simplify the control strategies for performing stable grasps due to their inherent shape adaptability. While at the beginning, the main research area was focused on developing human-like robotic hands for disabled people, in the last years, a new field of application appeared with the constant evolution of the industry: the implementation of a single underactuated gripper as a replacement of diverse dedicated fully-actuated grippers. However, two main issues are restraining its use: the stability of the grasp and the speed of performance. The first is an active topic as all underactuated grippers need to ensure the stability of the grasped object through an adequate kinematic design, while, the latter is not widely treated as there weren't many application fields where high-speed was required and, at the end, the quasi-static analysis must be also ensured.

For this reason, the present research work has been focused on the speed of the grasping. In the first place, an introduction to underactuated hands is made, and is followed by two main stability criteria. Then, the development of a model for an underactuated finger that allows analyzing the complete grasping sequence at high-speed along with a collision model are presented. Following, a design-based analysis to simplify the model is performed, and the *grasp-state volume* tool is introduced in order to inspect the impact of the design variables on the proposed criteria. In the last chapter, an optimization over the design space is performed and a design is chosen, crosschecked with ADAMS software and prototyped. Finally, an overview remarking the strengths and gaps in the research is presented in the form of conclusions, and closing them, future works that could be interesting to develop.

Acknowledgments

Before presenting this research work, I would like to express some words to the people that have guided me during my master studies and master thesis.

First of all, I would like to express a special thank to my research supervisors, Dr. Vincent Bégoc and Dr. Sébastien Briot, for the time they have shared with me and the advice provided in order to carry out this Master thesis. Their combined expertise and experience have been extremely appreciated and valuable for the fluent development of this research work. Moreover, I am extremely grateful for the balance they have put between guiding me and encouraging me to be autonomous during the research.

I also would like to thank the responsible of the ARIA-ROBA master program for accepting me in the second year of the master as an exchange student, granting me the opportunity to acquire a great knowledge in the robotics field and encouraging me to continue learning. Not only this, but for the opportunity to experience the life in a different country and to grow, not only in the scientific plane but, in the personal one too thanks to the nice environment provided by the university.

Finally, I would like to express my gratitude and love to my family and friends, for their never ending support.

Contents

List of Figures

List of Tables

List of Symbols

$[\ ]_\times$	Skew symmetric matrix representation
$\boldsymbol{\omega}$	Angular velocity of the rigid object
$\boldsymbol{\omega}_a$	Joint velocities vector
$\boldsymbol{\tau}, \tau_{ij}$	Torques on A_{ij} applied on to l_{ij}
$\boldsymbol{\tau}_{C2j}$	Contact wrenches applied in the generalized coordinates
$\boldsymbol{\tau}_s$	Wrench applied by the spring
$\boldsymbol{\xi}_i$	Twist of the contact point on phalanx i
$\boldsymbol{\zeta}_i$	Wrench on the contact point of phalanx i
$\boldsymbol{t}$	Simulation time vector
$\boldsymbol{x}_i$	Unitary vector defining the direction along the i^{th} phalanx
$\boldsymbol{y}_i$	Unitary vector defining the orthogonal direction to the i^{th} phalanx in the plane
$\boldsymbol{z}_i$	Unitary vector defining the out-of-the-plane direction of the i^{th} phalanx
$\circ$	Reciprocal product operator
δ_i	Self-locking inequality sign parameter
δ_{max}	Penetration transition zone
δ_n	Normal penetration distance
η_i	Torque friction coefficient of phalanx i
$\hat{\mathbf{n}}_p^T$	Contact constraint with the palm
$\dot{\mathbf{c}}^o$	Vector of contact points velocities of the object
$\dot{\mathbf{c}}^{y,o}$	Vector of contact points velocities attached to the object and projected on the normal vectors of the contact surfaces
$\dot{\mathbf{c}}^{y,p}$	Vector of the phalanx velocities along its normals
$\dot{\mathbf{c}}_i^o$	Contact points velocities
$\dot{\mathbf{u}}$	Vector of the object velocity
$\mathbf{A}, \mathbf{B}$	Matrices relating $\mathbf{q}_a$ with $\mathbf{x}$
$\mathbf{B}_{ti}$	Coriolis effects of the tree-structure
$\mathbf{c}$	Centrifugal, Coriolis and Gravity effects vector
$\mathbf{C}_{ti}$	Centrifugal effects of the tree-structure
$\mathbf{F}_{N2j}, \mathbf{F}_{T2j}$	Normal and Tangential contact forces vectors on P_{2j}
$\mathbf{G}$	Grasp matrix

$\mathbf{g}, \theta_g$ Gravity constant (9.81 m/s^2) and direction

$\mathbf{h}, \mathbf{h}_p, \mathbf{h}_d$ Closed-loop equations, reduced to $\mathbf{x}$ and reduced to $\mathbf{q}_d$ respectively

$\mathbf{J}$ Jacobian matrix

$\mathbf{J}_C$ Collision Jacobian matrix

$\mathbf{J}_{da}, \mathbf{J}_{ta}, \mathbf{J}_{td}$ Matrices relating $\mathbf{q}_a$ with $\mathbf{q}_d$

$\mathbf{J}_{P_{2j}}$ Jacodian of the contact point P_{2j}

$\mathbf{K}$ Stiffness matrix of the system

$\mathbf{M}$ Inertia matrix

$\mathbf{N}$ Matrix of contact constraints

$\mathbf{n}_i$ Contact constraint at point C_i^o

$\mathbf{P}$ Projection matrix

$\mathbf{q}_a, q_{ij}$ Actuated joints, also, generalized coordinates

$\mathbf{q}_d, q_{ij}$ Passive joints

$\mathbf{Q}_{ti}$ Gravity effects of the tree-structure

$\mathbf{S}$ Selection matrix

$\mathbf{T}$ Transmission matrix

$\mathbf{t}$ Input torque vector

$\mathbf{U}$ Matrix of unilateral constraints for underactuated mechanisms

$\mathbf{v}$ Linear velocity of the rigid object

$\mathbf{x}, x, y$ End-effector coordinates

μ, μ_s, μ_d Generic, static and dynamic friction coefficients

μ_i Tangential force friction coefficient of phalanx i

ω_i Angular velocity of the i^{th} phalanx

τ_i Torque applied by phalanx i

$\dot{\theta}a$ Velocity of the actuator

$\dot{\theta}i^a$ Velocity of the driven joint i

θ_a Configuration of the actuator

θ_i^a Configuration of the driven joint i

φ_{c2j} Collision angle measured from the center of the object

$\varphi_{c2j}, \varphi_{nc2j}$ Collision and Normal collision angles taken from the center of the object

φ_{ij} Angle between l_{ij} and t_{ij}

ζ_i Wrench on the contact point of phalanx i

$_{OC}$ Object Contact

$_{SC}$ Spring Contact

a Hertz contact radius

A_{ij} Joints definition

$base$ Horizontal distance between O and the center of the object

c_max Contact damper constant

C_i^p Contact point on the phalanx i

c_s Spring constant

d Configuration space dimension of the object

$depth$ Depth of the gripper

E^*, E_i, ν_i Compound Young's Modulus, the materials Young's Moduli and the Poisson Moduli

F_a Wrench applied by the actuator

F_i^a Wrench transmited to the output i

F_f Friction force

f_i Normal force applied by phalanx i

F_{N2j} Contact wrenches

f_{ti} Tangential force applied by phalanx i

F_t Tangent force

k Collision spring constant

l_{ci} Distance from O_i to C_i^p

l_{ij} Length of the mechanism links from joint to joint

l_i Length of the phalanx i

L_{ti}, E_{ti}, U_{ti} Lagrangian, Kinetic energy and Potential energy of the tree-structures

m_{ij}, I_{ij} Mass and Inertia around $\boldsymbol{z}_{ij}$ of l_{ij}

n Number of DOF of the system

n_c Number of unilateral contact constraints

n_g Dimension of the grasp configuration space

n_h Dimension of the hand configuration

n_k Number of unilateral constraints of the problem

n_p Number if phalanges of a finger

n_u Number of unidirectional mechanism constraints

O_i Origin of the phalanx i

q_0 Offset angle of the initial configuration

$q_{f,ij}$ Final geometric configuration

q_s, q_p Spring and Spring preload coordinates

R, R_i Compound radius of curvature and the respective objects' radii of curvature

r_i^a Transmission ratio of the output i

r_{μ_d} Ratio between μ_s and μ_d

r_c Radius of the object

r_h Maximum allowed heigh ratio

r_l Ratio l_{22}/l_{11}

r_{WC} Weighted criterion

$rebound$ Rebound criterion

s_{ij} Center of Mass position of l_{ij}

T_a Actuator torque

t_{ij} Tip phalanx length

T_i Torque on i^{th} joint

T_t Transmission ratio

$v_i^{\mathbf{x}}$ Component of the velocity along $\mathbf{x}_i$ at the contact point i

$v_i^{\mathbf{y}}$ Component of the velocity along $\mathbf{x}_i$ at the contact point i

v_{slip} Slipping velocity between finger and object

v_s, v_d Static and Dynamic transition zones between friction sections

w Width of the phalanges

Appendix Figures

Introduction

Context

This research thesis is developed in the framework of Master 2 ARIA-ROBA in École Centrale de Nantes and in collaboration with LS2N. Specifically, the following research work is the culmination of the Master degree. The main topic of this thesis is the design of underactuated grippers implemented on high-speed pick-and-place operations.

Underactuated grippers began to be studied around 60 years ago. At that time, the main field of application was to develop robotic hands for disabled people. A human hand has many degrees of freedom and actuators, hence, it was not possible (and nowadays is still a research topic), to fit all the actuators and control in a wearable hand. For this reason, underactuated systems started to impose over the fully-actuated ones. The main reason is that disposing of self-adaptable end-effectors can result attractive because they require few (if any) dedicated sensors than the current grippers, which translates to less control strategies, hence, simpler systems.

Over the years, new application fields for underactuated grippers appeared, and these mechanisms started to gain the interest of the researchers. One of the big topics in the late years are the collaborative robots. Robots that can interact with humans and perform tasks along with them either in public places or in the industry (main focus). However, many of these tasks require the grasping and the manipulation of different objects. Hence, here is where the interest in underactuated grippers resides in the industry: use a single end-effector to perform different tasks.

As, in general, this type of gripper lacks of sensors, the main objective is to ensure the stability of the grasped object, *i.e.*, ensure that the grasped object does not get loose and slips out of the gripper. In order to achieve the stability, the literature shows that only an adequate kinematic design is required. However, it still is an open research topic.

The second issue that limits the evolution of the underactuated grippers in the industry is the grasping cycle time. As the stability must be guaranteed in static (final phase of a grasping cycle), the previous phases, the dynamic phases that contemplate the approximation of the fingers and the interaction of the phalanges with the object, have not been widely researched. Hence, the performance of underactuated grippers is not competitive with the current solutions: suction cups and parallel jaws that can perform grasping cycles of less than 10 ms.

Summarizing, this research work proposes to study the whole grasping cycle of an industrial pick-and-place operation, and it has as a main objective, the design of an underactuated gripper able to perform stable pick-and-place operations being robust to position uncertainty and with a desired open/close cycle of less than 10 ms.

Problem formulation

A pick-and-place is a generic operation widely performed in industries and based in 3 single steps (see *Fig.1*): *(a)* pick the goods at one location, *(b)* transport them to a destination and *(c)* release the goods.

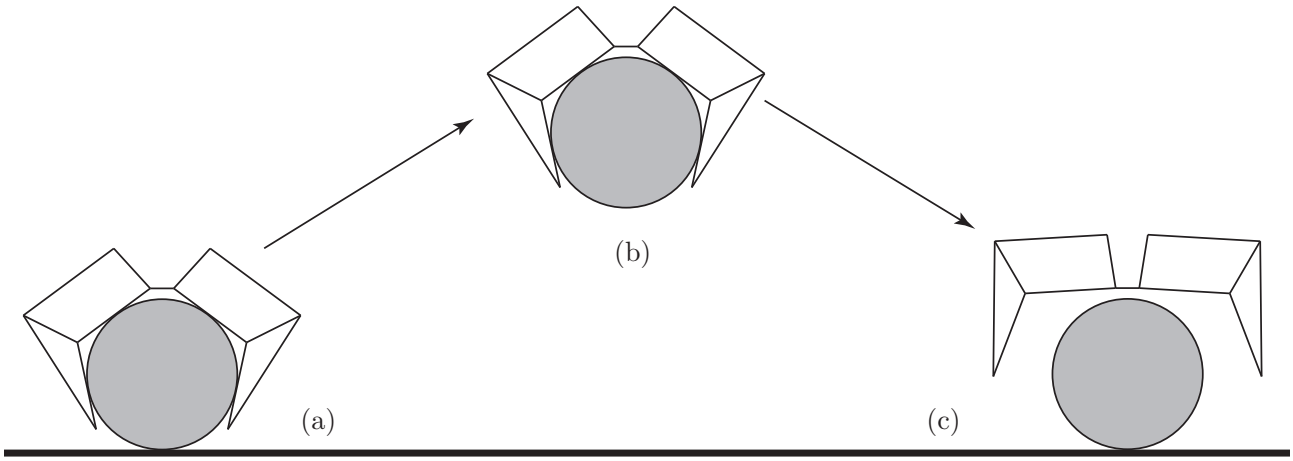

Figure 1: Pick-and-place diagram

Main issues with this operation appear when it is performed at high-speed. The reason is that, when the performance is at a high velocity, inertial forces are introduced into the system creating vibrations into the moving platform, which decrease repeatability and precision of the placement. Those parameters are critical when a grasping must be performed, mainly because of the gripper limitations.

Having the task defined and knowing its most important problems, the principal challenges can be defined:

- Compensate for positioning error and vibration during the grasping phase.
- Reduce closure and opening cycle time.
- Reduce weight.
- Model the dynamic behavior during the grasping phase and translational phase.
- Guarantee the stability of the object along with all the process.

Current grasping systems (mostly suction cups and parallel jaws) present some important drawbacks for the proposed challenges. Suction cups, even though they are designed for specific objects, have a built-in compliance that makes them really interesting, but are unable to apply tangential forces or torques, thus the objects would be lost in the translation phase. Referring to parallel jaws, they are not adaptable to the object's shape, even though it could happen in some specific configuration. A higher level of adaptability could be implemented on the parallel jaws, however, the weight would also increase.

Between all the existing kinds of grippers, underactuated grippers have been chosen because of their suitable qualities, given the previous requirements. With a proper design, underactuated grippers can:

- Adapt to different object's shapes.
- Be robust to vibrations of the moving platform.
- Be robust to positioning errors.
- Have low weight.

However, it must be proven that underactuated gripper are able of:

- Guarantee the stability of the object along all the process.
- Have low open/close cycle time.

Contributions

In order to position the current research work with respect to the state of the art, a short review of some of the most recent and relevant works on robotic hands are presented along with the main contributions of this thesis.

All the research related to underactuated design is based on ensuring stability at different phases of a required task when the gripper is in contact with the object. Inside this field, almost all the studied hands have been developed considering quasi-static conditions, *i.e.*, they

analyze the stability of the hand/gripper when the fingers are closed and considering the null movement of the object and contact points. Here is where the general contribution of this research is placed, as the main hypothesis is the consideration of a whole closing sequence of an underactuated gripper performed at high-speed, meaning that inertial effects due to great accelerations, and derived events, are taking part on the stability of the grasp.

In 2007, Birglen et al. presented *Underactuated Robotic Hands* [7], a book gathering their previous works, including a new proposition to unify and facilitate the quasi-static analysis of robotic hands and the stability determination. In Wu et al. 2009 [25] is presented an interesting approach to simulate the closing sequence of a finger in relation to the object. Unfortunately, only the kinematic model is proposed. First works related to the phases previous to the grasp were introduced by Massa et al. 2002 [21] and Kaneko et al. 2003 [12]. Massa introduces a dynamic model of the approaching phase using Lagrange equations and considering the finger as a serial robot; the presented results are interesting because they show the effects of the inertial forces, but the model overlooked the contact phase. In Kaneko's work, a dynamic preshaping of the fingers, modifying the distribution of the torques on them, was studied in order to reduce the closing cycle time, however, it does not allow a positioning error. Finally, one of the most recent works in the topic presents a quasi-dynamic approach (Saliba et al. 2016 [24]). This work differs from the quasi-static analysis in some hypotheses: the object is not fixed to the environment and considers the approaching and closing sequence of the finger. Yet, the basic hypotheses are not enough as fingers inertia are not considered and the collision is supposed ideal and without rebound.

Positioned with respect to the works presented above, this thesis has contributed to the development of a complete dynamic model for a two-phalanxed linkage-driven underactuated finger. The model not only takes into account the inertial effects, but the interactions with the target object too. In order to model the interactions, a Collision model has been proposed, allowing to include rebound events in the high-speed closing. In order to analyze the workspace given the task, the concept of the *grasp-state space* proposed by Birglen [7] is modified to obtain a *grasp-state volume* that can analyze up to five dimensions, helping to understand the influence of the variables on to some parameters/criteria. Finally, along with some static stability criteria, two dynamic stability criteria are proposed to analyze the performance.

Chapter 1

Underactuated grippers

1.1 Introduction to underactuated hands

Underactuated systems are widely known in control and robotics fields. These systems show the special characteristic of having more degrees of freedom (DOF) than degrees of actuation (DOA). These systems are interesting in robotics because control is simplified as fewer actuators need to act in coordination. However, as specified in Birglen et al. 2007 [7], underactuation must not be mistaken with coupling. A system is coupled if the kinematics of more than one body can be expressed with a single actuator.

Nowadays, robots can perform many tasks, such as pick-and-place operations, drive, assembly other robots, work together with humans or in hazardous environments. But, due to the end-effector, precision tasks that require some sensor feedback have been more limited because of the complexity of the system. One of the goals in end-effectors research field is then, try to match the dexterity of a hand.

> **dexterity**: *"the capability of changing the position and orientation of the manipulated object from a given reference configuration to a different one, arbitrarily chosen within the hand workspace".* (Bicchi 2000 [4])

Many research has been done in the understanding of how a human hand works, but, since a human hand has up to 27 DOF and is highly redundant, it is not an easy task. Some attempts to create a copy of human hands (anthropomorphic robotic hands) have been done divided into two main research areas: grasping and manipulating.

The motivation to introduce the underactuated systems in the grippers' framework is simple: if a proper mechanical design is performed, the gripper/hand will adapt automatically to the shape of an unknown object (see *Fig.1.1*) with a simple control law and usually without sensors. This built-in adaptability in the mechanical system is based on the force distribution,

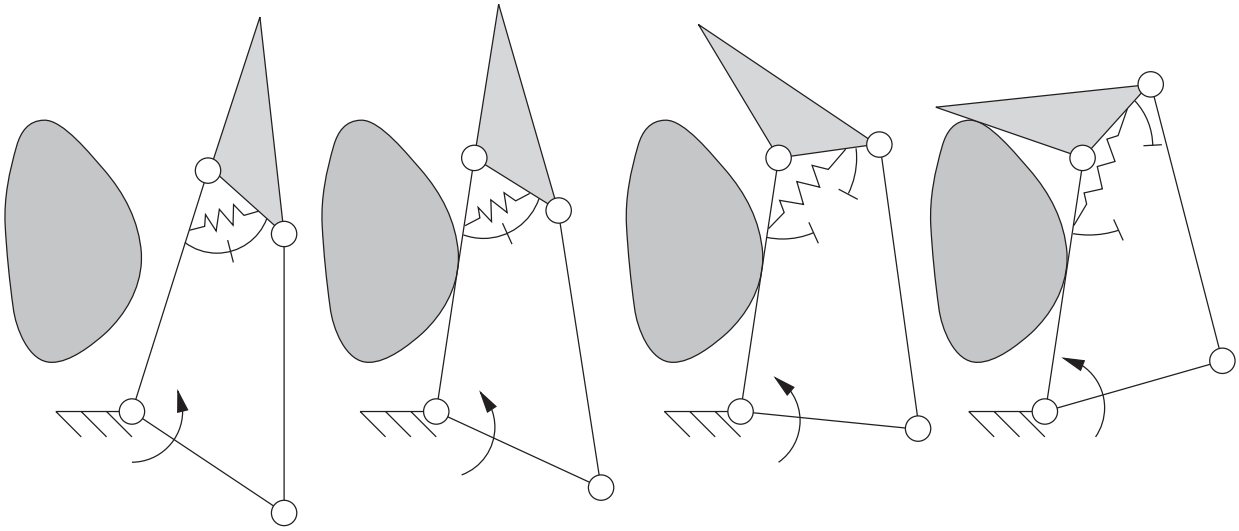

Figure 1.1: Underactuated mechanism with 2 DOF and 1 DOA [5].

i.e., systems that are able to divide up the input forces in several outputs depending on the interaction with the environment.

As the main basis of the research started in the morphological study of the hand, the parts of the grippers (see *Fig.1.2*) have been named in consequence as:

> **palm**: *the inside part of the hand, from the wrist to the base of the fingers.*
>
> **finger**: *any of the long, thin, separate parts of the hand, especially those that are not thumbs.*
>
> **thumb**: *the short, thick finger on the side of the hand that makes it possible to hold and pick things up easily by opposition placement.*
>
> **phalange**: *any one of the small bones of the fingers and toes.*
>
> > **proximal**: *near to the center of the body or to the point of attachment of a bone or muscle.*
> >
> > **intermediate**: *being between two other related things.*
> >
> > **distal**: *away from a particular point of the body.*

Online Cambridge Dictionary, December 2016

In the way to mimic the human hand, many different designs with different properties have been developed. In order to help the design decisions, some classifications are presented (is not an extensive summary). The first ones are related to underactuated hands mechanisms and the lasts are associated with the hand outlines.

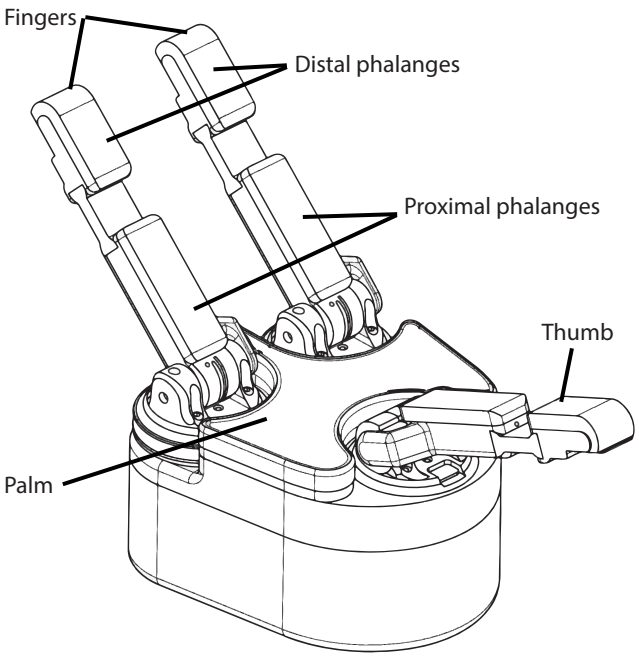

Figure 1.2: Definition of parts of a Robotic hand [9].

- Underactuated hands mechanisms:
  - Relation between actuator torque and output forces.
  - Driving mechanisms.
- Hands outlines:
  - Number of fingers.
  - Fingers DOF.

Relation between actuator torque and output forces

The first introduction to this classification can be found in Krut 2005 [18]. This work tried to classify the mechanism used to perform underactuation. To classify the mechanism, it uses the formulation based on the contact force expression in relation with the applied torques into the mechanism. After, in Bégoc et al. 2010 [19], a third class is added. Finally, mechanisms can be defined as:

- **Differential:** when supposing a kinetostatic state, the output wrench can be expressed by the input wrench and a transmission relation:

$$\begin{aligned} F_a &= F_1^a \, r_1^a = \cdots = F_n^a \, r_n^a \\ \dot{\theta}_a &+ \sum_{i=1}^{n} \frac{\dot{\theta}_i^a}{r_i^a} = 0 \end{aligned} \tag{1.1}$$

  where, n are the number of DOF of the system, θ_a and θ_i^a are the configuration of the system (the actuator and the driven bodies respectively), $\dot{\theta}_a$ and $\dot{\theta}_i^a$ are the joint velocities,

F_a is the actuator wrench (force or torque), F_i^a is the wrench transmitted to the output i and r_i^a are the transmission ratios.

- **Compliant:** when the output forces of the system depend on its configuration and on the stiffness of the elements in the mechanism:

$$[F_a \;\; F_1^a \;\; \dots \;\; F_n^a]^T = \mathbf{K}\,[\theta_a \;\; \theta_1^a \;\; \dots \;\; \theta_n^a]^T \tag{1.2}$$

where, $\mathbf{K}$ is the stiffness matrix of the system.

- **Self-locking:** this type of mechanism have the inherent ability to block any return motion of the elements independently of any external wrench applied. The self-locking property is achieved when the system configuration is constrained by a set of inequalities like:

$$\delta_i\,\dot{\theta}_i^a \geq 0 \qquad \forall i = \{1, \dots, n\} \tag{1.3}$$

where $\delta_i = \pm 1$ depending on the case.

All underactuated hands use one or more of this mechanisms as their properties vary depending on the design. *Table 1.1* summarizes them.

Types	**Strengths**	**Drawbacks**
Differential	Isotropic-force	Return system and Space
Compliant	Inherent adaptability	Short displacements
Self-locking	Blocking mechanism	Weight

Table 1.1: Comparison table of driving mechanisms.

Driving mechanisms

Driving mechanisms are related to how the torque is transmitted from the input to the output. From the existing works, two subdivisions based on the assembling structure are made: mechanisms to drive the fingers and to drive the phalanges. The major distinction is that the mechanism, generally, needs parallel outputs to transmit the movement to fingers, while phalanges are built in series, hence, a way to transmit progressively is needed.

Parallel outputs can be obtained with any of the three classes presented above and, are usually combined. Progressive serial outputs can be obtained with differential and self-locking mechanisms but no work with phalanges driven by compliant mechanisms has been developed, probably due to the stiffness property, which is well suited for parallel outputs but not for progressive serial ones.

Types	Strengths	Drawbacks
Pulley-cable	Adaptability and simplicity	Needs space, low force, lose of wrench by elasticity and high friction
Linkages	High wrenches, small mechanisms and easy manufacturing	Short transmission distance
Gears	High wrenches	Needs space, weight and short transmission distance
Pneumatic	High wrenches	Needs space and short transmission distance

Table 1.2: Comparison table of underactuation between fingers

Number of fingers and fingers DOF

Depending on the final purpose, hands can be classified by its number of fingers. Usually, two fingers are enough for planar applications, while for grasping objects in the space three fingers should be sufficient if well design. Many works, as they were aimed at the prosthetic field, emulate the human hand with five fingers.

The number of DOF of the finger are less clear to define as it depends on the stability requirements to accomplish. Most of the works design hands with 2 or 3 DOF in each finger (emulating the human hand), but other propositions like the Soft Gripper [13], with 10 links each finger, have been studied.

1.2 Stability

"A grasp is stable if and only if the finger is in static equilibrium."

(Birglen et al. 2007 [7])

As it has been already introduced, underactuated grippers are very interesting when referring to control vs. shape adaptability. Fully-actuated or over-actuated grippers rely on a dedicated control and feedback in order to grasp and hold an object stable, in contrast, underactuated grippers don't need any control nor feedback because **the adaptability and the stability depend only on the mechanical design (geometry)**. This is the reason why the research area is focused on developing different models that accomplish the required tasks avoiding instability.

In order to design an underactuated gripper, it is important to forget about using intuition because underactuation does not behave like a single body, coupled ones or independently of the other bodies. Therefore, the design must be based on design/stability criteria. Many can be found in the literature but, the aim is almost always the same, analyze two well-differentiated aspects (Kragten et al. 2009 [17]):

- Ability to grasp: the capability to grasp reaching a stable equilibrium with a range of objects that can move freely.
- Ability to hold: capability to keep a stable holding of the grasped object when external forces are applied.

For fully-actuated and over-actuated grippers, the latter abilities are well-defined in the literature as *form-closure* and *force-closure* respectively. However, as will be seen in the following sections, the main hypotheses of these criteria is that the mechanical system is fully controllable. Hence, they are not suited for underactuated systems and consequently, this chapter is dedicated to review the criteria used to analyze the performance of the underactuated grippers when performing *grasping* and *holding* tasks. First, a general kinetostatic model and a brief classification are presented. After, the most relevant criteria for this thesis are developed.

1.2.1 Static model for robotic fingers

For many years, the research have faced the topic of underactuated grippers either, only theoretically, focused on grasping and manipulating, or designing essentially by intuition. Finally, quite recently, Birglen et al. 2004 [6] presented a kinetostatic analysis for underactuated fingers[1] that relates the two approaches, a useful tool that gives the formulation to link the grasping theory with the design optimization. The purpose, was to create a common framework to analyze the contact forces because, until then, the existing models that formulated the finger's behavior were dependent of the finger, hence, different for each design.

This work has been widely accepted because the model is built in the same way independently of the differential transmission mechanism. The fact that the same model can be applied to different mechanisms will allow to compare diverse hands with the same criteria. For instance, it allows to compare the force distribution and to analyze the stability or if whether the fingers can exert or not, forces to the target.

1.2.1.1 General model

Based on the general layout of the fingers, the model below is based on the following working hypotheses (see *Fig.1.3*):

1. Fixed object: the object is attached to the environment and the fingers are already in contact with it (quasi-static condition).
2. Planar finger: each finger, individually, performs 2D motions; no abduction or adduction motions are considered.

[1]The model presented below is the updated one from Birglen et al. 2007 [7].

3. Revolute joints: all joints are revolute with parallel axes. First joint is fixed to the ground.

4. Single actuator: only one actuator transmits the power and the torque is applied to the first joint.

5. Springs on joints: as a return back method, springs are considered on the joints.

6. Friction: consideration of a tangential force in the contact points due to the Coulomb friction between the phalanges and the object.

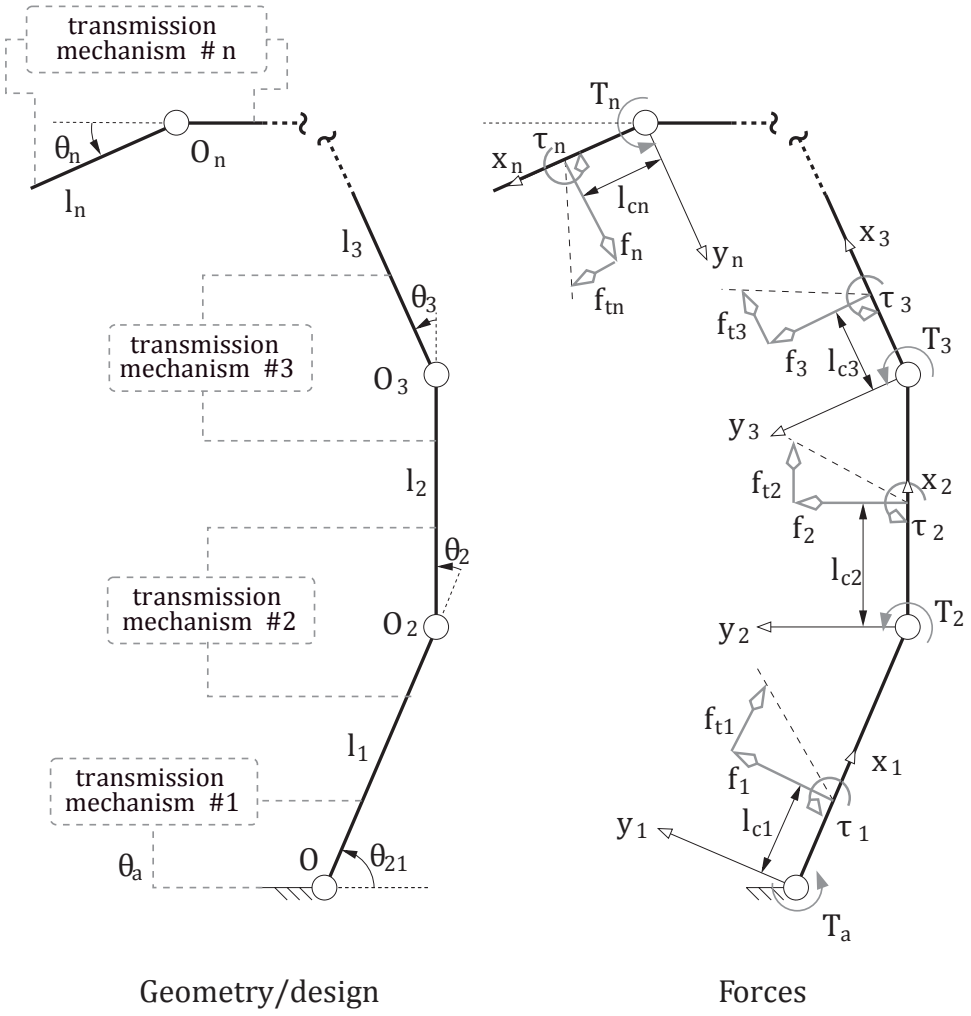

Figure 1.3: Underactuated finger's diagram [7].

The finger is composed of n_p phalanges. Each phalanx is formed by a revolute joint attached either, to the ground or the previous phalanx, and the phalanx itself of length l_i. All phalanges have, by definition, a frame fixed in the joint (point O_i) with the $\boldsymbol{x}_i$ axis along the phalanx, the $\boldsymbol{y}_i$ axis perpendicular to the phalanx and, orthogonal to them and pointing out of the plane, the $\boldsymbol{z}_i$ axis. Each phalanx can also have a contact point with the object, C_i^p, at a distance l_{ci} from O_i and along $\boldsymbol{x_i}$.

Given the finger model and based on the screw theory, the input and output virtual powers

of the system can be computed as:

$$\mathbf{t}^T \boldsymbol{\omega}_a = \sum_{i=1}^{n_p} \boldsymbol{\xi}_i \circ \boldsymbol{\zeta}_i \tag{1.4}$$

where $\mathbf{t}$ is the input torque vector exerted by the joints, $\boldsymbol{\omega}_a$ is the joints velocities vector, $\boldsymbol{\xi}_i$ and $\boldsymbol{\zeta}_i$ are the twist and the wrench of the contact point i (C_i^p, belonging to phalanx i), and the operator $\circ$ defines the reciprocal product operation. Being,

$$\mathbf{t} = \begin{bmatrix} T_a \\ T_2 \\ T_3 \\ \vdots \\ T_{n_p} \end{bmatrix}, \qquad \boldsymbol{\omega}_a = \begin{bmatrix} \dot{\theta}_a \\ \dot{\theta}_2 \\ \dot{\theta}_3 \\ \vdots \\ \dot{\theta}_{n_p} \end{bmatrix}, \qquad \boldsymbol{\xi}_i = \begin{bmatrix} \omega_i \\ v_i^{\mathbf{x}} \\ v_i^{\mathbf{y}} \end{bmatrix}, \qquad \boldsymbol{\zeta}_i = \begin{bmatrix} f_{ti} \\ f_i \\ \tau_i \end{bmatrix}, \tag{1.5}$$

where T_a and T_i are the actuator and the i^{th} joint torques. For $\boldsymbol{\omega}_a$, $\dot{\theta}_a$ and $\dot{\theta}_i$ are the actuator and the i^{th} joint velocities. For $\boldsymbol{\xi}_i$, ω_i, $v_i^{\mathbf{x}}$ and $v_i^{\mathbf{y}}$ are the angular and linear velocities at the contact point i. And finally, for $\boldsymbol{\zeta}_i$, f_{ti} and f_i are the tangential and normal forces applied by the phalanx i and, τ_i the torques applied by the phalanx i.

Grouping terms and developing, one can obtain

$$\mathbf{t}^T \boldsymbol{\omega}_a = \sum_{i=1}^{n_p} \left(f_i \left(\sum_{k=1}^{i} \dot{\theta}_k \ \mathbf{r}_{ki}^T \ \mathbf{x}_i - \mu_i \sum_{k=1}^{i} \dot{\theta}_k \ \mathbf{r}_{ki}^T \ \mathbf{y}_i + \eta_i \sum_{k=1}^{i} \dot{\theta}_k \right) \right) \tag{1.6}$$

with μ_i and η_i being coefficients relating the tangential force and the torque to the normal force through friction.

1.2.1.2 Contact matrix

The latter equation (1.6) can be grouped in matrices, obtaining

$$\mathbf{t}^T \boldsymbol{\omega}_a = \mathbf{f}^T (\mathbf{J} \dot{\boldsymbol{\theta}}) \tag{1.7}$$

where, $\mathbf{J}$ is a matrix that only depends on the contact points poses and the friction coefficients. In the literature it is introduced as the "Jacobian" matrix for robotic fingers. As will be seen later, it actually corresponds to the kinematic Jacobian of the contact points in a quasi-static analysis of the system. By identification of eq. (1.6), $\mathbf{J}$ for fingers with two phalanges and with friction is defined as (Birglen et al. 2007 [7]):

$$\mathbf{J} = \begin{bmatrix} l_{c1} & 0 \\ l_{c2} + l_1(\cos\theta_2 - \mu \sin\theta_2) & l_{c2} \end{bmatrix} \tag{1.8}$$

As explained above, **J** only depends on the configuration of the finger when the phalanges are in contact with the object, hence, the transmission system is not introduced in the model, facilitating in this way the comparison of the fingers only taking into account the geometric design. Even though, the encouragement of developing such model were the underactuated fingers, note that it can also be applied to fully actuated fingers. Regarding the friction parameters, the inclusion of them depend on if friction is considered

1.2.1.3 Transmission matrix

It is possible that, at some point, one is interested in modeling the fingers in function of their driving mechanism. For instance, in order to optimize the transmission ratios. This can be done with the model presented above introducing a new matrix in the system, derived from the virtual power equation (1.6),

$$\mathbf{t}^T \boldsymbol{\omega}_a = \mathbf{f}^T (\mathbf{J}\mathbf{T}\boldsymbol{\omega}_a) \tag{1.9}$$

where, $\mathbf{T}$ is the transmission matrix that relates the vector $\boldsymbol{\omega}_a$ to the time derivatives of the phalanx coordinates as: $\dot{\boldsymbol{\theta}} = \mathbf{T}\boldsymbol{\omega}_a$. For a two-phalanxed finger,

$$\begin{bmatrix} \dot{\theta}_1 \\ \dot{\theta}_2 \end{bmatrix} = \begin{bmatrix} 1 & R_t \\ 0 & 1 \end{bmatrix} \begin{bmatrix} \dot{\theta}_a \\ \dot{\theta}_2 \end{bmatrix} \tag{1.10}$$

where R_t is the transmission ratio relating the first link with the actuator and the second link. As will be seen later, $\mathbf{T}$ is a reformulation of the kinematic model relating the active joints with the passive ones.

1.2.2 Stability performance criteria

With the creation of new designs, new criteria have been introduced in the research works to analyze their performance. Following, a short classification (Kragten et al. 2009 [17]) aims to summarize them divided by if they do not require object information or, on the opposite, the target must be known.

1.2.2.1 Unknown object

Relative to the unknown object, two aspects can be considered: one corresponding to the motion of the fingers and, the other one, related to the contact forces with the object. The latter class is more relevant as it relates the stability with the interaction with the object through the configuration of the fingers. The main criteria considered on this class are:

1. Positiveness: as the fingers can only apply compression forces, the contact forces on the fingers must be positive or null for each studied configuration.

2. Resultant force direction: the resultant contact force must be facing the palm in order to keep the object.

1.2.2.2 Known object

In the case that the target object is known (shape, dimensions ans position), no assumptions need to be made, as happened with the latter case. Hence, three classes can be defined: contact forces, ability to grasp and ability to hold. The criteria regarding the first class, the contact forces, have been already defined in the previous subsection; yet, a small change is introduced as the position of the contact forces is known. In the second class, by definition, the ability to grasp includes a stable grasp. Hence, the proposed criteria aim to maximize some ranges where stability is ensured. Finally, the third class is related to the ability to hold an object. These criteria try to deal with the exterior forces applied to the object:

1. Modified Form-closure: as a specific case for non-backdrivable fingers, kinetically determines the number of non-backdrivable elements needed to acquire form-closure.

2. Force disturbances: evaluates the maximal wrench that the fingers are able to oppose.

This classification is far from extensive but, for the case of this thesis, where the grasping phase and the transporting phase can be considered static with some external wrench applied, there will be enough with the four previous criteria.

1.2.3 Force positiveness

As previously introduced, stability in underactuation grippers is when the final configuration of the fingers with the object is in static equilibrium (Birglen et al. 2007 [7]).

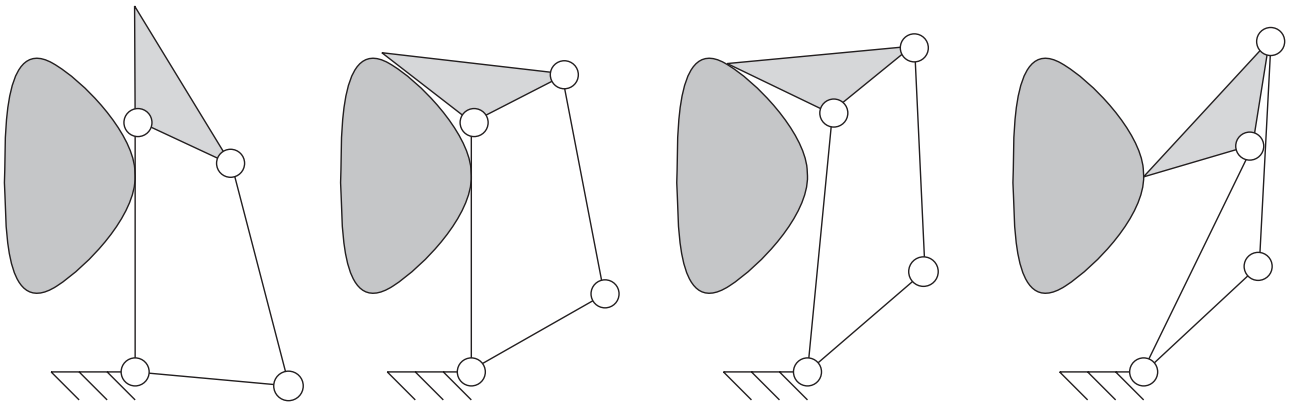

Figure 1.4: Ejection phenomenon of a two-phalanxed finger [7].

The forces on the system are only contact forces, *i.e.*, defined bigger or equal to zero as the fingers are not able to reproduce any pulling force. Namely, any phalanx in contact with the object should have a non-negative force and those that are not in contact, purely null forces. When this condition is not accomplished and some contact forces are negative, the phalanges in contact slip over the object giving the *ejection* phenomenon (see *Fig.1.4*). This event is also identified as instability and is the one that all grippers want to avoid because it can mean the

loss of the object. This section is then, dedicated to the study of the contact forces that define the criterion[2].

If all phalanges are in contact, the model proposed in the previous section is used in order to analyze the contact forces exerted by the finger. Specifically, from equations (1.7) and (1.9), next relation can be written:

$$\mathbf{f} = \mathbf{J}^{-T}\mathbf{T}^{-T}\mathbf{t} \tag{1.11}$$

Then, vector $\mathbf{f}$ can be computed with the latter relation (1.11), the geometric model of the finger and the transmission matrix. However, as only the geometry of the finger is known, the final values will be in function of the geometric parameters l_{ci} and θ_i. Thus, the stability of the grasp can be studied analyzing the positiveness of $\mathbf{f}$ in function of the contact configuration defined by the set of geometrical parameters pairs, l_{ci} and θ_i, which are grouped in the vectors

$$\mathbf{l}_c^\star = [l_{c2} \ \ldots \ l_{cn_p}]^T \qquad \boldsymbol{\theta}^\star = [\theta_2 \ \ldots \ \theta_{n_p}]^T$$

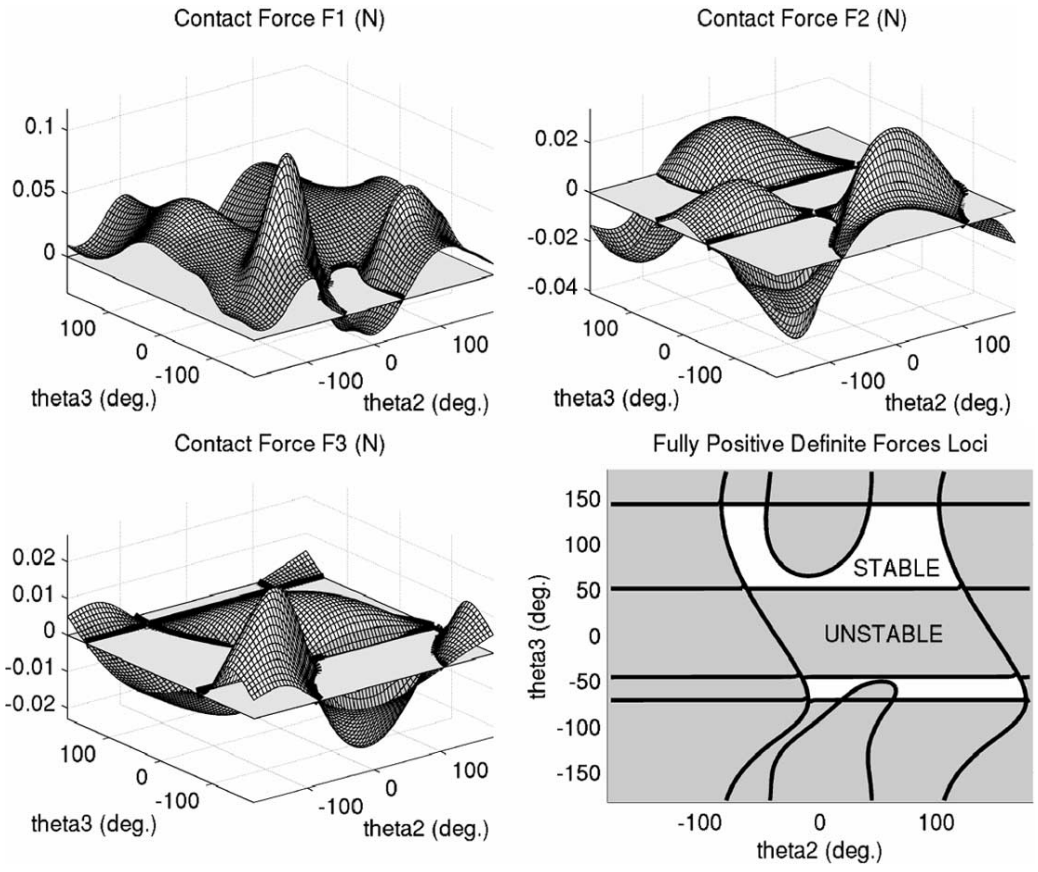

Figure 1.5: Forces on each phalanx and the finger's grasp-state space assuming the contact point is on the middle of the phalanges of a three-phalanxed finger [6].

With this tool, we are able to physically see the contact forces and the stability region of the finger. However, the ratios between the forces depend on the contact configuration and, not

[2]Main references for the following section are Birglen et al. 2004 [6] and Birglen et al. 2007 [7].

on the actuator. Hence, to achieve different ratios, the contact configuration must change, *i.e.*, the geometric design should be modified. In addition, it is important to notice that this results can be obtained only if all phalanges are in contact (a condition imposed by the existence of solution in equation (1.11)) but, other stable configurations may exist where not all phalanges are in contact with the object.

1.2.4 Form-closure

The form-closure property is a largely studied property in the literature. Introduced by Reuleaux 1875 [23], where defined the form-closure property as the capability of a system to constraint the motions of a grasped object, only depending on unilateral, frictionless contact constraints, *i.e.*, the form-closure property is a geometric property. In *Fig.1.6* there is an example of the form-closure grasp of a 2D square; in order to move the square, this would have to break the contact condition of non-penetration, hence, the grasp is form-closure. In the same figure, a partially form-closure grasp can be observed; this property, introduced by Lakshminarayana et al. 1978 [20], is a more general case of the form-closure where only some DOF want to be constrained.

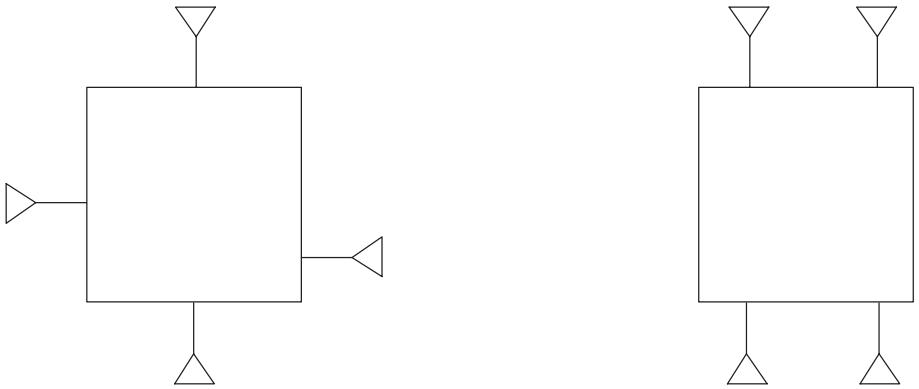

Figure 1.6: Left: form-closure grasp of a planar square. Right: partially form-closure grasp of a planar square [3].

1.2.4.1 General case

Coming, the general expressions for the form-closure analysis are presented[3]. Even though the general case takes into consideration some conditions that are not achievable by underactuated systems, the concept remains the same.

[3]This subsection is based in the work presented by Bicchi et al. 1995 [3]

Lets consider a rigid object (see *Fig.1.7*) with an infinitesimal motion in the space respect to a fix frame R. The working hypotheses are:

1. The motion is composed by a linear velocity, $\mathbf{v}$, applied in the origin of the object, O, and an angular velocity $\boldsymbol{\omega}$.
2. The motion of the object is fully constrained.
3. The constraints are applied on fixed contact points $C_i^o,\ i = 1, \ldots, n_c$, on the surface of the object.

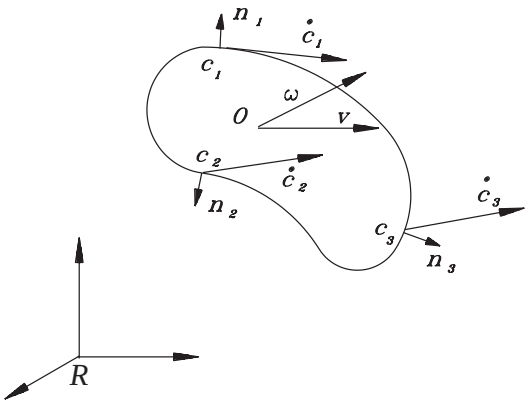

Figure 1.7: Form-closure parameters diagram [3].

4. The set of contact constraints prevent the contact points of having any velocity.
5. Contact points are considered frictionless, hence, the contact constraints are defined normal to the object's surface.

Given the previous hypotheses, the contact constraints and the velocity of the contact points can be defined in matrix form by:

$$\dot{\mathbf{c}}^o = \mathbf{G}^T \dot{\mathbf{u}} \tag{1.12}$$

$$\mathbf{N}^T \dot{\mathbf{c}}^o \geq 0 \tag{1.13}$$

where,

$$\dot{\mathbf{u}} = \begin{bmatrix} \mathbf{v} \\ \boldsymbol{\omega} \end{bmatrix}, \qquad \dot{\mathbf{c}}^o = \begin{bmatrix} \dot{\mathbf{c}}_1^o \\ \vdots \\ \dot{\mathbf{c}}_{n_c}^o \end{bmatrix}, \qquad \mathbf{G} = \begin{bmatrix} \mathbf{I}_3 & \ldots & \mathbf{I}_3 \\ [C_1^o]_\times & \ldots & [C_{n_c}^o]_\times \end{bmatrix}, \qquad \mathbf{N} = diag(\mathbf{n}_1, \ldots, \mathbf{n}_{n_c})$$

where, $\mathbf{n}_i$ is the unit vector defining the forbidden direction for the velocity of the i^{th} contact point and $\dot{\mathbf{c}}_i$ the velocity of such point expressed on the reference frame. $\mathbf{G}$ is the Grasp matrix (as called in the literature) in which, $[C_i^o]_\times$ are the skew symetric matrices for the contact points. In equation (1.13), the inequality is treated elementwise.

Definition *A set of contact constraints is defined Form-Closure if, for all object's motion* $\dot{\mathbf{u}}$*, at least one contact constraint is violated.*

Hence, the way to know if find a grasp is form-closed is to try to find a solution of (1.13) under (1.12). If no solution is found, means that the unilateral contact constraints are broken for any movement, hence, the grasp is form-closed. Two ways are usually used, one, solve a linear programming problem and find the kernel as a single solution. The second, compute the convex polytope of the grasp and check if the origin (kernel) lies inside it (proposed by Mishra

et al. 1987 [22]). As an extension of the linear programming problem, a necessary condition can be written:

Reuleaux-Somov [23] *The minimum number of contacts necessary to form-restrian an object in its configuration space is*

$$n_c \geq d + 1 \tag{1.14}$$

being d is the configuration space dimension of the object, for instance, $d = 3$ for planar cases and $d = 6$ in the three-dimensional space.

1.2.4.2 Underactuated case

One of the considered hypothesis of the form-closure is that the contact points are fixed in the space. For fully-actuated grippers means that, once a configuration is established, if the motors are not actuated, the configuration rests in the same pose. However, with underactuated grippers, this hypothesis is not always true, as presented in *Fig.1.8*. Applying (1.14) in the horizontal dimension, the necessary condition is respected, however, the object still moves, thus is proven that the definition as it is by now, is not suitable for underactuated mechanisms. Bégoc et al. 2010[4] [19] introduces a modified form-closure property to include the non-static contact points and also, the unilateral conditions that can be imposed by non-backdrivable mechanisms. The modified form-closure property is then reformulated as:

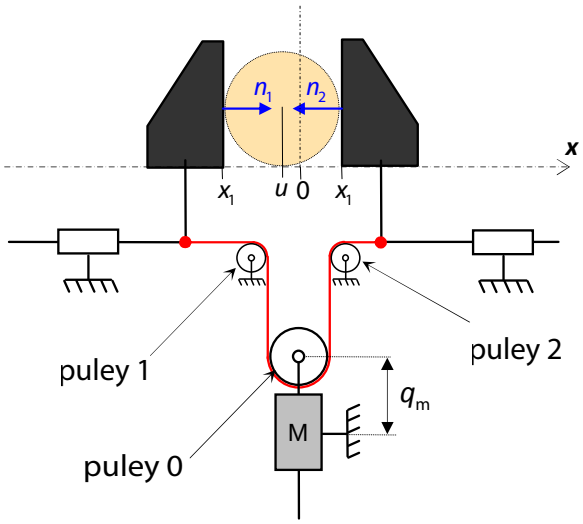

Figure 1.8: Non-form closure grasp for underactuated gripper [19].

Definition *A grasp is said to be formed-closure if, and only if, for any variation of the configuration of the grasp at least one of the unilateral kinematic constraints is violated.*

In comparison with the non-penetration condition (1.13), where the points are fixed, the displacement velocities of the phalanges are introduced into it:

$$\dot{\mathbf{c}}^{y,o} - \dot{\mathbf{c}}^{y,p} \geq 0 \tag{1.15}$$

$$\dot{\mathbf{c}}^{y,o} = \mathbf{N}^T\mathbf{G}^T\dot{\mathbf{u}} = \mathbf{P}\dot{\mathbf{u}}, \qquad \dot{\mathbf{c}}^{y,p} = \mathbf{J}\dot{\boldsymbol{\theta}} \tag{1.16}$$

where $\mathbf{P}$ is called Projection matrix, $\mathbf{J}$ is the one defined in the static model (1.8) under the assumption of frictionless contacts, $\dot{\mathbf{c}}^{y,o}$ is the vector of contact points velocities attached to the

[4]Work used as a base to develop the following subsection

object and projected on the normal vectors of the contact surfaces for all fingers and $\dot{\mathbf{c}}^{y,p}$ is the vector of the phalanx velocities along its normals for all fingers. The previous equations are valid if all phalanx are in contact, hence, $\mathbf{S}$ matrix is added as a Selection matrix, an identity matrix where the row of the phalanx not in contact is removed. The system then,

$$\mathbf{S}(\mathbf{P}\dot{\mathbf{u}} - \mathbf{J}\dot{\boldsymbol{\theta}}) \geq 0 \tag{1.17}$$

Nevertheless, checking the relative velocity is no enought, the introduction of non-backdrivable mechanisms is needed. The actuator transmission vector (1^{st} row of $\mathbf{T}$) computed in (1.10) can be group in a matrix as $\mathbf{T}^f = diag(\mathbf{T}_{n_{pk}})$. Finally, in order to check the kinematic constraints, they have been grouped in the vector $\mathbf{q}_c$, vector of unilateral constraints. Each component of the vector is defined negative if that constraint is violated, hence, the condition of form-closure will be given if all components are positive or zero. Namely,

$$\mathbf{q}_c = \mathbf{U}\boldsymbol{\omega}_g = \left[\begin{array}{c|c} \mathbf{SP} & -\mathbf{SJ} \\ 0 & \mathbf{T}^f \\ \hat{\mathbf{n}}_{palm}^T & 0 \end{array}\right] \begin{bmatrix} \dot{\mathbf{u}} \\ \dot{\boldsymbol{\theta}} \end{bmatrix} \tag{1.18}$$

where $\mathbf{U}$ is the matrix of unilateral constraints and $\boldsymbol{\omega}_g$ defines the motion of the grasp. The matrix $\hat{\mathbf{n}}_{palm}^T$ is the contact constraint with the palm because it is not included in $\mathbf{P}$. As the resulting system is still linear, it can be solved by a linear programming program to check the property.

Lastly, an extension of the minimum contact points to achieve the property is extended from the one in (1.14). Being,

- $n_g = n_h + d$ the dimension of the grasp configuration space with,
  - n_h the dimension of the hand configuration.
  - d the dimension of the object configuration.
- $n_k = n_c + n_u$ the number of unilateral constraints of the problem with,
  - n_c the number of unilateral contact constraints.
  - n_u the number of unidirectional mechanism constraints.

By analogy with (1.14),

$$n_k \;\geq\; n_g + 1 \qquad \Rightarrow \qquad n_c + n_u \;\geq\; n_h + d + 1 \tag{1.19}$$

And, in the general case where one contact per phalanx is assumed (including the palm), $n_c = n_p + 1 \;\Rightarrow\; n_u \;\geq\; d$, at least d non-backdrivable mechanisms are needed to ensure the form-closure property.

Chapter 2

Modeling

2.1 Finger model

As stated in the problem formulation, the main objective is to analyze the closing process of a high-speed gripper. The introduction of high-speeds and interactions with the environment (see *section 2.2*) shifts the need from studying quasi-static models to the necessity of considering a dynamic model of the system. In the following section, the dynamic model for the gripper is developed. To carry out the model, the outlines of the finger are presented and also the kinematic model is developed, as it is necessary for the computation of the dynamic model.

2.1.1 Geometry outline definition

From all the possible combinations that can be built using the classification presented previously (see *section 1.1*), a two-phalanxed linkage-driven finger was chosen. The major reasons to choose this composition is because:

1. The space dimension of the object will be 2: translations in $\boldsymbol{x}$ and $\boldsymbol{y}$ axis. Hence, applying the necessary condition imposed by the Form-closure (see (1.19)), three well-positioned contact points are sufficient to constrain the object. However, the gripper must be symmetric, thus two phalanges for each finger is the minimum affordable.

2. Linkage-driven mechanisms can support good wrenches, implying that the transmission is going to be robust and easy to block. Moreover, they can be small mechanisms with a low weight in comparison with others. Finally, the main drawback is the occupied space in large transmission distances but, given the general dimensions of the problem, it will not present an inconvenience.

The general lines of the studied finger are defined by a five-bar mechanism. This mechanism is defined by five links and five revolute joints of which two are fixed on the ground and the distance between them is null, so at sight, it resembles a four-bar mechanism (see *Fig. 2.1*). The type of system seen in the figure is called *closed-loop* mechanism because if the links are followed in order, the path ends in the initial point; this property is important because it changes the method to compute the models.

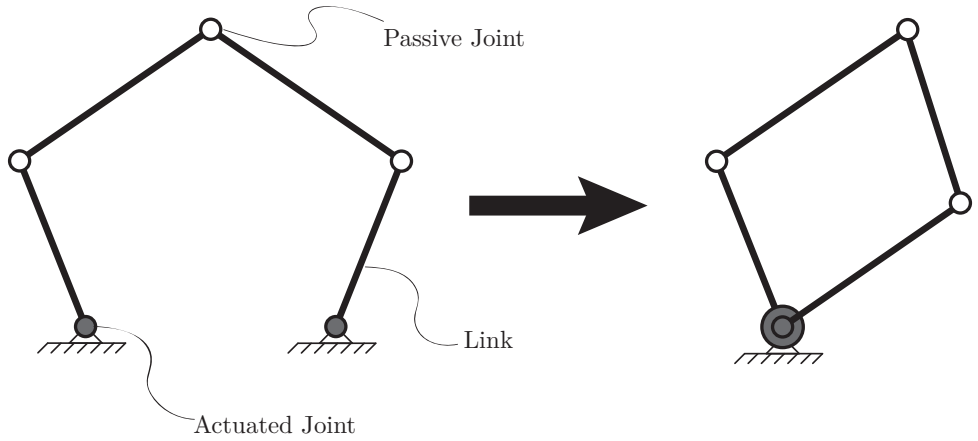

Figure 2.1: Finger mechanism outline.

Computing the degrees of freedom of the mechanism, one gets that two actuators are needed in order to fully constrain the system. These actuators are placed in the joints fixed to the ground. Note that, in the development of this thesis, only one actuator is considered as under-actuation is studied, however, for the kinematic model, a fully constrained model needs to be considered and after, due to the dynamic relations, one of the actuators is suppressed.

Based in *Fig. 2.2*, the model parameters are defined as:

- O, A_{ij}: the Origin and the joints position.
- *base*: the distance along $\boldsymbol{x}$ from O to the center of the object. Note that the object size is known and that it is considered in contact with the palm, so no vertical coordinate is needed.
- l_{ij}: the distance between joints of each link j of the serial mechanism i. Each link have a coordinate axis system centered in the joint shared with the precedent link, or the origin, and oriented with the $\boldsymbol{x}_{ij}$ axis along the link and the $\boldsymbol{z}_{ij}$ axis pointing out.
- t_{22}: the useful distance of the tip phalanx.
- φ_{22}: the angle between the l_{22} link and t_{22} defined in the vectorial positive direction.
- w: is the width of the finger measured from the link to one of the sides, thus the total width is $2w$.
- r_c: is the radius of the cylindric object.

- $\mathbf{q}_a$: the actuated coordinates of the system, defined between the system $\boldsymbol{x}$ axis and the link $\boldsymbol{x}_{ij}$ axis in the vectorial positive direction.

$$\mathbf{q}_a = [q_{11}, q_{21}]^T$$

- $\mathbf{q}_d$: the passive coordinates of the system, defined between the $\boldsymbol{x}_{i(j-1)}$ axis and the link $\boldsymbol{x}_{ij}$ axis in the vectorial positive direction. The joint A_{13} is defined as the end-effector, hence, q_{13} is read as the orientation of the link l_{22} from $\boldsymbol{x}$ axis in the vectorial positive direction.

$$\mathbf{q}_d = [q_{12}, q_{13}, q_{22}]^T$$

- $\mathbf{x}$: the end-effector position, placed in the A_{13} joint and expressed in reference to O.

$$\mathbf{x} = [x, y]^T$$

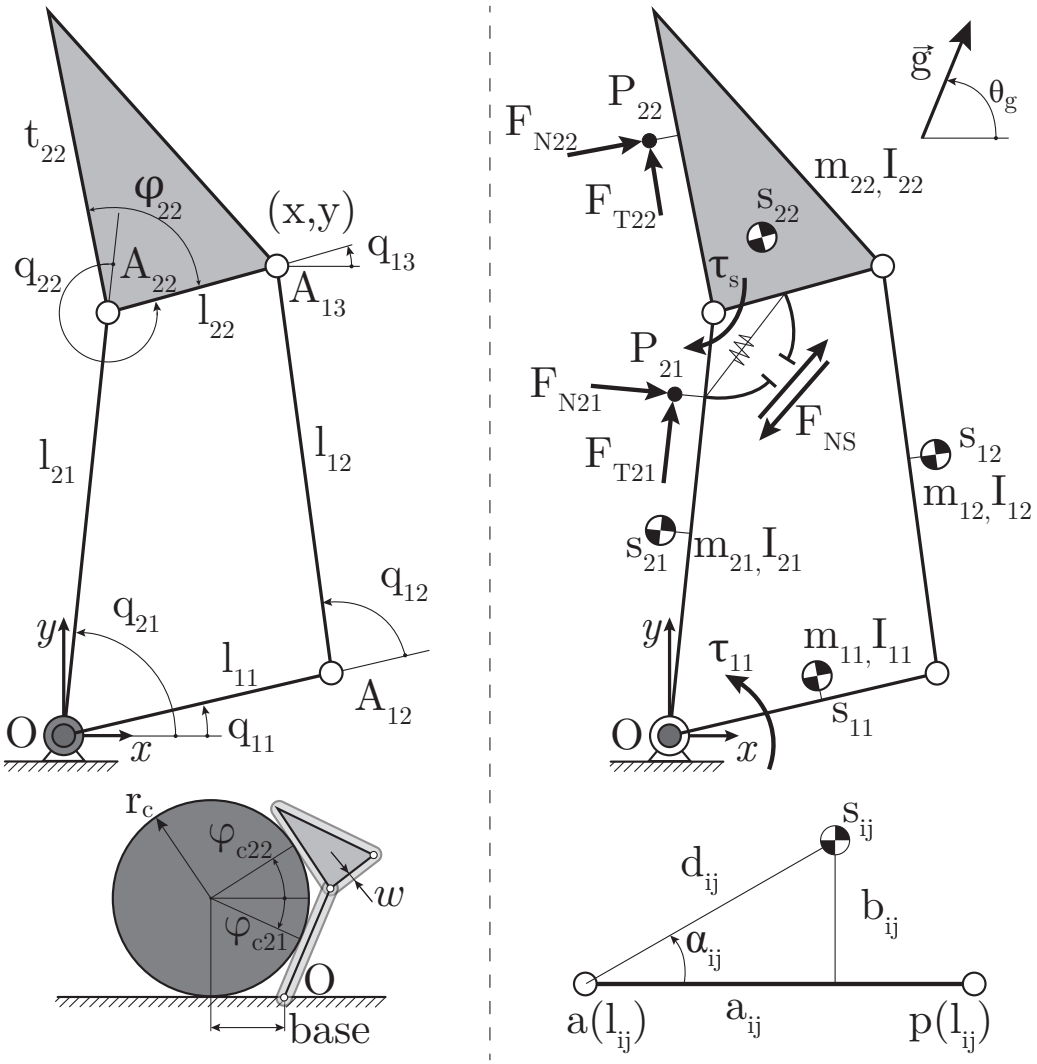

Figure 2.2: Finger parameters definition. Left, geometric parameters. Right, dynamic parameters.

- s_{ij}: the center of mass (CoM) position defined by the distance a_{ij} along the $\boldsymbol{x}_{ij}$ axis and

the distance b_{ij} along the $\boldsymbol{y}_{ij}$ axis.

- m_{ij}, I_{ij}: the mass of the link and the inertia along the $\boldsymbol{z}_{ij}$ in the CoM.
- $\mathbf{g}, \theta_g$: the gravity vector and its orientation with respect to the reference $\boldsymbol{x}$ axis.
- $\boldsymbol{\tau}$: the actuator efforts of the system, defined as torques in the vectorial positive direction. Note that, only the one applied on to the link l_{11} is active because the system is underactuated.

$$\boldsymbol{\tau} = [\tau_{11}, \tau_{21}]^T = [\tau_{11}, 0]^T$$

- $\boldsymbol{\tau}_s$: the wrench applied by the spring.
- F_{N2j}, F_{NS}: the normal contact forces applied either in the collision/contact points P_{2j} and defined positive pointing towards the finger, or in the joint limit contact force.
- F_{T2j}: the friction forces at the points of contact.

Note that in the latter graphics, mostly are a line-diagram to simplify the understanding of the parameters. However, due to the width (w), the contact points P_{2j} are separated from the links in the diagram (*Fig. 2.2*).

2.1.2 Modeling of closed-loop systems

In the following paragraphs is presented the general methodology used to compute the system relations between the generalized coordinates, their velocities and their accelerations $(\mathbf{q}_a, \dot{\mathbf{q}}_a, \ddot{\mathbf{q}}_a)$ with the end-effector ones $(\mathbf{x}, \dot{\mathbf{x}}, \ddot{\mathbf{x}})$, or the set of passive coordinates ones $(\mathbf{q}_d, \dot{\mathbf{q}}_d, \ddot{\mathbf{q}}_d)$, for closed-loop systems. Along with the methodology, the results for the proposed finger are also presented.

2.1.2.1 Direct Geometric Model

The direct geometric model (DGM) expresses the existent relation between the actuated coordinates and the end-effector only relying in the geometric configuration as $\mathbf{x} = dgm(\mathbf{q}_a, \gamma)$, being γ the assembly mode. If the system is closed-loop, there will be passive coordinates which can be computed from the actuated ones and the end-effector as $\mathbf{q}_d = passive\_joints(\mathbf{q}_a, \mathbf{x})$. As the architecture the finger is quite simple, the DGM has been extracted by direct inspection of the architecture as

$$\mathbf{x} = dgm(\mathbf{q}_a, \gamma) \quad \rightarrow \quad \overline{OA_{13}} = \overline{OA_{12}} + \overline{A_{12}H} + \overline{HA_{13}} \qquad (2.1)$$

with,

$$\overline{A_{12}H} = \frac{a}{\left|\overline{A_{12}A_{22}}\right|}\overline{A_{12}A_{22}}$$

$$\overline{HA_{13}} = \gamma\frac{b}{a}\begin{bmatrix}0 & -1\\ 1 & 0\end{bmatrix}\overline{A_{12}H}$$

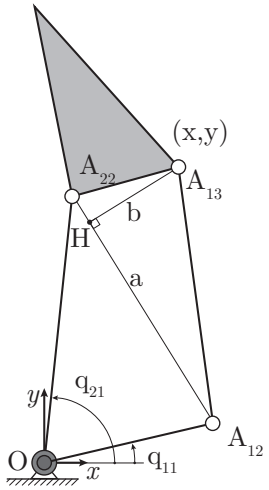

Figure 2.3: DGM parameters diagram.

Once the DGM is computed, the expression of the passive joints is

$$\mathbf{q}_d = passive\_joints(\mathbf{q}_a, \mathbf{x}) \quad \rightarrow \quad q_{i2} = tan^{-1}\left(\frac{y - l_{i1}\sin(q_{i1})}{x - l_{i1}\cos(q_{i1})}\right) - q_{i1}, \quad \forall i = 1, 2 \qquad (2.2)$$

2.1.2.2 Direct Kinematic Model

The direct kinematic model (DKM) relates the velocities of the generalized coordinates with the end-effector as $\dot{\mathbf{x}} = dkm(\mathbf{q}_a, \dot{\mathbf{q}}_a, \mathbf{q}_d, \mathbf{x})$ by the Jacobian matrix $\mathbf{J}$, which can be obtained from the following relation:

$$\mathbf{A}\dot{\mathbf{x}} + \mathbf{B}\dot{\mathbf{q}}_a = 0 \quad \rightarrow \quad \dot{\mathbf{x}} = -\mathbf{A}^{-1}\mathbf{B}\dot{\mathbf{q}}_a \quad \rightarrow \quad \dot{\mathbf{x}} = \mathbf{J}\dot{\mathbf{q}}_a \qquad (2.3)$$

In order to obtain the previous relation, one has to differentiate the proper geometric equations. If the architecture of the legs is complex, an analysis through the application of the Screw theory can be used, however, in the current case, it has been obtained from the closed-loop equations of the robot that are of the form $\mathbf{h}(\mathbf{x}, \mathbf{q}_a, \mathbf{q}_d) = 0$ (2.4). As there is no interest on the passive coordinates for computing the DKM, one can reduce the closed-loop equations to $\mathbf{h}_p(\mathbf{x}, \mathbf{q}_a) = 0$ (2.5). Finally, differentiating the latter w.r.t. time, the equation (2.3) is obtained with

$$\mathbf{A} = \frac{\partial \mathbf{h}_p}{\partial \mathbf{x}} = \begin{bmatrix}x - l_{11}\cos(q_{11}) & y - l_{11}\sin(q_{11})\\ x - l_{21}\cos(q_{21}) & y - l_{21}\sin(q_{21})\end{bmatrix} \qquad (2.6)$$

$$\mathbf{B} = \frac{\partial \mathbf{h}_p}{\partial \mathbf{q}_a} = \begin{bmatrix}xl_{11}\sin(q_{11}) - yl_{11}\cos(q_{11}) & 0\\ 0 & xl_{21}\sin(q_{21}) - yl_{21}\cos(q_{21})\end{bmatrix} \qquad (2.7)$$

And again, as the system is closed-loop, the passive coordinates velocities can be computed from the actuated ones and the end-effector through differentiating (2.4) w.r.t. time. Moreover, to obtain a simplified form, the closed-loop equations have been transformed to $\mathbf{h}_d(\mathbf{q}_a, \mathbf{q}_d)$, so

they do not depend on the end-effector parametrization. Hence, differentiating the latter w.r.t. time, the passive joints velocities can be computed as:

$$\mathbf{J}_{ta}\dot{\mathbf{q}}_a + \mathbf{J}_{td}\dot{\mathbf{q}}_d = 0 \quad \rightarrow \quad \dot{\mathbf{q}}_d = -\mathbf{J}_{td}^{-1}\mathbf{J}_{ta}\dot{\mathbf{q}}_a \quad \rightarrow \quad \dot{\mathbf{q}}_d = \mathbf{J}_{da}\dot{\mathbf{q}}_a \tag{2.8}$$

with

$$\mathbf{J}_{ta} = -\frac{\partial \mathbf{h}_d}{\partial \mathbf{q}_a} = -\begin{bmatrix} -l_{11}\sin(q_{11}) - l_{12}\sin(q_{11}+q_{12}) & l_{21}\sin(q_{21}) + l_{22}\sin(q_{21}+q_{22}) \\ l_{11}\cos(q_{11}) + l_{12}\cos(q_{11}+q_{12}) & -l_{21}\cos(q_{21}) - l_{22}\cos(q_{21}+q_{22}) \end{bmatrix} \tag{2.9}$$

$$\mathbf{J}_{td} = -\frac{\partial \mathbf{h}_d}{\partial \mathbf{q}_d} = -\begin{bmatrix} -l_{12}\sin(q_{11}+q_{12}) & l_{22}\sin(q_{21}+q_{22}) \\ l_{12}\cos(q_{11}+q_{12}) & -l_{22}\cos(q_{21}+q_{22}) \end{bmatrix} \tag{2.10}$$

2.1.2.3 2^{nd} Order Direct Kinematic Model

The 2^{nd} order direct kinematic model (DKM2) relates the accelerations of the system with the ones of the actuated coordinates as $\ddot{\mathbf{x}} = dkm2(\mathbf{q}_a, \dot{\mathbf{q}}_a, \ddot{\mathbf{q}}_a, \mathbf{q}_d, \dot{\mathbf{q}}_d, \mathbf{x}, \dot{\mathbf{x}})$. This model is the direct differentiation w.r.t. time of the DKM:

$$\mathbf{A}\ddot{\mathbf{x}} + \mathbf{B}\ddot{\mathbf{q}}_a = -(\dot{\mathbf{A}}\dot{\mathbf{x}} + \dot{\mathbf{B}}\dot{\mathbf{q}}_a) \quad \rightarrow \quad \dot{\mathbf{x}} = -\mathbf{A}^{-1}(\mathbf{B}\ddot{\mathbf{q}}_a + \mathbf{b}) \tag{2.11}$$

with,

$$\dot{\mathbf{A}} = \begin{bmatrix} \dot{x} + \dot{q_{11}}l_{11}\sin(q_{11}) & \dot{y} - \dot{q}_{11}l_{11}\cos(q_{11}) \\ \dot{x} + \dot{q_{21}}l_{21}\sin(q_{21}) & \dot{y} - \dot{q}_{21}l_{21}\cos(q_{21}) \end{bmatrix} \tag{2.12}$$

$$\dot{\mathbf{B}} = \begin{bmatrix} (\dot{x}l_{11}\sin(q_{11}) + x\dot{q}_{11}l_{11}\cos(q_{11})) - (\dot{y}l_{11}\cos(q_{11}) - y\dot{q}_{11}l_{11}\sin(q_{11})) & \\ 0 & \\ & 0 \\ & (\dot{x}l_{21}\sin(q_{21}) + x\dot{q}_{21}l_{21}\cos(q_{21})) - (\dot{y}l_{21}\cos(q_{21}) - y\dot{q}_{21}l_{21}\sin(q_{21})) \end{bmatrix} \tag{2.13}$$

As with the DKM, the accelerations of the passive joints can also be obtained by differentiating the equation (2.8) w.r.t. time:

$$\mathbf{J}_{ta}\ddot{\mathbf{q}}_a + \mathbf{J}_{td}\ddot{\mathbf{q}}_d = -(\dot{\mathbf{J}}_{ta}\dot{\mathbf{q}}_a + \dot{\mathbf{J}}_{td}\dot{\mathbf{q}}_d) \quad \rightarrow \quad \ddot{\mathbf{q}}_d = \mathbf{J}_{da}\ddot{\mathbf{q}}_a + \mathbf{J}_{td}^{-1}\mathbf{d}_c \tag{2.14}$$

with,

$$\dot{\mathbf{J}}_{ta} = \begin{bmatrix} \dot{q}_{11}l_{11}\cos(q_{11}) + (\dot{q}_{11}+\dot{q}_{12})l_{12}\cos(q_{11}+q_{12}) & -(\dot{q}_{21}l_{21}\cos(q_{21}) + (\dot{q}_{21}+\dot{q}_{22})l_{22}\cos(q_{21}+q_{22})) \\ \dot{q}_{11}l_{11}\sin(q_{11}) + (\dot{q}_{11}+\dot{q}_{12})l_{12}\sin(q_{11}+q_{12}) & -(\dot{q}_{21}l_{21}\sin(q_{21}) + (\dot{q}_{21}+\dot{q}_{22})l_{22}\sin(q_{21}+q_{22})) \end{bmatrix} \tag{2.15}$$

$$\dot{\mathbf{J}}_{td} = \begin{bmatrix} (\dot{q}_{11}+\dot{q}_{12})l_{12}\cos(q_{11}+q_{12}) & -(\dot{q}_{21}+\dot{q}_{22})l_{22}\cos(q_{21}+q_{22}) \\ (\dot{q}_{11}+\dot{q}_{12})l_{12}\sin(q_{11}+q_{12}) & -(\dot{q}_{21}+\dot{q}_{22})l_{22}\sin(q_{21}+q_{22}) \end{bmatrix} \tag{2.16}$$

2.1.2.4 Direct Dynamic Model

The dynamic model gives the relation between the efforts applied on the actuated coordinates and the position, velocities, accelerations and external forces on the system. Hence, the direct dynamic model can be expressed as $\ddot{\mathbf{q}}_a = ddm(\boldsymbol{\tau}, \mathbf{q}_a, \dot{\mathbf{q}}_a)$. The model has been calculated using the Lagrange formulation, which one of its extension to parallel robots is (Ibrahim and Khalil, 2010 [14]):

1. Virtually open the closed-loop to create virtual tree structures composed of serial fully-actuated manipulators (two in the case of the finger model) and a virtual free-moving platform (see *Fig. 2.4*).
2. Compute the inverse dynamic models for the tree structures.
3. Close the loop again, using the loop-closure equations and the Lagrange multipliers.

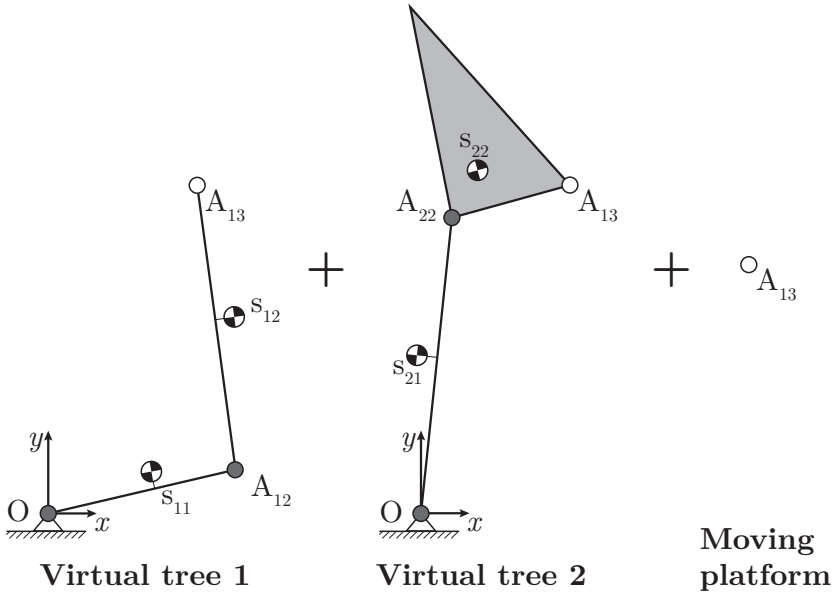

Figure 2.4: Finger decomposition into tree structures.

Applying the Lagrange formulation, the efforts of the tree structures can be computed as

$$\begin{gathered} \boldsymbol{\tau}_{ti} = \frac{d}{dt}\left(\frac{\partial L_{ti}}{\partial \dot{\mathbf{q}}_{ti}}\right)^T - \left(\frac{\partial L_{ti}}{\partial \mathbf{q}_{ti}}\right)^T, \quad i = 1, 2 \\ L_{ti} = E_{ti} - U_{ti} \end{gathered} \tag{2.17}$$

For any rigid robot, the Lagrange formulation leads to the following expression (Khalil and Dombre, 2002 [16]):

$$\begin{aligned} \boldsymbol{\tau}_{ti} &= \mathbf{M}_{ti}(\mathbf{q}_{ti})\ddot{\mathbf{q}}_{ti} + \mathbf{c}_{ti}(\mathbf{q}_{ti}, \dot{\mathbf{q}}_{ti}) \\ \mathbf{c}_{ti} &= \mathbf{B}_{ti}\dot{q}_{i1}\dot{q}_{i2} + \mathbf{C}_{ti}[q_{i1}^2, q_{i2}^2]^T + \mathbf{Q}_{ti} \end{aligned} \tag{2.18}$$

where $\boldsymbol{\tau}_{ti} = [\tau_{i1}, \tau_{i2}]^T$ is the actuators efforts' vector, $\mathbf{q}_{ti} = [q_{i1}, q_{i2}]^T$ is the vector of the generalized coordinates of the tree structure; note that for the case of the finger, the virtual tree

structures are composed by 1 actuated joint and 1 passive. L_{ti} is the Lagrangian of the tree structure, E_{ti} is its kinematic energy and U_{ti} is its potential energy. Once the equations are developed for each tree structure, $\mathbf{M}_{ti}$ is the mass matrix and $\mathbf{c}_{ti}$ is the vector containing the centrifugal ($\mathbf{C}_{ti}$), Coriolis ($\mathbf{B}_{ti}$) and gravity ($\mathbf{Q}_{ti}$) effects. The virtual tree structures have been computed using the *Christoffel symbols* formulation, which gives:

$$\mathbf{M}_{ti} = \begin{bmatrix} m_{i1}d_{i1}^2 + m_{i2}(l_{i1}^2 + d_{i2}^2 + 2l_{i1}(a_{i2}\cos q_{i2} - b_{i2}\sin q_{i2}) + I_{i1} + I_{i2}) & & \\ m_{i2}(d_{i2}^2 + l_{i1}(a_{i2}\cos q_{i2} - b_{i2}\sin q_{i2}) + I_{i2}) & & \\ m_{i2}(d_{i2}^2 + l_{i1}(a_{i2}\cos q_{i2} - b_{i2}\sin q_{i2}) + I_{i2}) & \\ m_{i2}d_{i2}^2 + I_{i2} \end{bmatrix} \quad (2.19)$$

$$\mathbf{B}_{ti} = \begin{bmatrix} -2m_{i2}l_{i1}(a_{i2}\sin q_{i2} + b_{i2}\cos q_{i2}) \\ 0 \end{bmatrix} \quad (2.20)$$

$$\mathbf{C}_{ti} = \begin{bmatrix} 0 & -2m_{i2}l_{i1}(a_{i2}\sin q_{i2} + b_{i2}\cos q_{i2}) \\ 2m_{i2}l_{i1}(a_{i2}\sin q_{i2} + b_{i2}\cos q_{i2}) & 0 \end{bmatrix} \quad (2.21)$$

$$\mathbf{Q}_{ti} = [-m_{i1}g(a_{i1}\sin(\theta_g - q_{i1}) - b_{i1}\cos(\theta_g - q_{i1})) - m_{i2}g(l_{i1}\sin(\theta_g - q_{11}) + a_{i2}\sin(\theta_g - q_{i1} - q_{i2}) - \\ -b_{i2}\cos(\theta_g - q_{i1} - q_{i2})), \quad -m_{i2}g(a_{i2}\sin(\theta_g - q_{i1} - q_{i2}) - b_{i2}\cos(\theta_g - q_{i1} - q_{i2}))]^T \quad (2.22)$$

Finally, closing the loop with the constraint equations and the Lagrange multipliers, the direct dynamic model for the finger is:

$$\ddot{\mathbf{q}}_a = \mathbf{M}^{-1}(\mathbf{q}_a)(\boldsymbol{\tau} - \mathbf{c}(\mathbf{q}_a, \dot{\mathbf{q}}_a)) \quad (2.23)$$

with,

$$\mathbf{M}(\mathbf{q}_a) = [\mathbf{I}_{2\times 2}\ \mathbf{J}_{da}^T]\mathbf{S}^T\mathbf{M}_t\ \mathbf{S}\begin{bmatrix}\mathbf{I}_{2\times 2} \\ \mathbf{J}_{da}\end{bmatrix}$$

$$\mathbf{c}(\mathbf{q}_a, \dot{\mathbf{q}}_a) = [\mathbf{I}_{2\times 2}\ \mathbf{J}_{da}^T]\mathbf{S}^T\left(\mathbf{c}_t + \mathbf{M}_t\ \mathbf{S}\begin{bmatrix}\emptyset_{2\times 1} \\ \mathbf{J}_{td}^{-1}\mathbf{d}_c\end{bmatrix}\right)$$

where,

- $\mathbf{M}_t$ groups the mass matrices as
$$\mathbf{M}_t = \begin{bmatrix}\mathbf{M}_{t1} & \emptyset_{2\times 2} \\ \emptyset_{2\times 2} & \mathbf{M}_{t2}\end{bmatrix}$$
- $\mathbf{c}_t = [\mathbf{c}_{t1}, \mathbf{c}_{t2}]^T$
- $\mathbf{J}_{td}, \mathbf{J}_{da}, \mathbf{d}_c$ are defined in (2.8), (2.8) and (2.14) respectively.
- $\mathbf{S}$ is a sorting matrix. It sorts the active joint elements first and the passive ones after.
$$\mathbf{S} = \begin{bmatrix}1 & 0 & 0 & 0 \\ 0 & 0 & 1 & 0 \\ 0 & 1 & 0 & 0 \\ 0 & 0 & 0 & 1\end{bmatrix}$$

Note that, by now, $\boldsymbol{\tau} = [\tau_{11}, \tau_{21}]^T$, which means that the system's model is not considering underactuation. Next section, will introduce the necessary to eliminate τ_{21}.

2.1.3 External efforts models

The dynamic model presented in the previous section only contemplates the relation between the evolution of the system and the actuator efforts. However, the studied case is involved in an environment, which leads to the need of developing the models of external forces applied on to the system. Specifically, there will be two types of external efforts: contact forces on the phalanges of the finger and a torque between two of the links. As the dynamic model is additive, the external wrenches' contributions can be directly added into the DDM giving as a result:

$$\ddot{\mathbf{q}}_a = \mathbf{M}^{-1}(\mathbf{q}_a)((\boldsymbol{\tau}_a + \boldsymbol{\tau}_s + \boldsymbol{\tau}_{C21} + \boldsymbol{\tau}_{C22}) - \mathbf{c}(\mathbf{q}_a, \dot{\mathbf{q}}_a)) \tag{2.24}$$

where $\boldsymbol{\tau}_a = [\tau_{11}, 0]^T$ is the actuator torque, $\boldsymbol{\tau}_s$ is the contribution of the spring and $\boldsymbol{\tau}_{C2j}$ are the contributions of the contact forces. To compute the effect of these external wrenches on to the system, a well-known relation in robotics has been used, the static model, which states

$$\boldsymbol{\tau} = \mathbf{J}_n^T \mathbf{w}_n \tag{2.25}$$

where $\mathbf{J}_n$ is the kinematic Jacobian matrix of the studied point belonging to any of the system links, and $\mathbf{w}_n$ the wrench applied in such point.

2.1.3.1 External forces

The finger will have two external forces applied on to it, one for each contact between the phalanx and the grasped object. Each of the forces have a normal and a tangential (friction) component. The computation of the normal and the tangent forces are given in the next section.

The contact point on l_{21} is defined as P_{21} (see *Fig. 2.5*) and its contribution to the system following (2.25) is

$$\boldsymbol{\tau}_{C21} = \mathbf{J}_{P_{21}}^T(\mathbf{F}_{N21} + \mathbf{F}_{T21}) = \begin{bmatrix} 0 \\ -l_{C21} - \mu w \end{bmatrix} F_{N21} \tag{2.26}$$

The contact point on t_{22} is defined as P_{22} (see *Fig. 2.5*) and its contribution to the system has been computed following the same method. The kinematic Jacobian of P_{22} is

$$\mathbf{J}_{P_{22}}^*(\dot{q}_{21}, \dot{q}_{22}) = \begin{bmatrix} -l_{21}\sin q_{21} - l_{C22}\sin(q_{21}+q_{22}+\varphi_{22}) - w\cos(q_{21}+q_{22}+\varphi_{22}) \\ l_{21}\cos q_{21} + l_{C22}\cos(q_{21}+q_{22}+\varphi_{22}) - w\sin(q_{21}+q_{22}+\varphi_{22}) \end{bmatrix}$$
$$\begin{bmatrix} -l_{C22}\sin(q_{21}+q_{22}+\varphi_{22}) - w\cos(q_{21}+q_{22}+\varphi_{22}) \\ l_{C22}\cos(q_{21}+q_{22}+\varphi_{22}) - w\sin(q_{21}+q_{22}+\varphi_{22}) \end{bmatrix} \tag{2.27}$$

Note that this Jacobian is expressed in function of $\dot{q}_{21}$ and $\dot{q}_{22}$, therefore, it has been transformed to depend on the active joints only as

$$\mathbf{J}_{P_{22}} = \begin{bmatrix} \mathbf{J}^*_{P_{22}}(1,2) & \mathbf{J}^*_{P_{22}}(1,1) \\ \mathbf{J}^*_{P_{22}}(2,2) & \mathbf{J}^*_{P_{22}}(2,1) \end{bmatrix} \begin{bmatrix} \mathbf{J}_{da}(2,1) & \mathbf{J}_{da}(2,2) \\ 0 & 1 \end{bmatrix} \tag{2.28}$$

Finally, the effort of the contact force is expressed as

$$\boldsymbol{\tau}_{C22} = \mathbf{J}^T_{P_{22}}(\mathbf{F}_{N22} + \mathbf{F}_{T22}) = \mathbf{J}^T_{P_{22}} \begin{bmatrix} \cos\varphi_{c22} + \mu \, |\cos(\varphi_{c22} - \varphi_{nc22})| \cos\varphi_{nc22} \\ \sin\varphi_{c22} + \mu \, |\cos(\varphi_{c22} - \varphi_{nc22})| \sin\varphi_{nc22} \end{bmatrix} F_{N22} \tag{2.29}$$

where,

- l_{C2j} is the distance from the precedent joint of the link to P_{2j} along the axis x_{2j}.
- w is the distance from the link to P_{2j} along the axis y_{2j}.
- F_{N2j} and F_{T2j} are the normal and tangent contact forces.
- F_{C22} is the generalized contact force in the tip with a collision angle φ_{c22}.
- μ is the friction coefficient and it is developed in the next section.
- φ_{nc22} is the normal contact orientation, which can be also expressed as $\varphi_{nc22} = q_{21} + q_{22} + \varphi_{22} - \pi/2$.

Remark that the differentiation between the orientation of the tip phalanx and the normal contact is necessary as the phalanx can slip until the tip, losing the normality of the contact.

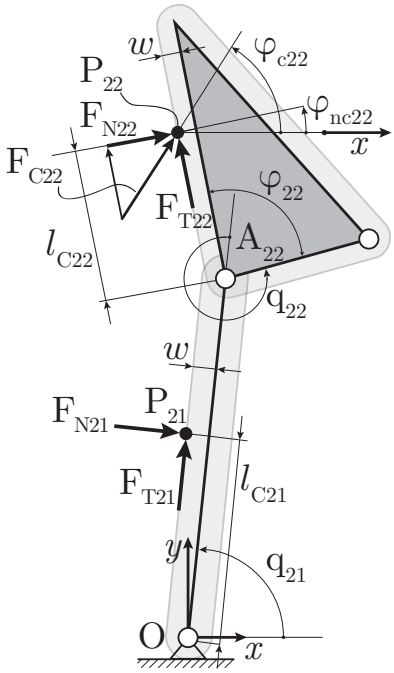

Figure 2.5: Contact parameters definition.

2.1.3.2 External torque

Finally, the finger will also have a torsional spring between two consecutive links in order to restrain the missing actuator in q_{21}, to a certain degree. Using the method presented above, the spring torque in function of the active joints is expressed by the angle formed in between the two consecutive links (q_s) as

$$\boldsymbol{\tau}_S = \left[\frac{\partial q_s}{\partial \mathbf{q}_a}\right]^T (c_s - \tau_{limit})(q_p + \Delta q_s) = \begin{bmatrix} \mathbf{J}_{da}(2,1) \\ \mathbf{J}_{da}(2,2) \end{bmatrix} k_s \tag{2.30}$$

where c_s is the constant of the spring, τ_{limit} is the value of the joint limit contact torque that will modify the total spring constant, q_p the preload angle, Δq_s the increment of the spring coordinate. Note that, $k_s = (c_s - \tau_{limit})q_p$, *i.e.*, k_s is the spring constant of a constant spring

(force does not vary with the deformation of the spring but, as a mathematic solution, the joint limit modifies it); also note that it is placed in the point A_{22}, between the links l_{21} and l_{22}. The reason of these decisions is solved in the next chapter (see *section 3.3.2.3*).

2.1.4 Static equilibrium model

As it has been introduced, Birglen 2007 [7] presents a generalized model to study the finger performance in static equilibrium. However, the study is presented in pieces, analyzing the impact of including one of the three following hypotheses at a time:

1. Consideration of springs.
2. The phalanges width.
3. Friction.

The model required to compute the stability of the current finger must incorporate all three hypotheses at the same time (have a spring, phalanx width, and friction) as all of them are considered. Through the analysis of the analytical results of the model presented in this chapter, the equivalent model to Birglen can be developed by applying the static equilibrium condition (null velocity and acceleration of all the joints) on the final configuration of the finger in the full model equation (2.24), obtaining

$$\boldsymbol{\tau}_a + \boldsymbol{\tau}_s + \boldsymbol{\tau}_{C21} + \boldsymbol{\tau}_{C22} = 0 \tag{2.31}$$

As it is explained in the next chapter (see *Chapter 3*), the actuator torque and the spring constant are computed with respect the geometry and the closing time condition, thus, the normal contact forces depend on them through the static equilibrium model as:

$$\begin{bmatrix} F_{N21} \\ F_{N22} \end{bmatrix} = -\mathbf{J}_C^{-1}(\boldsymbol{\tau}_a + \boldsymbol{\tau}_s) \tag{2.32}$$

with,

$$\mathbf{J}_{C,(2\times 2)} = [\mathbf{J}_{C21}, \mathbf{J}_{C22}], \quad \mathbf{J}_{C2j,(2\times 1)} = \mathbf{J}_{P2j}^T \left(\frac{\mathbf{F}_{N2j}}{|\mathbf{F}_{N2j}|} + \frac{\mathbf{F}_{T2j}}{|\mathbf{F}_{T2j}|} \right)$$

Then $\mathbf{J}_C$ is defined as the Jacobian matrix of the collisions and is the same matrix presented by Birglen in [7] (see (1.8)) but with the incorporation of all the hypothesis at once.

2.2 Interactions

As explained before, the main point of this thesis is the development of a model that allows the analysis of the whole closing sequence of an underactuated gripper at high-speed. This is the

reason why, besides the dynamic model, also the external wrenches due to the collision between the finger and the object, and between the links of the finger have been considered. These interactions can be modeled by a contact model that expresses their magnitude. This section will model a collision model for the above-mentioned phenomenon which will allow the analysis of the transition between having the fingers freely moving in the environment and the static phase. To ensure that the model is working properly, a crosschecking with ADAMS software is done. ADAMS is an MSC software widely used for dynamics simulation and model checking of multi-body systems. Due to its extended use among researchers, can be considered as Ground Truth when it comes to check new models or to use the results for highly complex systems. This software includes many possibilities for modeling physical phenomena, such as collision and friction between two bodies. The specific final equations to compute the variables values have been placed in *Appendix B.2.1* as they are mainly geometric relations.

2.2.1 Hertz contact and Coulomb's friction theory

The contact and friction phenomena are a well-known issue in the modeling of systems by its complex mathematical characterization. Nevertheless, these phenomena exist and can highly influence the model, thus they must be taken into consideration.

2.2.1.1 Hertz contact

Collisions or interactions between different solids are a substantial topic of research because it is a complex problem to understand and model. When an interaction occurs, many physical phenomena are happening simultaneously and, in addition, the problem can not be isolated as all the interacting bodies' properties are exerting an influence on the output of the studied region. As some of the physical phenomena have a not so obvious models by themselves and many data is usually missing (for instance, precise geometry around contact point or accurate models for the non-linear phenomena), the collision models tend to be simple and take some compromise in the accuracy, as long as the practical applications are respected.

Two types of contact models can be found in the bibliography (Chatterjee 1997 [8]), Algebraic and Incremental models. The first is mainly based on the satisfaction of some inequations where the parameters of the model appear, these models depend on the impulse response rigidity (f.e. the restitution coefficient). The second group is defined by the evolution of the interaction expressed as a set of ODEs and depend on the force response rigidity. The fisrt group includes models like Poisson functions, based on the restitution coefficient (energy conservation on the collision). The second group contemplates models like the Hertz model, which computes the contact force values. Extending the Herts model with a damper, energy loss can be introduced in the collisions (Giesbers 2012 [11]).

A small reminder in Hertz contact theory based on Johnson 1987 [15], beginning by the assumptions that it incorporates:

1. Adhesion is neglected. No force tries to tie both bodies after the collision.

2. Initial contact is a point or a line.

3. Only elastic deformations occur around the contact point.

4. Deformation is much smaller than the objects' curvature radii.

5. There is no friction.

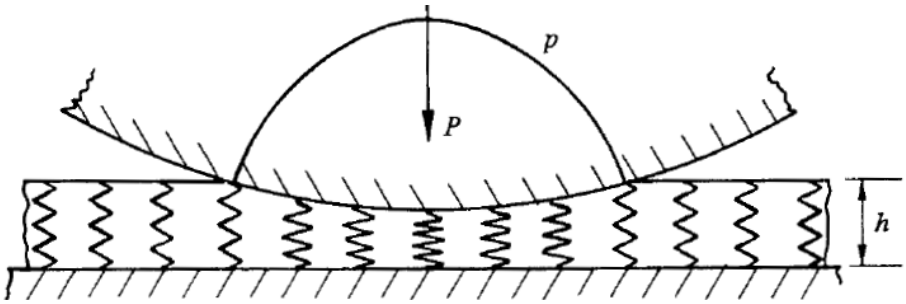

Figure 2.6: Spring Bed model simplification

The contact force is computed using the interference volumes of two spheres (an imaginary volume that penetrates the opposed object if no deformation is considered). The Hertz theory develops the pressure distribution due to this penetration. A simplification of this theory is the Spring Bed approach, where the two bodies are changed by a single body with the shape equal to the sum of the two penetrated volumes and a space of springs that compress under the object collision (see *Fig. 2.6*). Finally, the solution of this model relates the penetration of the spheres with the contact force under the shape

$$F_n = k\,\delta_n^{3/2} \tag{2.33}$$

Where, F_n is the normal contact force, k is the contact stiffness and δ_n the normal penetration distance. The contact stiffness is a variable that depends on both objects to be determined and can be defined as

$$k = 2aE^* \tag{2.34}$$

with,

$$a = \left(\frac{3L_N R}{4E^*}\right)^{1/3}, \qquad R = \left(\frac{1}{R_1} + \frac{1}{R_2}\right)^{-1}, \qquad E^* = \left(\frac{1-\nu_1^2}{E_1} + \frac{1-\nu_2^2}{E_2}\right)^{-1}$$

Where, a is the Hertz contact radius, R the combined radius of curvature, E^* the combined Young's modulus, L_N the normal load with which both objects are pressed together, R_i the respective radius of curvature, ν_i the respective Poisson's moduli and E_i the respective Young's moduli.

2.2.1.2 Coulomb friction

Friction between solids is a complex phenomenon that depends on many parameters. The most used and known model to evaluate friction is Coulomb's friction model. It establishes a relation between (see *Fig. 2.7a*) the friction force F_f (tangential) opposed to a motion produced by the tangential force F_t of an applied force F_{app} and the normal force of contact between the two solids F_n, with a friction coefficient μ as

$$F_f = \mu F_n \tag{2.35}$$

One can differentiate static friction (stiction) and kinetic friction (sometimes called dynamic friction) with two different coefficients. As one can feel by trying to move an object on a table, the friction is more important when the object is static and then it decreases with the slipping of the object. This relation can be defined by Coulomb's Friction Cone (see *Fig. 2.7b*) as

$$\begin{cases} \texttt{if:} \quad F_t \leq \mu_s F_n \;\rightarrow\; \mu_s \geq \dfrac{F_t}{F_n} = \tan(\theta_f) \quad \texttt{then:} \quad F_f = \mu_s F_n & (2.36) \\ \texttt{else:} \quad F_f = \mu_d F_n & (2.37) \end{cases}$$

where, μ_s is the static friction coefficient, μ_d is the kinetic friction coefficient and θ_f is the Cone angle respect the vertical. Equation (2.36) expresses the fact that if a randomly force applied on to the object (F_{app}) is not great enough, the object will remain static. While, if F_{app} is greater enough, the object will slip with an opposing force as in (2.37). Usually, the value of the coefficient is between 0 and 1, but specific cases/materials can have bigger friction coefficients. Note that, as the transition between static and kinetic friction is instantaneous, in the transition a discontinuity appears.

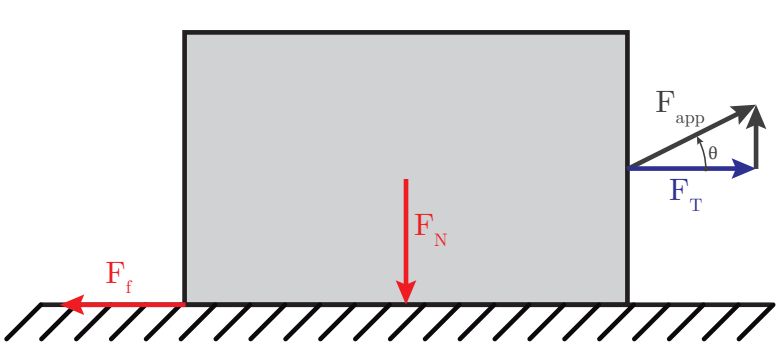

(a) Simple representation of Coulomb friction

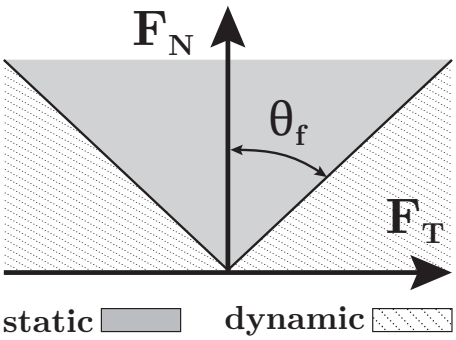

(b) Coulomb's friction cone

2.2.2 Normal contact force model

As it has been introduced previously, a normal contact model has been developed. This contact model is defined by two parts, a spring (as the Hertz model indicates) and a damper, which

is the responsible for the non-elastic collisions (see *Fig. 2.8*). Hence, the normal contact force have the following structure:

$$F_{cn} = k(\delta_n)^e - STEP(c_{max}, \delta_{max}, \boldsymbol{x}, \dot{\boldsymbol{x}}) \tag{2.38}$$

where, F_{cn} is the normal contact force, k the contact stiffness, δ_n the normal penetration distance and e the exponent of the penetration, as defined in (2.33) by the Hertz model. The $STEP$ function makes reference to the damper part of the system. In the real world, the damper system (as the spring system) acts as soon as the contact begins. However, in the spring system the force value is continuous and progressively increasing from 0, while in the damper system, the damper goes from null effect to full influence. The behavior of the damper results in a problem when integrating the model because the discontinuous force induces the integrator to oscillate around the equilibrium point and it can lead to unstable solutions or long convergences. For this reason, is a usual practice to provide this kind of functions with a transition zone, approximated by a continuous function (as the model is checked with ADAMS, a cubic function has been chosen to match the results with the software [2]), to eliminate the discontinuities. In this case, the STEP function is defined as

$$STEP(c_{max}, \delta_{max}, \boldsymbol{x}, \dot{\boldsymbol{x}}) = c\dot{\boldsymbol{x}} \tag{2.39}$$

with $c(c_{max}, \delta_{max}, \boldsymbol{x})$ being the damper constant defined as

$$\begin{cases} \texttt{if no contact:} & c = 0 \\ \texttt{elseif } \delta_n > \delta_{max} & c = c_{max} \\ \texttt{else} & c = a(\delta_n)^3 + b(\delta_n)^2 \quad \text{with} \quad a = \dfrac{2c_{max}}{\delta_{max}^3}, \quad b = \dfrac{3c_{max}}{\delta_{max}^2} \end{cases}$$

where, c_{max} is the value of the damper constant when it is over the transition zone, δ_{max} is the width of the transition zone.

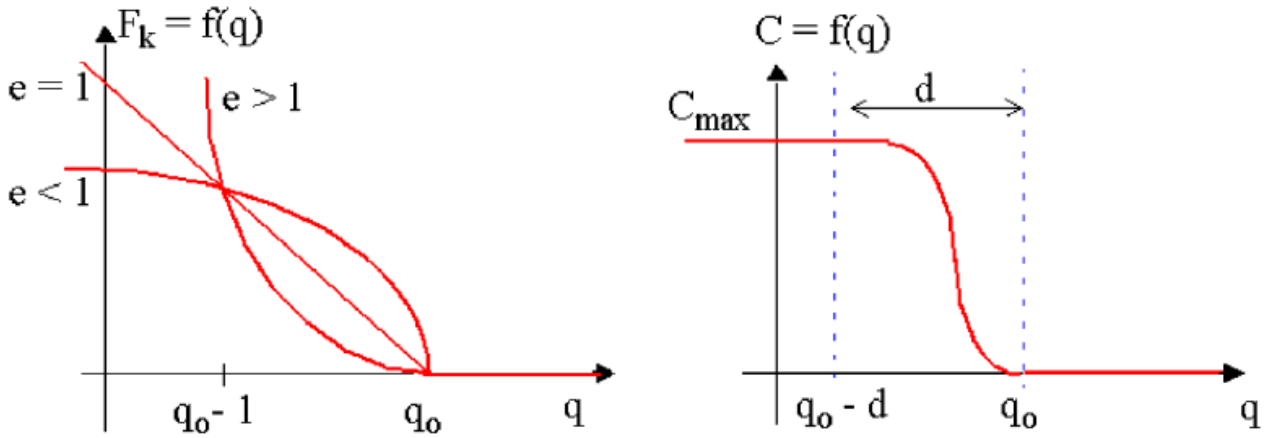

Figure 2.8: ADAMS Spring (left) and Damper (right) functions [2].

2.2.3 Friction force model

As it has been introduced previously, a model Coulomb's friction model is used. The Friction force model, as presented before in equation (2.35) is:

$$F_f = \mu F_n$$

where μ is a generic value of the friction coefficient and computed in the following paragraphs.

Following the same methodology as in the previous model, the transition zone for the discontinuous friction coefficient has been modeled according to ADAMS [2] in order to obtain the same results in the crosschecking. The used parameters are: *Coulomb Friction, Static Coefficient, Dynamic Coefficient, Stiction Transition Vel.and Friction Transition Vel.* As it has been stated, the friction model used will be the Coulomb's model. The two first parameters refer to the already explained coefficients μ_s and μ_d. The other two parameters that one can set are the *Stiction Transition Velocity* (v_s) and the *Friction Transition Velocity* (v_d). These coefficients will set the transition zone because the friction coefficients do not follow a continuous function (as they are different), which implies that there is a discontinuity when the object starts slipping. The friction coefficient function is based on the slipping velocity between phalanx and object (see *Fig. 2.9*).

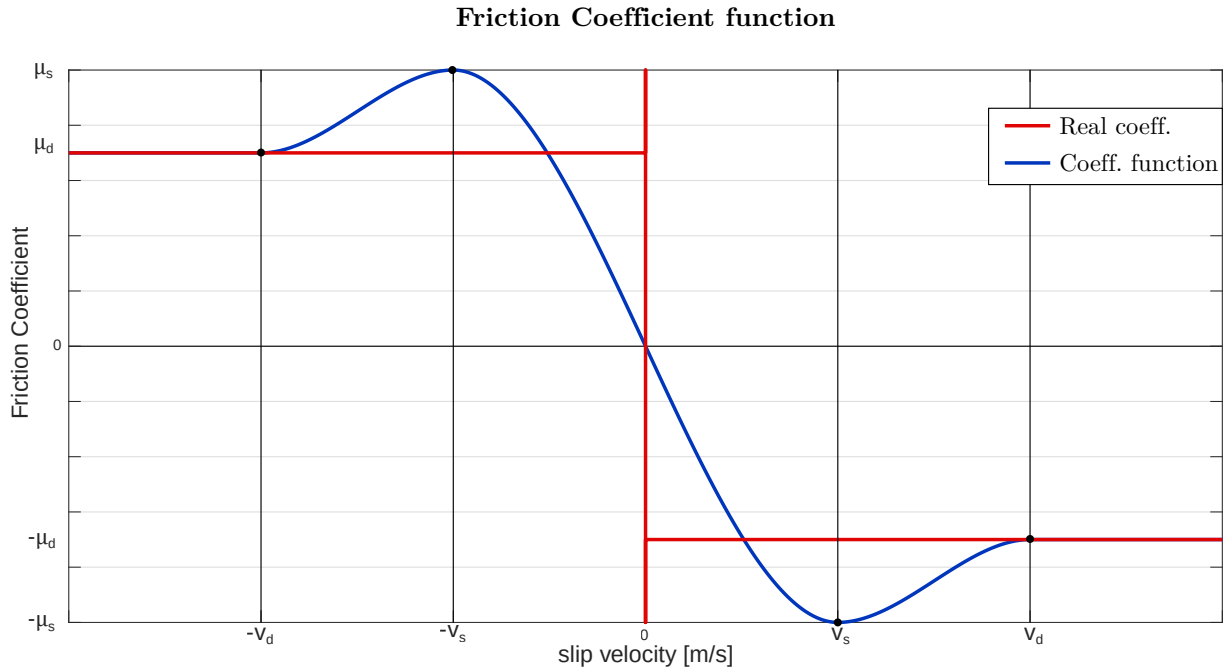

Figure 2.9: Friction coefficient function vs. real coefficient behavior.

Taking into account this graphic, in equation (2.35), the friction parameter is defined as $\mu = \mu(v_{slip})$, where v_{slip} is the slipping velocity between the two contacting objects. This antisymmetric chart can be divided in five sections (two of them antisymmetric) that allow to

define $\mu(v_{slip})$:

$$\begin{cases} |v_{slip}| > |v_d| & \rightarrow \mu = -\text{sign}(v_{slip})\mu_d \\ |v_s| < |v_{slip}| < |v_d| & \rightarrow \mu = -\text{sign}(v_{slip})\left[av_{slip}^3 + bv_{slip}^2 + \mu_d\right] \\ -v_s < v_{slip} < v_d & \rightarrow \mu = \left[cv_{slip}^3 + dv_{slip}^2 - \mu_s\right] \end{cases}$$

with

$$a = \frac{-2(\mu_s - \mu_d)}{(v_d - v_s)^3}, \quad b = \frac{3(\mu_s - \mu_d)}{(v_d - v_s)^2}, \quad c = \frac{-2(2\mu_s)}{(2v_s)^3}, \quad d = \frac{3(2\mu_s)}{(2v_s)^2}$$

Chapter 3

Grasp Analyses

3.1 Design theory

In the previous chapters, the main idea has been presented several times:

The performance of an underactuated gripper is directly related to its mechanical design.

Therefore, this chapter is dedicated to analyzing the model in order to get the best possible design. Before proceeding to the analysis, a short recall on design process methodology is hereafter presented.

There are several methodologies for a design process, however, optimization belongs to the end of the design loop. A general design methodology (French et al. 1985 [10]):

1. Need: the design is born from a need to cover requisites. This necessity becomes the main objective around which the design evolves.
2. Analysis: once the need is formulated, it is analyzed. This analysis performs mainly two actions,
   (a) a study of the current or similar solutions, if existing.
   (b) the study of the potential tools to develop a new one.
3. Problem statement: having acquired the general knowledge on the topic, it is possible to state which are the actual tools and the missing ones to solve the main objective.
4. Conceptual design and selection: only one in a thousand times, the first design is the good one. For this reason, it is advised to start with very different simple concepts and little by little narrow them down. It depends on the problem.

5. Embodiment: usually, the main objective includes the general dimensions or performances that are expected. These allow to scale or give to the drafts a set of base parameters to define them to a higher order. Sometimes, in this phase, the set of possible solutions is narrowed to one.

6. Detailing: here is where optimization takes part. The possible solutions must be analyzed in order to select the best one. Hence, optimization (and simulation) is a useful tool to analyze the performances of the different options to create and objective selection.

7. Testing: once the model is fully completed, it is time to prototype and check that the results were the expected ones.

Due to feasibility and improving issues, is usual to go back to the analysis of the problem or the conceptual designs to change them and getting feedback, starting a design loop.

3.2 Gripper requirements

In the following section, the finger requirements and hypotheses considered are detailed in order to have a general overview of the achievements the finger must accomplish. Beginning by the problem formulation,

- the gripper must grasp and hold stable and fixed 2D cylindric object of ⌀40 mm subject to gravity to perform planar pick-and-place operations.
- the gripper must be underactuated and perform the closing operation in less than 10 ms.
- the gripper must be symmetric.
- the gripper must be robust in front of vibrations, however, the positioning error is assumed to be null.
- the gripper must be robust in front of the object's material.
- while accomplishing the previous tasks, total mass, actuator torque and contact forces should be the smallest possible.

Apart from the requirements stated by the problem, there is a set of conditions that are interesting when considering the high-speed closing of the system. As can be seen in Massa et al. 2002 [21], when there is a fast movement of the finger, the underactuated DOF act as a coupled mechanism. This event is used in Kaneco et al. 2003 [12] to design the finger such as it makes contact with all phalanges at the same time. However, this method is only applicable if the object position is known and with the drawback that the design is useful only for a single object. For this reason, in the present thesis, the same study has been used but in the opposite sense of Kaneco et al. 2003 [12] as the exact position could be unknown. Then, the desired behavior of the fingers is

- to perform the approaching phase (from the beginning until the first collision) as if it were a rigid solid, *i.e.*, the spring must be stiff enough to maintain the finger links in null relative velocity, only rotating around the actuator joint. Which means that the finger will have a progressive closing.

3.3 Model analyses and settings

In the following section, some analysis over the model has been done in order to define the design parameters and the methodologies to ensure the requirements stated in the previous section.

3.3.1 Model variables and constants

The first analysis is regarding the number of design variables that have to be set for a single finger. Having defined the outline of the fingers and the models, the design variables go up to sixty if no hypotheses are considered and no values are given. After some considerations and values decisions using ADAMS, the design is reduced down to eight (see *Table 3.1*).

Class	**Variables**	**After Reduction**
Geometry	13	4
Mass	18	0
Spring	9	2
Contacts	20	1
Actuator	1	1
Total	**60**	**8**

Table 3.1: Design variables summary and reduction.

The 8 design variables over which the model is expressed are:

- $base, l_{21}, \varphi_{22}, r_l (= l_{22}/l_{11})$
- c_s, spring type and placement
- μ_s
- τ_{11}

Some of the values have been chosen as a dimensioning of the finger by direct inspection of the conceptual designs and simulations with ADAMS:

Geometry	**Spring Contact**	**Object Contact**
$l_{11} = 15$ mm $w = 2.5$ mm $q_0 = 25°$ $\varphi_{c21m} = 0°$ $\varphi_{c22m} = 5°$ $r_h = 0.9375$ $depth = 40mm$	$k_{SC} = 10^{11}$ N/m $e_{SC} = 2.2$ $c_{maxSC} = 10^9$ N·s/m $d_{maxSC} = 10^{-5}$ m $\mu_{SC} = 0$	$k_{OC} = 10^8$ N/m $e_{OC} = 2.2$ $c_{maxOC} = 10^6$ N·s/m $d_{maxOC} = 10^{-5}$ m $r_{\mu_d} = 0.7$ $v_d = 2v_s = 0.2$ m/s

Table 3.2: Chosen parameters for the model.

where, the initial orientation of the finger is defined as the first collision angle plus an offset of $q_0 = 25°$, the minimum collision angle for l_{21} is φ_{c21m} and the minimum for l_{22} is φ_{c22m} and the maximum reachable height of the finger when closing is defined as height ratio r_h of the object's diameter. To simplify the contact with the object, $\mu_d = r_{\mu_d}\mu_s$.

The hypotheses assumed for the development of the reductions and the general relations are[1] (see *Appendix B.2.2* for the complete functions):

- Geometry
  - The links width are constant and equal for all links.
  - The initial configuration is a right trapezoid ($q_{11} = 0°, q_{21} = 90°$).
  - The palm normal is in $+\mathbf{y}$ axis direction.

  $\rightarrow [l_{21min}, l_{21max}] = f(base),\ [\varphi_{c2j}, t_{22}] = f(base, l_{21}),\ l_{12} = f(l_{21}, l_{12}, l_{22}, \varphi_{22})$

- Mass
  - Links are made of homogeneous ABS of density ρ_{ABS}.
  - Geometry studied is a planar section of the part.

  $\rightarrow [m_{ij}, a_{ij}, b_{ij}, I_{ij}] = f(\text{body volume})$

- Contacts: contact properties between the phalanges and the object are equal for any link (defined in *Table 3.2*).

- Actuator: is driven by a non-backdrivable mechanism.

- Gravity is in $+\mathbf{y}$ axis direction, pulling the object away from the palm.

[1]Note that the functions only include the variables dependency but not the constants.

3.3.2 Requirements analyses

Following the requirements presented in section 3.2, this section presents the relations and results that arise from them. The direct results are:

- The symmetry of the system, and the null positioning errors with respect the object allow simplifying the study to a single finger.
- In order to grasp the object stable, static stability criteria must be used: force positiveness, palm force positiveness and form-closure.
- In order to hold stable the object, some of the previous criteria can be used: form-closure.
- In order to be robust to the fingers' and object's material, friction must be neglected if possible.
- Closing the grasp in less than 10 ms will determine the minimum constant spring and actuator torque.
- In order to reduce the spring and the actuator's torque, the placement of the spring is also important. These last two analyses are further developed hereafter.

3.3.2.1 Test trajectory

In order to ensure that the finger can perform the closing trajectory (see *Fig. 3.1*) in at least 10 ms, a test trajectory is computed given, the time to perform it (10 ms), the *base*, the set of geometrical variables and q_0. The function used is a 7^{th} order polynomial that will ensure that the initial and final velocities, accelerations and jerks of the link l_{11} are null.

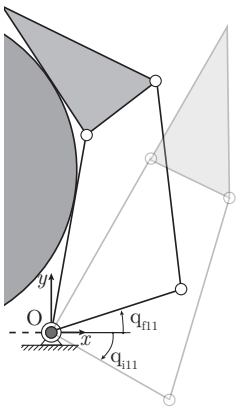

Figure 3.1: Evolution of the desired trajectory.

3.3.2.2 Minimum spring constant and actuator torque

In order to respect the desired behavior of the finger, moves as a rigid solid until the first contact, the adequate spring constant c_s must be chosen. Applying the rigid solid constraints into the model and simulating the system using the test trajectory as the input, the right side of the IDM is computed, leaving the left side as the computation of two torques equaled to a constant that varies along the trajectory:

$$\begin{bmatrix} \tau_{11} \\ 0 \end{bmatrix} + \left[\frac{\partial q_s}{\partial \mathbf{q}_a} \right]^T c_s = \mathbf{cnt}(t) \tag{3.1}$$

From the two equations that can be extracted, the minimum $c_s(t)$ and its respective $\tau_{11}(t)$ can be computed. Finally, the minimum spring constant that respects the criteria is $c_s = \max(c_s(t))$ and the torque that accomplished the trajectory in at least 10 ms is $\tau_{11} = \text{RMS}(\tau_{11}(t))$. Note that, the trajectory is going to be faster than 10 ms as the torque is a constant and not a continuous function.

3.3.2.3 Spring placement

Given a trajectory and the computation of the minimum spring constant, four q_s can be experimented in order to know in which of the joints the spring is the smallest. As the behavior conditions are the same for any of the spring positions, the resultant torque is not affected by them. The expressions of q_s are:

1. $q_{s1} = q_{21} - q_{11}$
2. $q_{s2} = q_{12}$
3. $q_{s3} = q_{22}$
4. $q_{s4} = q_{11} + q_{12} - (q_{21} + q_{22})$

In *Fig. 3.2* can be seen that k_{s3} and k_{s4} have the lowest values. Even though, the figure only shows a single experiment, the result is the same in all the experiments. As stated previously, the interest is to find the minimum spring constant with the same performances, however, taking into account the similarity between k_{s3} and k_{s4}, the first is preferred in front of the latter because it is a traction spring, while the latter is a compression spring. The preference arises from the mechanical design of the finger, in which implementing a joint limit and the spring attachments to the links is for easier and comfortable. Thus, the best placement for the spring is in the joint q_{22}, between the links l_{21} and l_{22}.

3.3.2.4 Spring type

The last analysis around the spring is regarding the spring type: constant or torsional. The difference between both types is only noticeable when the first collision occurred and the spring is incrementing its coordinate. The best spring type is the one that causes lower actuator torques. Given the best placement for the spring and a trajectory, using the equation (2.30) for the contribution of generic springs, the process of the last experiment is repeated, obtaining *Fig. 3.3*. As can be appreciated in the figure, the constant spring causes smaller torques than the torsional spring during the extension phase, hence, the best spring type is the constant spring.

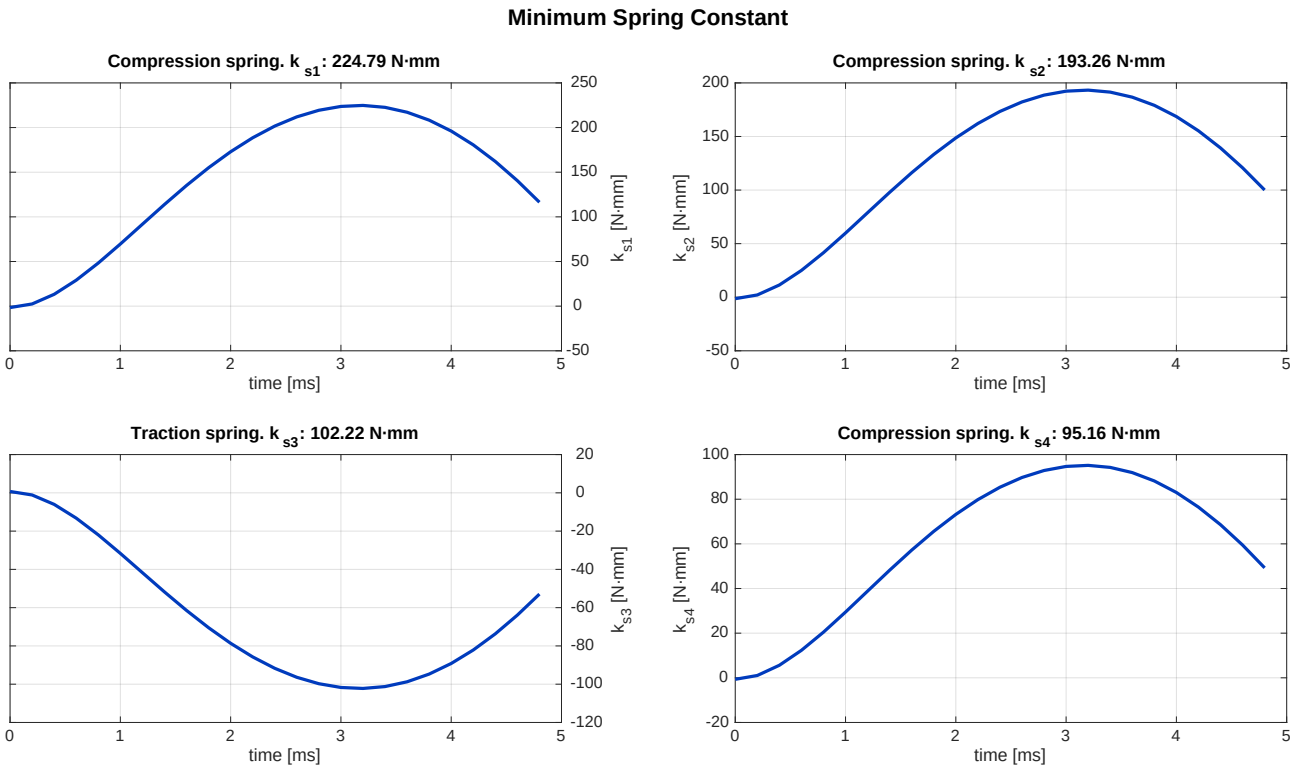

Figure 3.2: Example of the Minimum spring constant required along the test trajectory with $base = 12$ mm, $l_{21} = 18.9$ mm, $\varphi_{22} = 100°$ and $r_l = 0.5$.

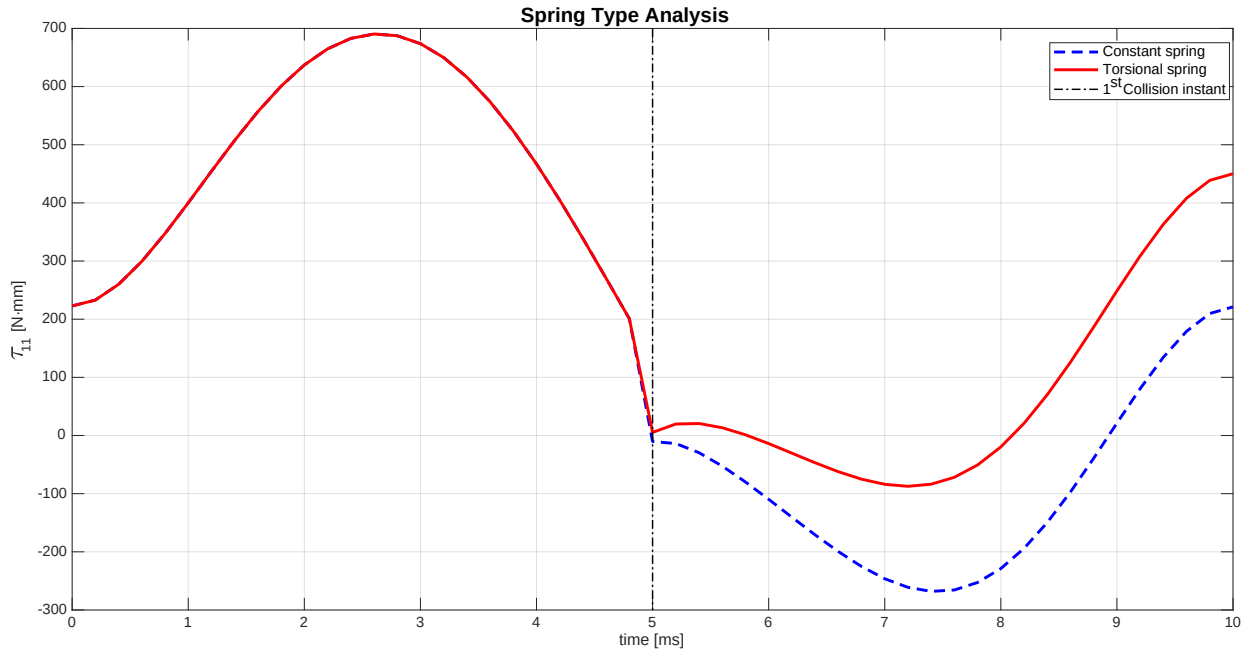

Figure 3.3: Example of the Spring type comparison using the test trajectory with $base = 12$ mm, $l_{21} = 18.9$ mm, $\varphi_{22} = 100°$ and $r_l = 0.5$.

3.4 Workspace analysis: *Grasp-state Volume*

Given the model, the hypotheses and the relations, the design variables are left to study. In order to get a general overview of how the system behaves in statics and to ensure that at least the finger in statics respects the requirements, a workspace analysis tool has been developed. The main idea of this tool is based on the *grasp-state space* presented by Birglen in [7], where, given a geometry, makes an analysis of its stability around the configuration workspace. Nevertheless, the case of this thesis is the opposite as the one presented by Birglen as the object is known and its position is chosen but, the geometry of the finger is the focus of the study.

The tool developed is a *grasp-state volume*, an atlas of the workspace mixed with the considered criteria, that is capable of showing up to five dimensions: three geometric parameters, stability (defined by Birglen's *Force positiveness* of the contacts), and an extra criterion. The arrangements decided for this tool are: given a *base* distance and a static friction coefficient μ_s, the three axis of the volume belong to $l_{21}(\%), \varphi_{22}$ and r_l. Over this volume, the useful zone is determined by the stability of the finger in statics through the use of the *force positiveness* criterion (see *Fig. 3.4*). Is in the remaining region that the finger properties can be analyzed as a fifth dimension. As there are many volumes' figures commented hereafter, they have been placed in the *Appendix A.1*.

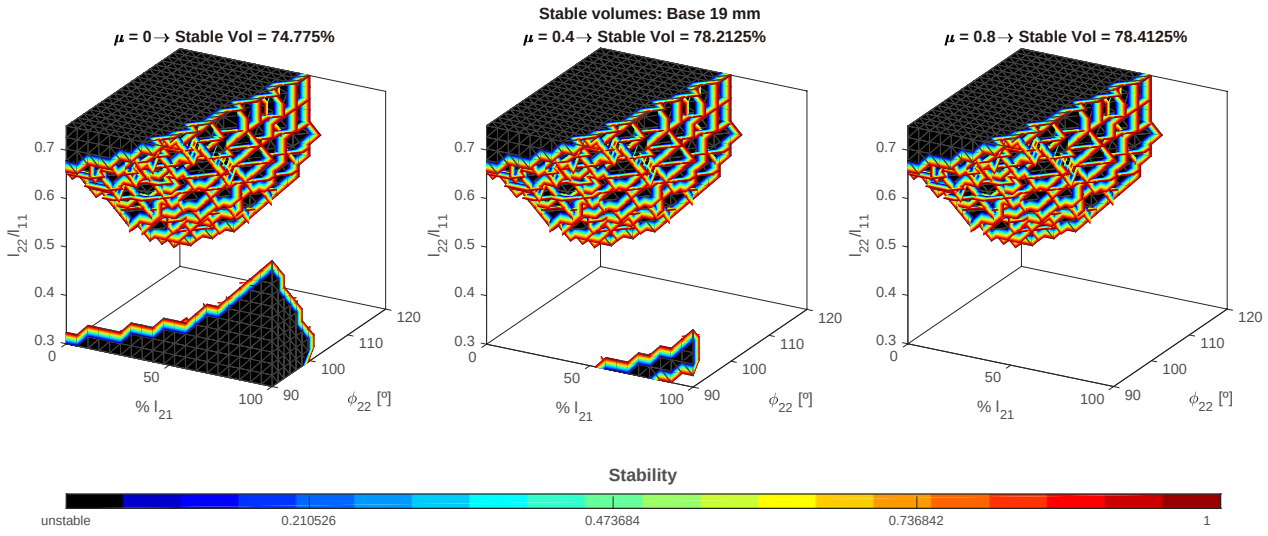

Figure 3.4: Volumes for *base* = 19 mm and three friction conditions. The black volume is the unstable (by *force positiveness*) region and the empty one the useful workspace.

3.4.1 Stability by *force positiveness*

In order to compare the influence of the *base* and μ_s, the following table (see *Table 3.3*) presents the useful workspace volume over the whole studied volume from computing the *force positiveness* criterion using the static equilibrium model presented in *Section 2.1.4*. As can be seen

Base	$\mu_s = 0$	$\mu_s = 0.4$	$\mu_s = 0.8$
12 mm	93.66%	93.91%	93.91%
15.5 mm	89.29%	92.11%	92.11%
19 mm	74.7%	78.21%	78.41%
22.5 mm	26.05%	26.64%	26.64%
Intersection	23.26%	26.44%	26.64%

Table 3.3: Volume stability percentage in function of the *base* and μ_s.

in *Table 3.3*, the parameter that influences the most the useful volume is the *base* parameter. As it grows bigger, the volume that is stable shrinks up to a 70%. However, the reduction is exponential in relation to the *base*, which means that, if possible, the working range of the finger in relation with the *base* should be kept far from the higher limits. A result that is also interesting is the *intersection*, which is computing how much useful volume is common to al *base* dimensions. It is in the analysis of the latter that the contribution of μ_s can be slightly appreciated, as the introduction of friction contributes to the increase of the stable volume. Nevertheless, it can be observed that, apparently, the value of the friction coefficient does not have a notorious influence. Lastly, analyzing the distribution of the useful volumes (see *Appendix A.1*), for any *base*, it can be seen that the combination of $\downarrow l_{21}, \uparrow \varphi_{22}$ and $\uparrow r_l$ leads to instability.

3.4.2 Palm Force Positiveness

In order to compare the influence of the *base* and μ_s, the following table (see *Table 3.4*) adds the analysis of the palm force positiveness, to the useful workspace volume previously presented. This criterion analyzes the resultant force from all the contacts between the phalanges and the object in the palm normal direction (as the component parallel to the palm is neutralized by the symmetry of the design) as:

$$\begin{aligned} PFP = {} & F_{N22}(\sin(q_{21} + q_{22} + \varphi_{22} - \pi/2) + \mu \sin(q_{21} + q_{22} + \varphi_{22}) \\ & -F_{N21}(\cos(q_{21} - \pi/2) + \mu \sin q_{21}) \end{aligned} \tag{3.2}$$

The expected result is to obtain a negative reaction, which means that the palm is applying a unidirectional contact force, *i.e.*, it is not pulling the object (as it cannot). As can be seen in *Table 3.4*, the parameter that influences the most the useful volume is μ_s. When it is null, the *base* lower values are highly affected. The reason of this lies in the fact that lower *base* dimensions decrease the collision angle of l_{21}, leading to smaller collision angle of l_{22}. In such configuration, the first phalanx vertical component is much bigger than the tip phalanx one. Moreover, in the larger values of *base*, the effect is just the opposite, allowing the tip phalanx to push towards the palm. As can be observed, the introduction of friction rises the useful volume of the lower *base* values (as the bigger ones are not affected) as well as the PFP results.

	$\mu_s = 0$			$\mu_s = 0.4$			$\mu_s = 0.8$		
Base	Stb.Ref.	%Vol.	Max. [N]	Stb.Ref.	%Vol.	Max. [N]	Stb.Ref.	%Vol.	Max. [N]
12 mm	93.66%	0.3%	2.47	93.91%	1.3%	5.47	93.91%	68.21%	24.58
15.5 mm	89.29%	9.54%	2.05	92.11%	81.46%	10.92	92.11%	92.11%	28.21
19 mm	74.7%	21.3%	2.24	78.21%	78.21%	10.5	78.41%	78.41%	21.37
22.5 mm	26.05%	26.05%	2.11	26.64%	26.64%	8.94	26.64%	26.64%	16.45
Base Intersection	23.26%	0%	-	26.44%	0%	-	26.64%	26.24%	-

Table 3.4: Useful volume percentage analyzing the PFP over the stable workspace in function of the *base* and μ_s. *Stb.Ref.* are the Stability Reference results from *Table 3.3*.

Finally, analyzing the distribution of the useful volumes (see *Appendix A.1*), for any *base* can be seen that the combination of $\uparrow l_{21}, \uparrow \varphi_{22}$ and $\downarrow r_l$ leads to the higher PFP values if there is no friction. When friction is introduced, the maximums moves to the $\uparrow r_l$ region.

3.4.3 Form-Closure

In order to compare the influence of the *base*, the following table (see *Table 3.5*) adds the analysis of the form-closure, to the useful workspace volume previously presented. Recall: this criterion analyzes the capability of the gripper to constrain the grasped object without using friction, which means that this criterion is independent of friction. To respect the form-closure, the gripper must at least respect the inequality presented in (1.19). Note that in the current case, the gripper is composed of a pair of two-phalanxed linkage-driven finger with non-backdrivable actuators; in addition, the cylinder dimension space is considered as two, because no rotation of it will appear. Finally,

$$n_c + n_u \geq n_h + d + 1$$
$$4 + 1 + 2 \geq 4 + 2 + 1$$
$$7 \geq 7$$

where, recall that, n_c is the number of contacts (phalanges and palm), n_u is the number of non-backdrivable mechanisms, n_h is the dimension of the hand configuration space and d is the dimension of the object's configuration space. Nevertheless, this is a necessary but not sufficient condition, as can be seen in the results table *Table 3.5*. As can be seen in it, the form-closure criterion is quite restrictive over all the workspace as in the best of the cases, the useful volume decreases from 90% until 23%. Moreover, from the results it can be seen that the best values of *base* to work on, are not placed in the extremes as the previous results showed. Fortunately, the performance of the finger in the middle range *base* dimensions is competent with the best values proposed in the previous paragraphs. Finally, analyzing the distribution of the useful volumes (see *Appendix A.1*), notice that it is interesting the fact that even though the form-closure criterion is purely geometric, there is not any apparent correlation between

Base	**Stability Ref.**	**%Volume**
12 mm	93.66%	9.98%
15.5 mm	89.29%	22.68%
19 mm	74.7%	2.61%
22.5 mm	26.05%	0%
Intersection	23.26%	0%

Table 3.5: Useful volume percentage analyzing the Form-Closure over the stable workspace in function of the *base* and μ_s.

the different *base* values, while a small relation can be guessed between the increment of φ_{22} and the existence on form-closure.

Chapter 4

Results

In the following chapter, first, different finger designs are analyzed and, then, the method used to select the final design is presented along with the results and the final design that has been used to create the prototype of the gripper. In the previous chapter, the *graps-state volumes* (section 3.4) have been introduced and through their analysis, the existence of solutions has been proofed. However, given the fact that any new analyzed geometry needs to be simulated over a range of time in order to compute the dynamic stability, the design optimization has been performed over the discretization of a bounded design space.

4.1 Criteria

Some of the criteria used to analyze the validity of the geometric models have been presented when the *graps-state volumes* have been developed. These criteria belong the static analysis checking and are:

- Force Positiveness
- Palm Force Positiveness
- Form-Closure

Nevertheless, the current static criteria do not contribute with any information of the dynamic performance. For this reason, dynamic criteria have been set.

4.1.1 Dynamic criteria

In order to determine if the performance of the design is good enough, two parameters are checked. In order to obtain these parameters, the full model must be simulated (developed in next *section 4.2*) because it is not possible to determine the dynamic evolution of the finger from the geometric analysis, yet.

4.1.1.1 Time to stability

The first dynamic parameter is the *time to stability* (*tts*), *i.e.*, the time that the finger requires to reach a static configuration. Note that this criteria is highly related to the *force positiveness* one, as in order to know if the finger has reached a static configuration:

- The finger dynamic configuration must be equal to the geometrical final configuration $q_{f,ij}$ computed, thus: $q_{ij} = q_{f,ij} \pm \epsilon$, where ϵ is a threshold to take into account the penetration depth δ_n of the phalanges into the object.
- Must respect the *force positiveness* criterion:
  - The contact forces must be positive.
  - The contact forces of the dynamic model at the *tts* must match those computed through the static model (*force positiveness*).

To respect the requirements, the *tts* should be smaller than 10 ms. However, to expand the solutions scope, the criteria has been set to 15 ms.

4.1.1.2 Rebound

The second dynamic parameter is the *rebound*, expressed as the percentage of time that the finger needs to reach the *tts* from the instant in which it reaches the geometrical final configuration $q_{f,ij}$ for the first time, *i.e.*, as there may be rebound, the first time that the finger is inside the thresholds defined in the paragraph above, does not necessarily imply that the finger is in equilibrium already:

$$rebound(\%) = 100 \left| \frac{\text{mean}(\boldsymbol{t}(q_{f,ij} : end))}{\text{mean}(\boldsymbol{t}(stable : end))} - 1 \right| \tag{4.1}$$

where, $\boldsymbol{t}(q_{f,ij} : end)$ is the time vector between reaching the geometric stability and the end of the simulation, and $\boldsymbol{t}(stable : end)$ is the time vector between reaching stability and the end of the simulation. Note that the parameter depends on the simulation length and the time to stability, hence, the thresholds can change depending on it. This expression of the rebound has been chosen to take into account that designs need a shorter time to stabilize, can have bigger rebound values. This criterion can divide the dynamic behavior into three classes:

- Stable: $rebound = 0\%$. The finger does not rebound on the contact.
- Semi-stable: $rebound \leq 5\%$. The finger does rebound but for a short-period.
- Unstable: $rebound > 5\%$. The finger rebound could cause instability due to the contact forces and the time passed without contact.

4.1.2 Weighted criterion

Hereafter, in the design selection phase (see *section 4.3*), will be seen that some results accomplish the requirements, so in order to characterize the design with the best performance a weighted criterion is proposed, grouping the main characteristics that are desired from the gripper:

- The highest *Palm Force Positiveness* (PFP).
- The shortest *time to stability* (tts).
- The best composed normal contact forces to achieve PFP with less friction:
  - Small F_{N21}.
  - High F_{N22}.

After converting the previous values, of the selectable finger designs, to a ratio in the range [0-1], the weighted criterion is defined as the mean of the four performances. All the ratios have been considered of the same importance, thus all of them are weighted equally, however, this can change if in further analyses it considered that any of them is more critical than the rest. For the current hypothesis:

$$r_{WC} = \text{mean}(r(PFP),\ (1 - r(tts)),\ r(F_{N21}),\ (1 - r(F_{N22}))) \tag{4.2}$$

4.2 Simulation

As introduced in the above paragraphs, one of the most efficient ways to optimize the design is to discretize a bounded design space and analyze its results. This process can be iterated around the solution of the previous iteration, however, the method have not been iterated in the present thesis. The design space where the finger has been searched is:

- $base$ = [12, 15.5, 19, 22.5] mm
- $l_{21} = l_{21,min} + [0, 1/4, 1/2, 3/4](l_{21,max} - l_{21,min})$, where $l_{21,min}$ and $l_{21,max}$ are determined in function of *base* (see *Appendix B.2.2* for the complete functions)
- φ_{22} = [90, 100, 110, 120]°
- $r_l = l_{22}/l_{11}$ = [1/3, 1/2, 2/3]
- μ_s = [0, 0.8]

Given the design space, composed of 192 different designs in two different friction conditions, they have been simulated over a time of 20 ms. Note that the simulation is two times the length required in order to be able to check that the model is stable for a longer time and that no delayed effects from the collision are taking place.

4.2.1 Simulation Results

A short analysis of the experimentation results is presented having decided the design space and acquired the simulation data. In *Appendix A.2* can be found all the results figures that are not in the current chapter due to the large quantity of them. *Fig. 4.1* shows a summary of the geometrical combinations of the 192 experiments along with the repercussion they have in the computation of the model parameters and the dynamic performance. Note that all the results are expressed in function of the experiment index, thus *Fig. 4.1* is the base of the results analysis.

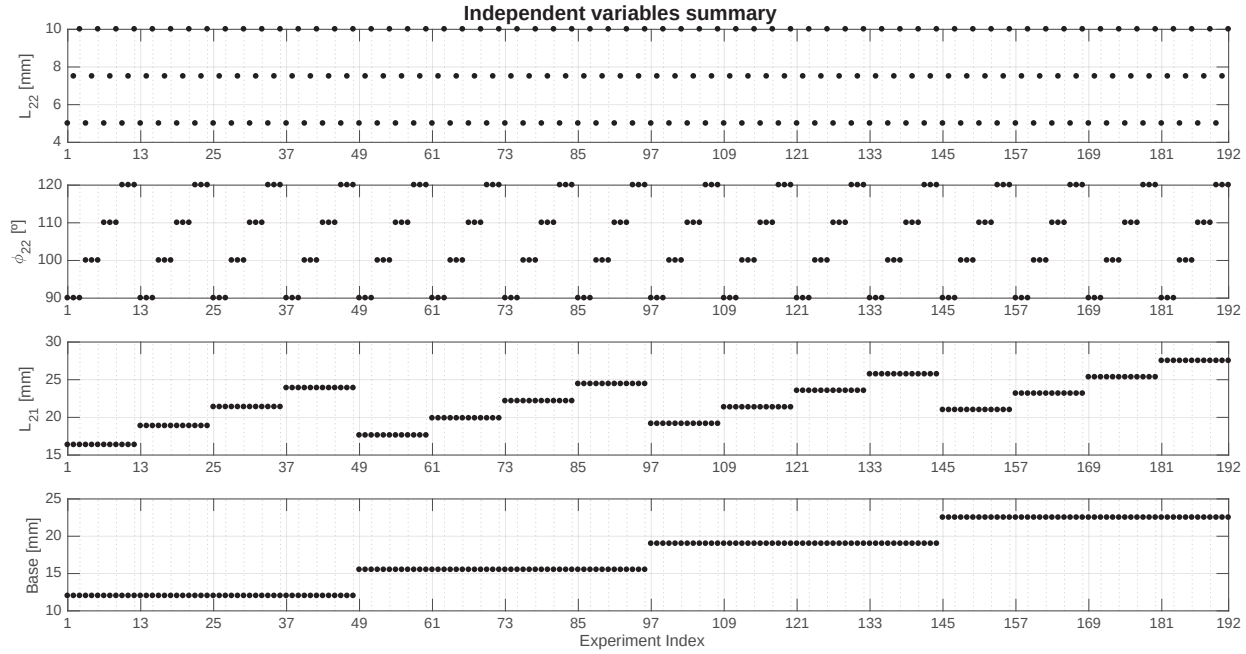

Figure 4.1: Summary of the geometric combinations of the 192 experiments simulated.

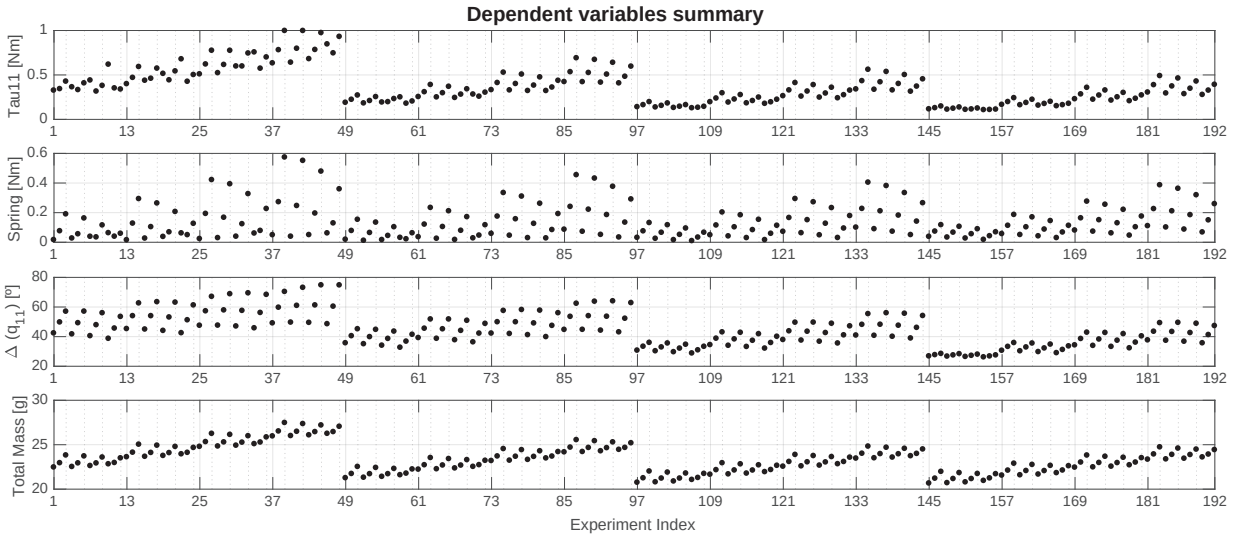

Figure 4.2: Summary of the dependent variables along the experiments in relation to the independent ones.

4.2.1.1 Parameters variation

In the case of the current thesis, can be observed that the total mass (without springs and axes) of a single finger (see *Fig. 4.2*) is in between 20.6 g and 27.5 g, a difference that can be considered insignificant, thus, not necessary to take into account in the decision variables. However, is important to remark the strong correlation that exists between the design variables and the total mass, as the tip phalanx is responsible for almost the 50% of the weight. Note that it is also the most remote part, meaning that, the inertia it introduces to the system must be taken into account for bigger designs.

Regarding the total test trajectory each experiment has to perform, can be observed in *Fig. 4.2*, that it oscillates between 26° and 75°. The r_l ratio has a big influence as it is directly influencing the transmission ratio between links l_{11} and l_{22} but, the bigger variation is introduced by the *base* value as de proximity between the two collision points decreases when *base* increases.

As all the model is geometrically related, is not coincidence that there is a relation between τ_{11} and, the total length of the test trajectory and the total mass of the finger (see *Fig. 4.2*). For k_s also a correlation can be guessed, however, it is lighter because k_s depends only on the maximum point and not the whole evolution of the system.

4.2.1.2 Dynamic performance

The main analyzed characteristic in the dynamic performance is the consideration of friction forces into the model. In order to analyze the effects they produce, several comparisons have been carried out. In *Fig. 4.3*, the Birglen stability with and without friction is contrasted, obtaining an increase of 5% more of stable results if friction is considered, outcome that concurs with the ones obtained analyzing the *grasp-state volumes* in *Table 3.3*.

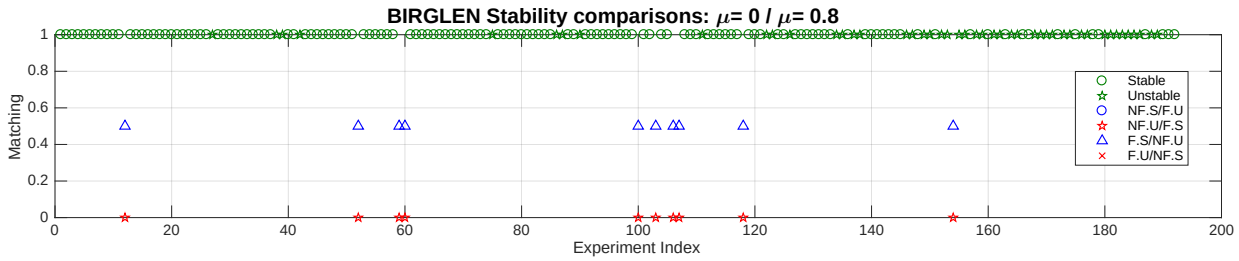

Figure 4.3: Birglen stability checking with and without stability. (F: friction, NF: no friction, S: stable, U: unstable).

Going further into the analysis of the stability, in *Fig. A.15*, the simulation results are compared to Birglen obtaining the summarized *Table 4.1*. In it can be appreciated that, while in the static analysis the contribution of friction is minor, the friction in the dynamic analysis

has a strong influence. This can be explained by the concept of friction, which by definition opposes to the movement and produces non-conservative work, *i.e.*, dissipates the finger energy faster. The extra energy dissipation during the collision produces smaller penetrations δ_n, thus, smaller collision forces that lead to less rebound and more stability.

	$\mu_s = 0$		$\mu_s = 0.8$		Comparison	
Class	Static (%)	Dynamic (%)	Static (%)	Dynamic (%)	ΔStatic (%)	ΔDynamic (%)
Stable	70.3%	28.1%	75.5%	50%	↑5.2%	↑21.9%
Unstable	29.7%	71.9%	24.5%	50%	↓5.2%	↓21.9%

Table 4.1: Stable designs over the discretized design space in statics and, in dynamics, with and without friction.

In *Fig. 4.4* and *Fig. A.19*, the design variables are presented sorted by its individual iteration order without and with friction respectively, allowing to analyze each design variable effects over the system when changed and class them in four groups:

- stable: no rebound and stable in less than 15 ms.
- semi-stable: small rebound but stable in less than 15 ms.
- semi-unstable: large rebound but stable in less than 20 ms.
- unstable: negative contact forces (Birglen) or stable in more than 20 ms.

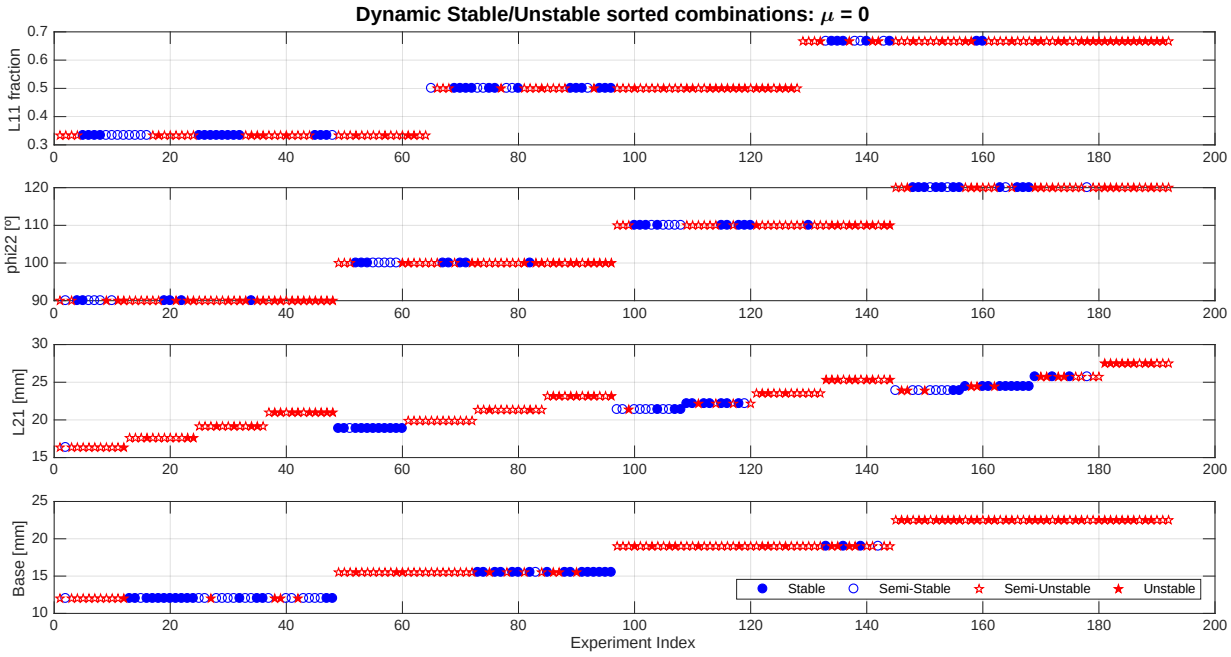

Figure 4.4: Dynamic stability analysis without friction in function of each one of the design variables.

The interest of the latter graphics lie in the fact that they allow to identify correlations between dynamic stability and the geometry of the design. Namely, in the case of the finger, can be guessed that some combinations of *base* and l_{21} lead to semi-unstable results, *i.e.*, large rebounds. No further analysis have been done in these outcomes as they fall out of this thesis scope, however, can be an interesting topic to study if any relation exist between the rebound and the system configuration.

Regarding the Form-Closure criterion, can be observed in *Fig. A.24* that it is rather restrictive, as from the 192 experiments (as friction does not have any effect on it) only twenty-two respect it. Thus, the design solution is highly bounded due to it. However, with this criterion one can ensure that the object is going to be blocked by the geometry without relying on the existing friction.

Finally, in *Fig. 4.5*, can be observed the *palm force positiveness* of each experiment with and without friction. As has been checked during the analysis of the *grasp-state volumes* (see *Table 3.4*), in theory exists a design solution that will respect the specified criteria without friction, nevertheless, the useful volumes are a quarter of the design space at its best and none of the discretized designs respect the *PFP* with null friction.

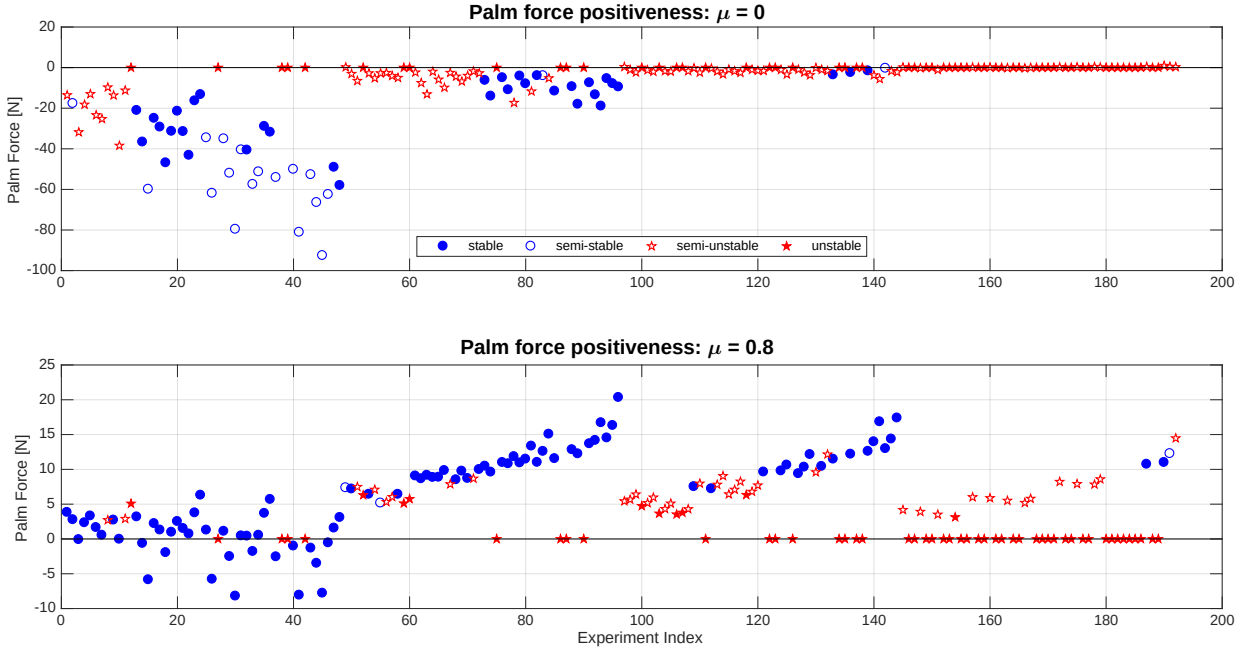

Figure 4.5: Palm force positiveness with and without friction.

4.2.1.3 Extension of the results

Through minor adaptations, the obtained results can deal with the elimination of one of the base hypotheses: the assumption of null positioning error. The main change into the study is that two complementary fingers must be studied simultaneously, hence, the design variables

must be adjusted to respect the finger condition symmetry with the use of the two extremes of the *base* parameter, in order to ensure the design robustness in front of such parameter values.

In the first place, the determination of the palm width is necessary in order to match the complementary pair of fingers that must be studied. In the current case and, under the assumption that the model could be used in the IRSBot-2, a $\pm 2^\circ$ oscillation of the moving platform along a 10 cm distance from it until the gripper palm are considered. Then, the possible positioning error of the center of the palm is bounded to ± 3.5 mm, leading to at least a $palm \geq 2base_{min} + 2 \cdot 3.5 \text{ mm} = 31 \text{ mm}$. Finally, with some security coefficient, an acceptable palm width could be 34 mm.

Once the palm width is decided, the experimentation can be repeated setting the right (^{r}) and left (^{l}) fingers parameters to:

- Initial position as $q_{i,11}^{r,l} = \min(q_{i,11}^r, q_{i,11}^l)$.
- Torque and spring as $\tau_{11}^{r,l} = \max(\tau_{11}^r, \tau_{11}^l)$ and $k_s^{r,l} = \max(k_s^r, k_s^l)$

In the analysis of the *grasp-state volumes* (see *Tables 3.3, 3.4* and *3.5*), *intersection* parameters are presented. Those parameters can be used in the current hypothesis in order to check if a solution exists where the design is robust in front of the *base*. Static stability can be achieved without friction, *PFP* requires high friction in order to present robustness in front the *base* dimensions and, unfortunately, there is no volume intersection for the *Form-Closure*. However, note that, in the case of symmetric base (null positioning error), *Form-Closure* is most likely to be given.

In summary, a design robust to the positioning error cannot be ensured to exist due to the fact that the *Form-Closure* criterion is considered necessary for the specific case of high-speed closing and moving. Nevertheless, further investigation on the evolution of the contact could be made in order to analyze if a *non-form-closed* configuration could lead to *form-closed* configurations due to the non-compensated horizontal forces of the grasp actuating as an automatic control of the system.

4.3 Design selection

Finally, the design is computed from the experimentation performed in the previous section through the use of the criteria presented at the beginning of the chapter. A summary graphic can be observed in *Fig. 4.6*. From the 384 design options, only eighteen remained after the requirements checking. Note that all the results are in the domain of friction existence, this is mainly because of the *palm force positiveness* checking, as (unfortunately) the discretization is not inside of the useful workspace of the *grasp-state volumes* without friction.

Following the weighted criterion, the best performance is given by the experiment 95 with a $r_{WC} = 0.67$, with:

- $PFP = 16.3$ N
- $tts = 7$ ms
- $F_{N21} = 23.6$ N
- $F_{N22} = 8.3$ N

and the design variables:

- $base = 15.5$ mm
- $w = 2.5$ mm
- $l_{11} = 15$ mm
- $l_{21} = 24.4$ mm
- $l_{12} = 22.4$ mm
- $l_{22} = 7.5$ mm
- $t_{22} = 12.6$ mm
- $\varphi_{22} = 120°$
- $\tau_{11} = 480$ N·mm
- $k_s = 132.6$ N·mm

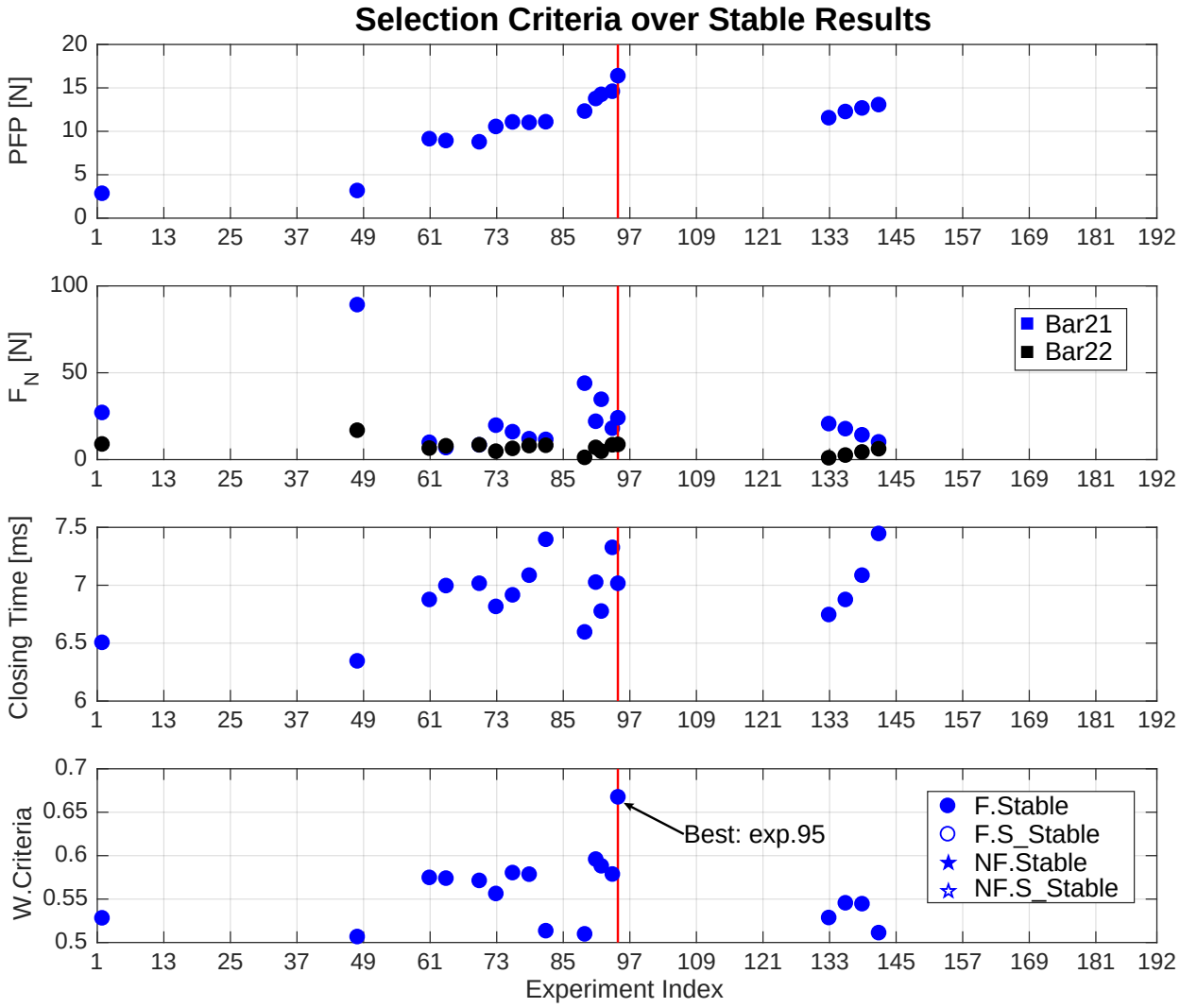

Figure 4.6: Summary of the selection results.

4.4 CAD model

Once the design has been selected, a real design of the finger has been done respecting the given dimensions and adapting the interpenetrations between the links in the joints zone to be able to build a prototype[1]. In order to ensure that the design works properly, it has been simulated in ADAMS MSC to analyze its performance. Although, the mass of the axis and the spring have been neglected, the results are considered satisfactory.

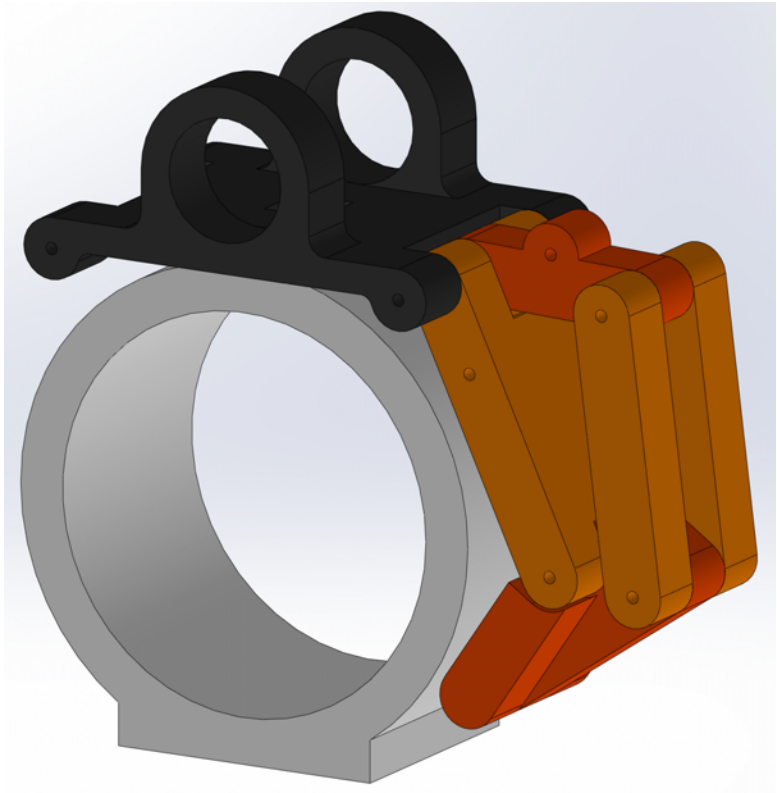

Figure 4.7: CAD model of the finger along with the object and the palm.

An interesting remark, on the obtained results, is the time the finger needed to reach stability (see *Fig. 4.8*), dropping the stabilization time from 7 ms to 4.7 ms. This behavior can be explained by the mass difference (see *Table 4.2*) between the extruded planar links used to compute the simulations and the final design of the parts, while the applied torque and the spring have not been changed. This result show the fact that the torque can be reduced in order to attain the 10 ms milestone, which will improve the general result of the design by reducing the collision efforts and the grasping forces applied onto the target object.

Regarding the transmission mechanism between the fingers, although it falls out of the studied scope of the current research work, a proposition is made only for the sake of building a complete prototype. In order to reduce to the maximum the number of actuators, the robot arm will provide the closing torque to the gripper, actuating it when contacting the object (on the case of

[1]The prototype is a 2:1 scale of the design meant to show the kinematics of the system and not to perform tests. Its drawings can be found in *Appendix C*

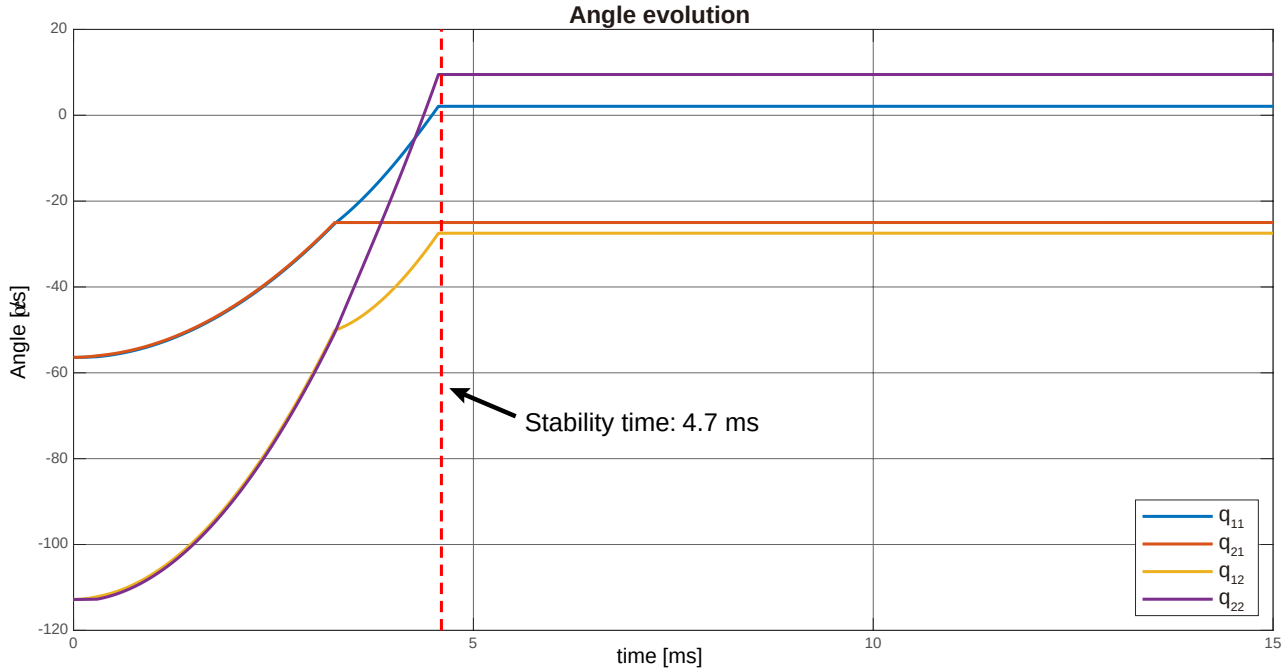

Figure 4.8: Angles evolution of the closing cycle for the real model.

Links	**Simulated design [g]**	**Final design [g]**	**Variation (%)**
l_{11}	4.28	2.18	49.07%
l_{21}	6.29	4.73	24.80%
l_{12}	5.86	2.78	52.56%
l_{22}	8.21	4.63	43.61%
Total	24.64	14.24%	42.21%

Table 4.2: Difference between the finger's mass used in the simulated model and the final design.

the current prototype will be the hand). With this configuration, a blocking (non-backdrivable) mechanism is needed. Any actuator could provide this blockage, nonetheless, it should be able to block the mechanism with a variable actuating distance, as a proposition, an electromagnet would do the job.

To transmit the torque from the robot arm to both fingers (see *Fig. 4.9*), a planar seesaw (a differential mechanism) has been implemented in order to divide the force isotropically while adapting to the contact conditions of the system. This system consists of a obtuse triangle where the larger angle is placed in a translational joint, and the extremes transmit the force forward.

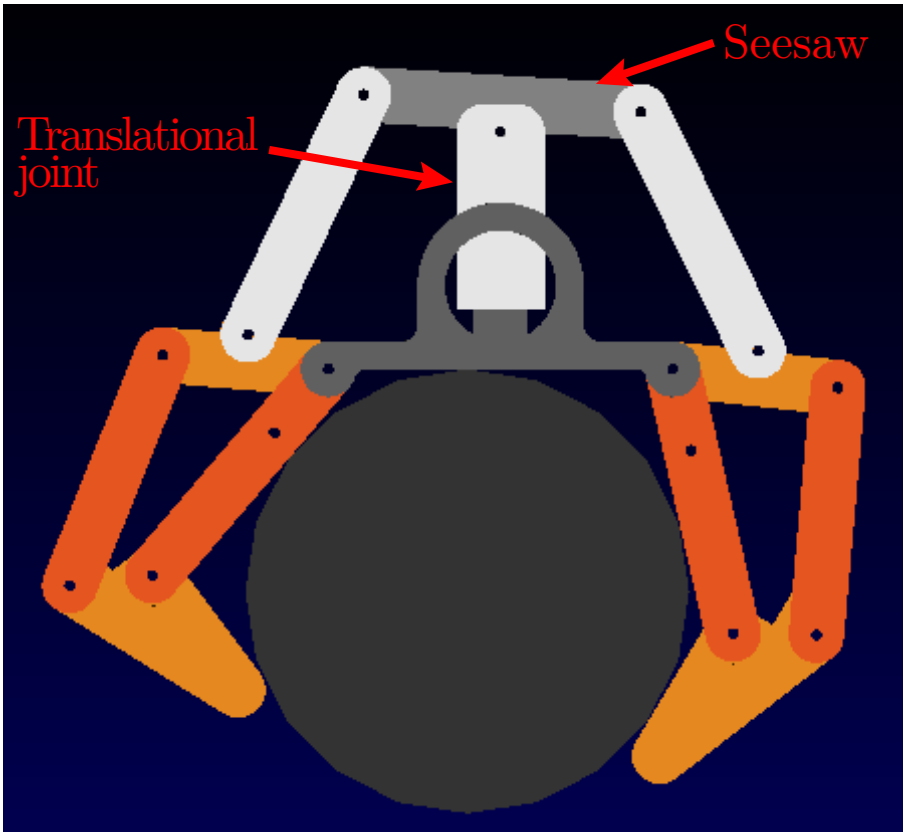

Figure 4.9: Two-finger gripper adapting to a non-symmetric contact condition through the seesaw mechanism.

Conclusion

Conclusions

This research work has provided a first design of an underactuated gripper that is capable of performing a stable closing cycle in less than 10 ms. The results of this thesis are not only relevant because the main objective has been accomplished but, because through the development of this research, an important gap in the literature of underactuated hands has started to be studied: the use of a dynamic model for analyzing the complete grasping cycle (from the approaching phase until reaching stability), and how the interactions between the gripper and the object affects the stability. Moreover, it also proofs that the underactuated grippers can offer an interesting performance and be competitive in the industry. However, cannot be forgotten that the adequate design has to be found in order to reach a stable grasp.

After the contextualization of this thesis and a brief problem statement, in the contributions is presented an abbreviated survey of the current methodologies to design underactuated fingers. In it, a main idea is highlighted: the current State of the Art of underactuated fingers hardly considers non-static design problems, probably due to the lack of applications until now.

The first chapter of this thesis introduces the general concepts related to underactuated hands and outlines their inherent characteristic of adapting to unknown objects, provided by a suitable geometric design and without the need of a dedicated control. As the behavior of the underactuated mechanism is unknown a priory, the design must rely on criteria. Hence, two of the main static stability criteria are defined as they are imperative constraints and the main guidelines in the design development. The importance of considering static design criteria, in a dynamic environment, is due to the fact that, if the gripper is not stable in statics, neither will by in dynamics. The presented static criteria are the *force positiveness* and the *form-closure*.

The modeling chapter is where most of this research work has been done, divided into two sections, provides the models to study the complete dynamic closing cycle. In the first part of the chapter, the geometric, kinematics and dynamic models are developed. In the latter model,

the condition of underactuation is applied on the model through the elimination of one actuator, and the addition of a spring to partially exert some control on the system while providing it with a return-back mechanism. It is, also, on the dynamic model where the external wrenches of the contact forces are applied. The second section of this chapter develops the models developed to obtain the dimension of the contact forces. These models are based on the simulations with ADAMS software, as a manner to obtain a direct comparison between the models and the recognized simulator software. The theory behind the models, the Hertz contact theory and the Coulomb's friction theory, is recalled before introducing them. The latter models are handful, as they allow the introduction of rebound into the system. However, obtain the correct constants values for the contacts is still an open problem.

Following, the recalling of the basic steps of design theory introduce the third chapter. Following these steps, the complete list of the gripper requirements, along with the desired behavior, is presented. The main requirements are the closing cycle time inferior to 10 ms and the robustness in front of vibrations (as, for now, the positioning error falls out of the scope). After performing some analyses over the proposed models, the number of variables is highly reduced (from sixty to eight), and the torque and the spring are defined. Finally, a new tool is presented to analyze the effects of the variables on the stability and other the criteria: the *grasp-state volumes*. This tool allows identifying if a proposed design is at least stable in statics, along with other possible criteria, for the required task.

Finally, in the last chapter, the dynamic criteria to determine the validity of a proposed design are presented. Then, the results are analyzed over a set of 192 designs in two different friction conditions. As can be observed in the chapter, friction plays an important role in the defined stability criteria, as it reduces the time needed to reach stability and increases the strength of the grasp. However, the *form-closure* criteria played an important role in the selection process, as it appears to be quite restrictive. At the end, from 384 possible designs, only eighteen respected the proposed criteria. Between these, the dynamic performance has been evaluated, obtaining a design that performs above the requirements with a closing cycle time of 7 ms.

Future work

The focus of this research work has been in the development of a model for an underactuated finger that allows analyzing the complete closing cycle, from the approaching until reaching a stable grasp. However, as the topic is extensive and not deeply studied, many works can follow the one presented.

The main direction of further study is introduced in *section 4.2.1.3*, where an extension of the proposed hypotheses is introduced and slightly analyzed. This thesis simplified the first

studies by assuming that the positioning error is minimal, hence, it has been disregarded. This assumption simplifies the design by considering a single finger in the study, however, if some error is introduced, the design space that respects the generic problem conditions shrinks. Moreover, the torques and initial conditions will be varied and the system evolution not symmetric anymore.

The introduction of the latter hypothesis opens new problems. The first is the non-symmetry of the collisions, for which is considered that would be interesting to study the system if the object is free (as has been already introduced in Saliba [24]). Secondly, as can be observed in *Table 3.5*, the non-symmetry of the grasp does not allow to ensure that any configuration exists by which the grasp is formed-closed, hence, a second non-static study can be performed: evolution of the configuration due to the horizontal components of the contact forces.

Finally, as has been already introduced in the analysis of the simulation results, would be interesting being able to relate in some manner, the design variables *base* and l_{21} with the existence of rebound, as some relation appears to exist (see *Fig. 4.4* and *Fig. A.19*).

In addition to the theoretical part of the design, the actuator and the transmission mechanism need to be design and optimized. As a first guess, the actuator needs to be able to perform the target torque independently of the actuated distance. After some analyses of the system, a blocking mechanism based on an electromagnet is proposed in conjunction with a mechanism tha actuates the gripper by contacting the object.

Bibliography

[1] "MSC SimCompanion - Adams Solver Help (for Adams 2017.2)," 2017. [Online]. Available: https://simcompanion.mscsoftware.com/infocenter/index?page=content{&}id=DOC11448{&}actp=LIST

[2] "MSC SimCompanion - Adams View Help (for Adams 2017.2)," 2017. [Online]. Available: https://simcompanion.mscsoftware.com/infocenter/index?page=content{&}id=DOC11451{&}actp=LIST

[3] A. Bicchi, "On the closure properties of robotic grasping," *The International Journal of Robotics Research*, vol. 14, no. 4, pp. 319–334, 1995.

[4] ——, "Hands for dexterous manipulation and robust grasping: A difficult road toward simplicity," *IEEE Transactions on robotics and automation*, vol. 16, no. 6, pp. 652–662, 2000.

[5] L. Birglen and C. M. Gosselin, "Geometric Design of Three-Phalanx Underactuated Fingers," *Journal of Mechanical Design*, vol. 128, no. 2, p. 356, 2006. [Online]. Available: http://mechanicaldesign.asmedigitalcollection.asme.org/article.aspx?articleid=1448876

[6] L. Birglen and C. Gosselin, "Kinetostatic analysis of underactuated fingers," pp. 211–221, 2004. [Online]. Available: http://ieeexplore.ieee.org/xpls/abs{_}all.jsp?arnumber=1284408http://ieeexplore.ieee.org/document/1284408/

[7] L. Birglen, C. M. Gosselin, and T. Laliberté, "Underactuated robotic hands," 2007.

[8] A. Chatterjee, *Rigid body collisions: some general considerations, new collision laws, and some experimental data*. Cornell University Ithaca, NY, 1997.

[9] M. Claffee and N. R. Corson, "Compliant Underactuated Grasper," 2014. [Online]. Available: http://www.google.ch/patents/US20140132018

[10] M. J. French, J. Gravdahl, and M. French, *Conceptual design for engineers*. Springer, 1985.

[11] J. Giesbers, "Contact mechanics in msc adams," *Faculty of Engineering Technology Applied Mechanics*, p. 20, 2012.

[12] M. Higashimori, M. Kaneko, and M. Ishikawa, "Dynamic preshaping for a robot driven by a single wire," in *2003 IEEE International Conference on Robotics and Automation (Cat. No.03CH37422)*, vol. 1. IEEE, pp. 1115–1120. [Online]. Available: http://ieeexplore.ieee.org/document/1241742/

[13] S. Hirose and Y. Umetani, "The development of soft gripper for the versatile robot hand," *Mechanism and machine theory*, vol. 13, no. 3, pp. 351–359, 1978.

[14] O. Ibrahim and W. Khalil, "Inverse and direct dynamic models of hybrid robots," *Mechanism and machine theory*, vol. 45, no. 4, pp. 627–640, 2010.

[15] K. L. Johnson and K. L. Johnson, *Contact mechanics*. Cambridge university press, 1987.

[16] W. Khalil and E. Dombre, "Modeling, identification and control of robots hermes," *Penton., Paris et Londre*, 2002.

[17] G. A. Kragten and J. L. Herder, "The ability of underactuated hands to grasp and hold objects," *Mechanism and Machine Theory*, vol. 45, no. 3, pp. 408–425, 2009.

[18] S. Krut, "A Force-Isotropic Underactuated Finger," in *Proceedings of the 2005 IEEE International Conference on Robotics and Automation.* IEEE, pp. 2314–2319. [Online]. Available: http://ieeexplore.ieee.org/document/1570458/

[19] S. Krut, V. Bégoc, E. Dombre, and F. Pierrot, "Extension of the form-closure property to underactuated hands," *IEEE Transactions on Robotics*, vol. 26, no. 5, pp. 853–866, oct 2010. [Online]. Available: http://ieeexplore.ieee.org/lpdocs/epic03/wrapper.htm?arnumber=5560878

[20] K. Lakshminarayana, "Mechanics of form closure," *ASME*, no. 78-DET-32,, pp. 2–8, 1978.

[21] B. Massa, S. Roccella, M. Carrozza, and P. Dario, "Design and development of an underactuated prosthetic hand," in *Proceedings 2002 IEEE International Conference on Robotics and Automation (Cat. No.02CH37292)*, vol. 4. IEEE, pp. 3374–3379. [Online]. Available: http://ieeexplore.ieee.org/document/1014232/

[22] B. Mishra, J. T. Schwartz, and M. Sharir, "On the existence and synthesis of multifinger positive grips," *Algorithmica*, vol. 2, no. 1-4, pp. 541–558, 1987.

[23] F. Reuleaux, *Theoretische Kinematik: Grundzüge einer Theorie des Maschinenwesens.* F. Vieweg und Sohn, 1875, vol. 1.

[24] M. Saliba and C. de Silva, "Quasi-dynamic analysis, design optimization, and evaluation of a two-finger underactuated hand," *Mechatronics*, vol. 33, pp. 93–107, 2016.

[25] L. Wu, G. Carbone, and M. Ceccarelli, "Designing an underactuated mechanism for a 1 active DOF finger operation," *Mechanism and Machine Theory*, vol. 44, no. 2, pp. 336–348, 2009.

Appendix A

Figures

A.1 *Grasp-state volumes*

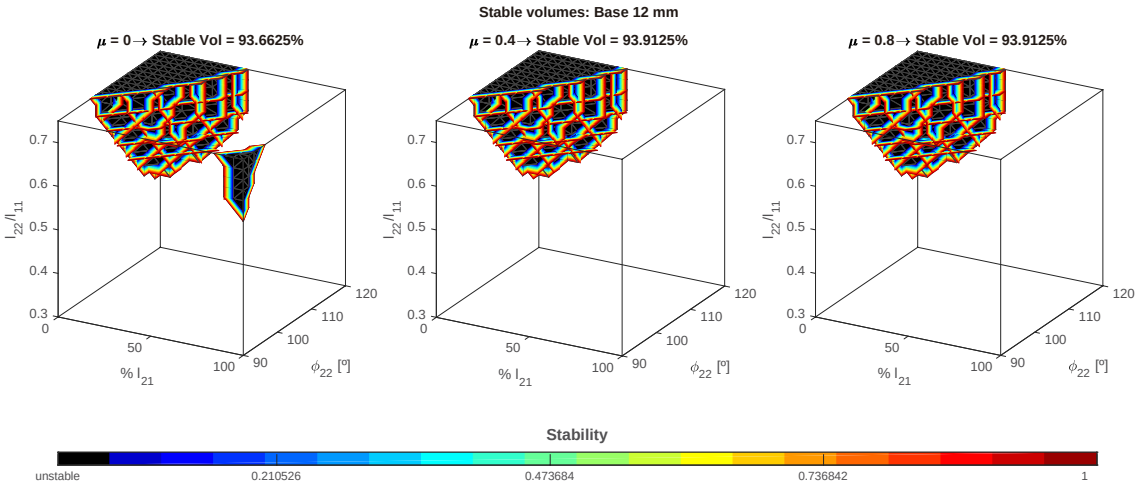

Figure A.1: *Grasp-state volume* analyzing the stability with different friction and *base* = 12 mm.

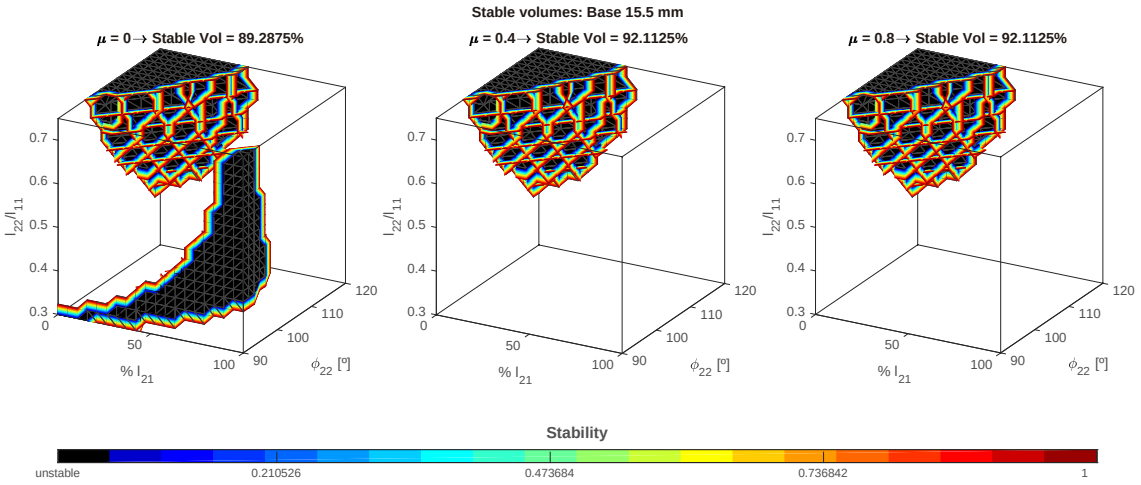

Figure A.2: *Grasp-state volume* analyzing the stability with different friction and *base* = 15.5 mm.

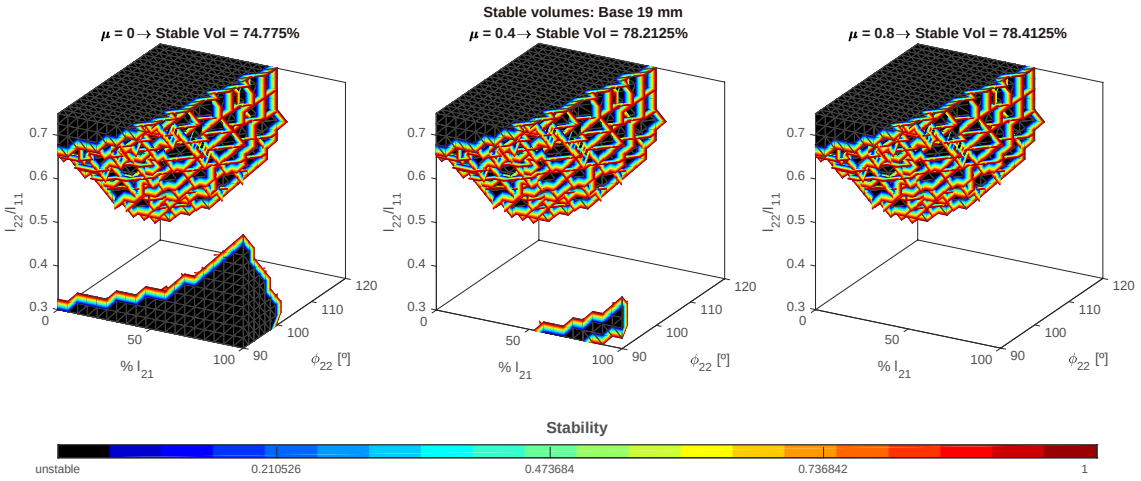

Figure A.3: *Grasp-state volume* analyzing the stability with different friction and *base* = 19 mm.

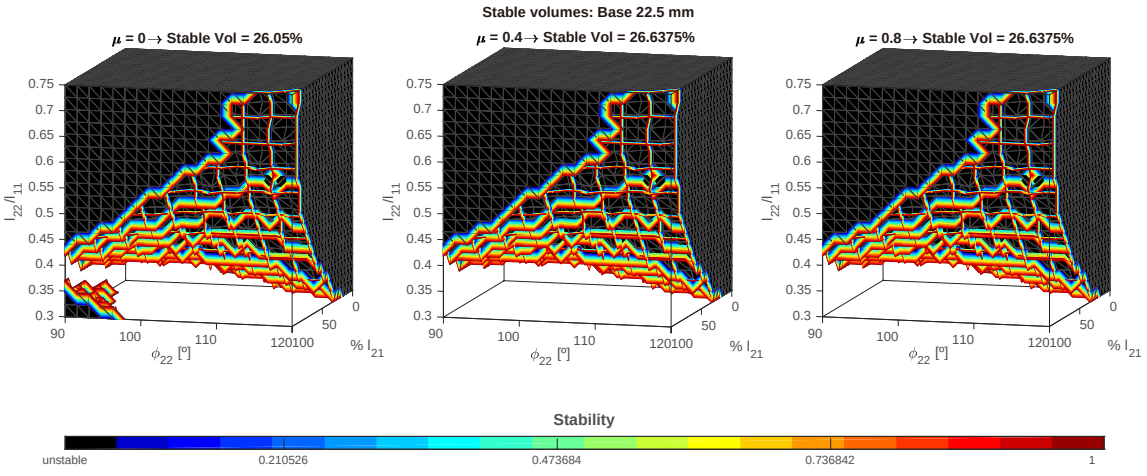

Figure A.4: *Grasp-state volume* analyzing the stability with different friction and *base* = 22.5 mm.

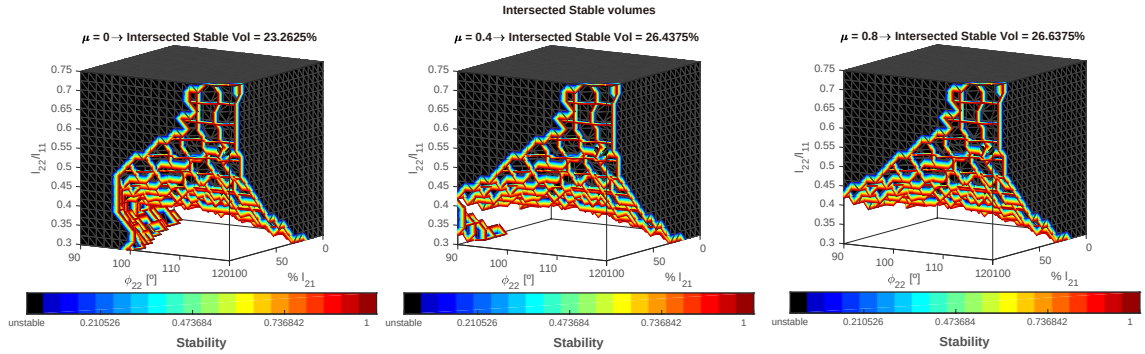

Figure A.5: *Grasp-state volume* analyzing the stability with different friction and the intersection of all *base* dimension.

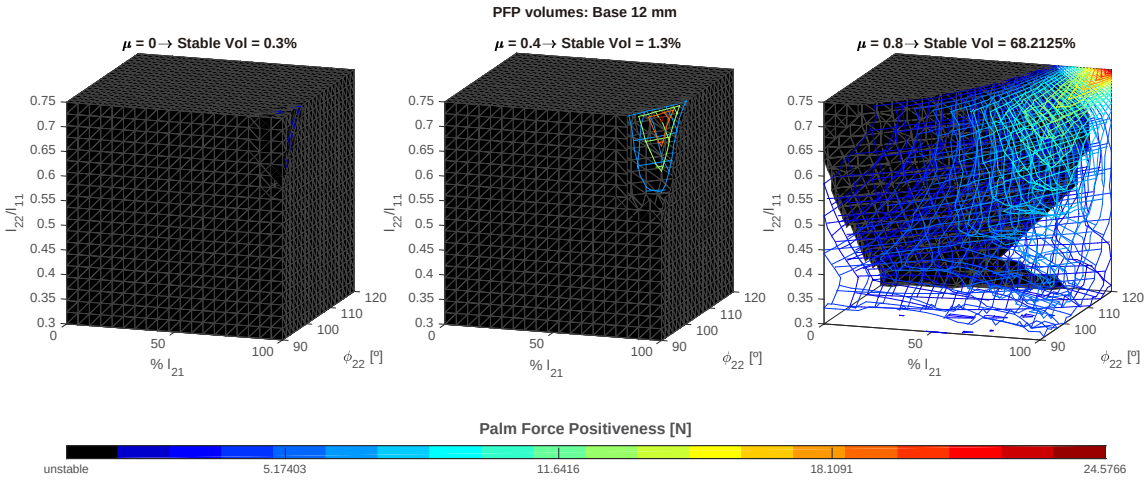

Figure A.6: *Grasp-state volume* analyzing the PFP with different friction and *base* = 12 mm.

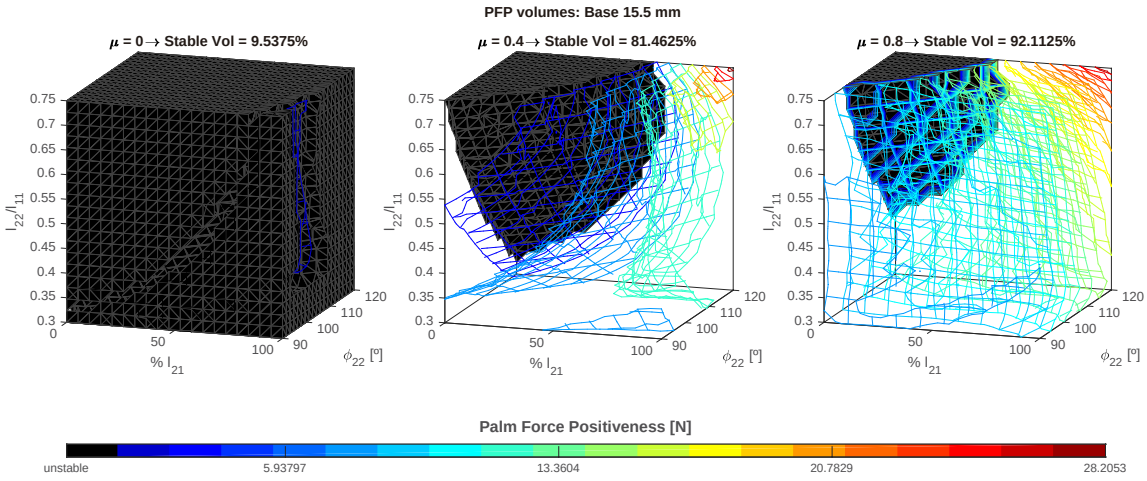

Figure A.7: *Grasp-state volume* analyzing the PFP with different friction and *base* = 15.5 mm.

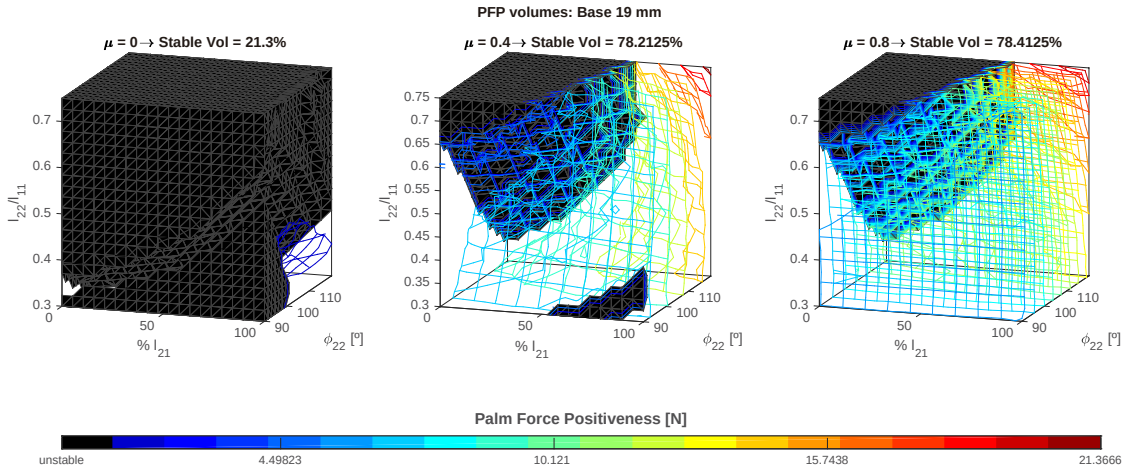

Figure A.8: *Grasp-state volume* analyzing the PFP with different friction and *base* = 19 mm.

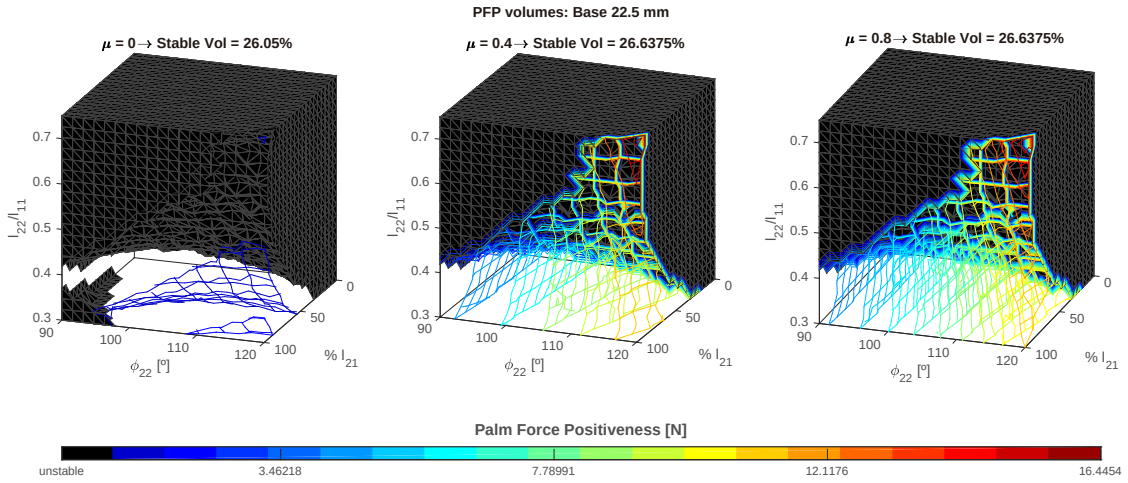

Figure A.9: *Grasp-state volume* analyzing the PFP with different friction and *base* = 22.5 mm.

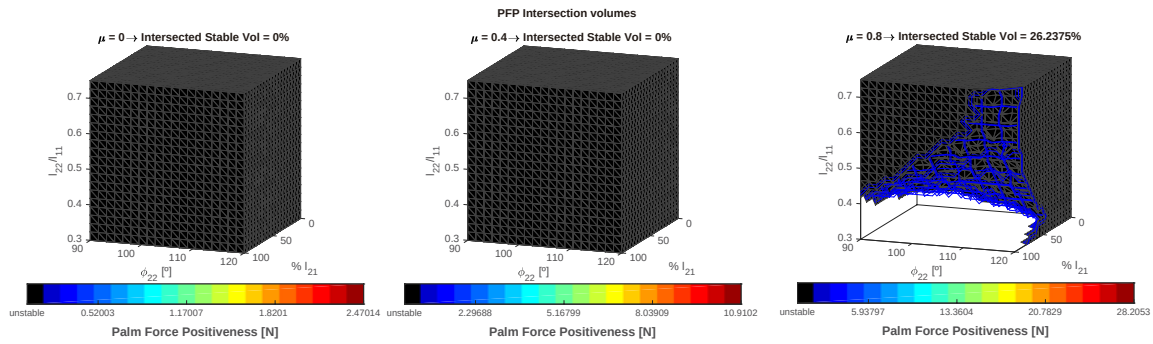

Figure A.10: *Grasp-state volume* analyzing the PFP with different friction and the intersection of all *base* dimension.

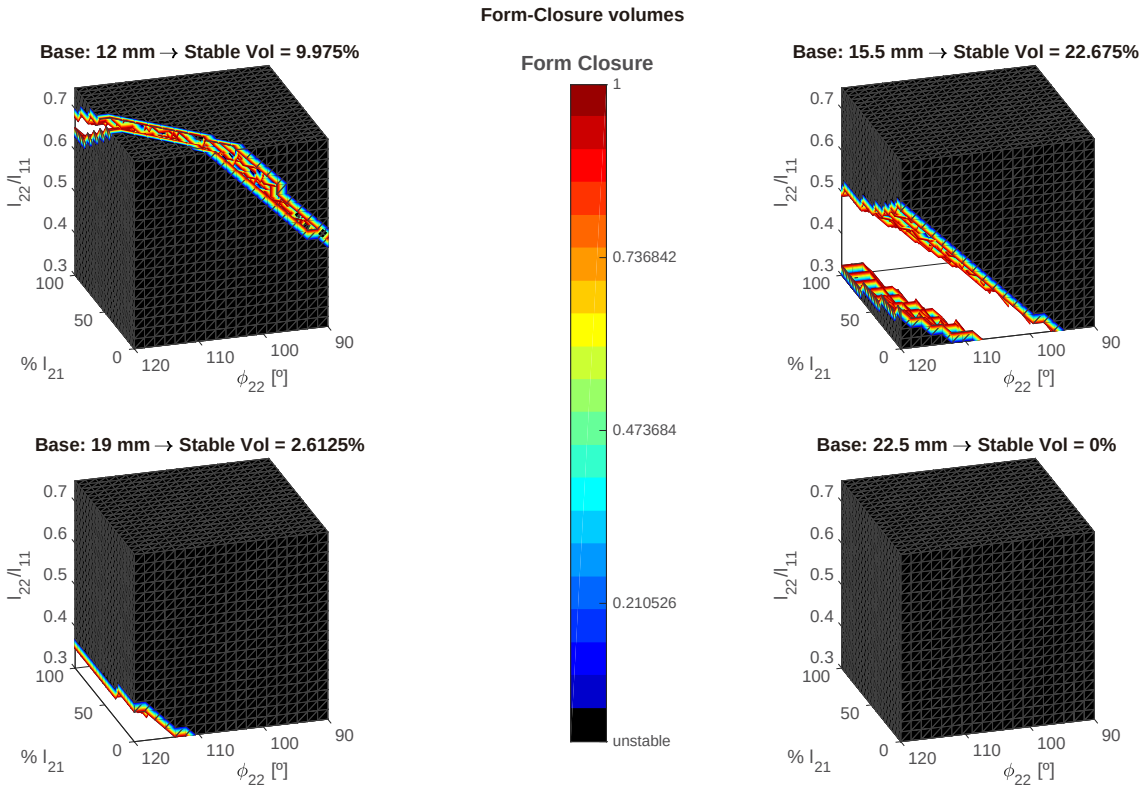

Figure A.11: *Grasp-state volume* analyzing the Form-Closure with different *base* dimension.

A.2 Simulation Results

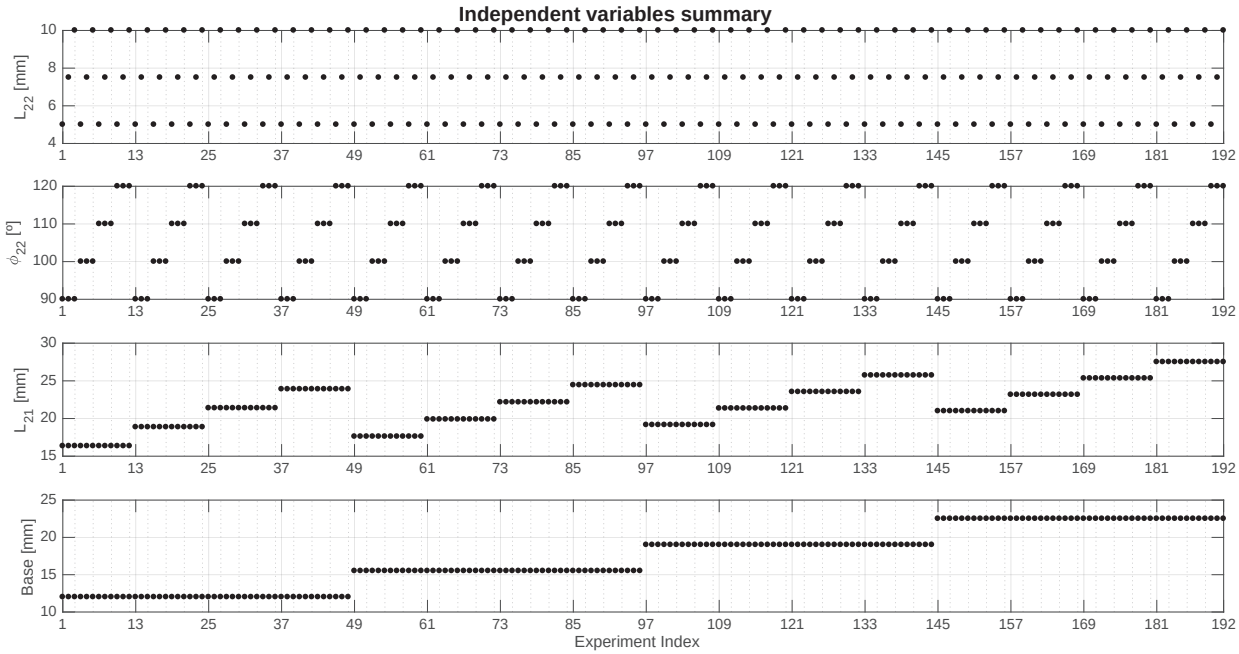

Figure A.12: Summary of the geometric combinations of the 192 experiments simulated.

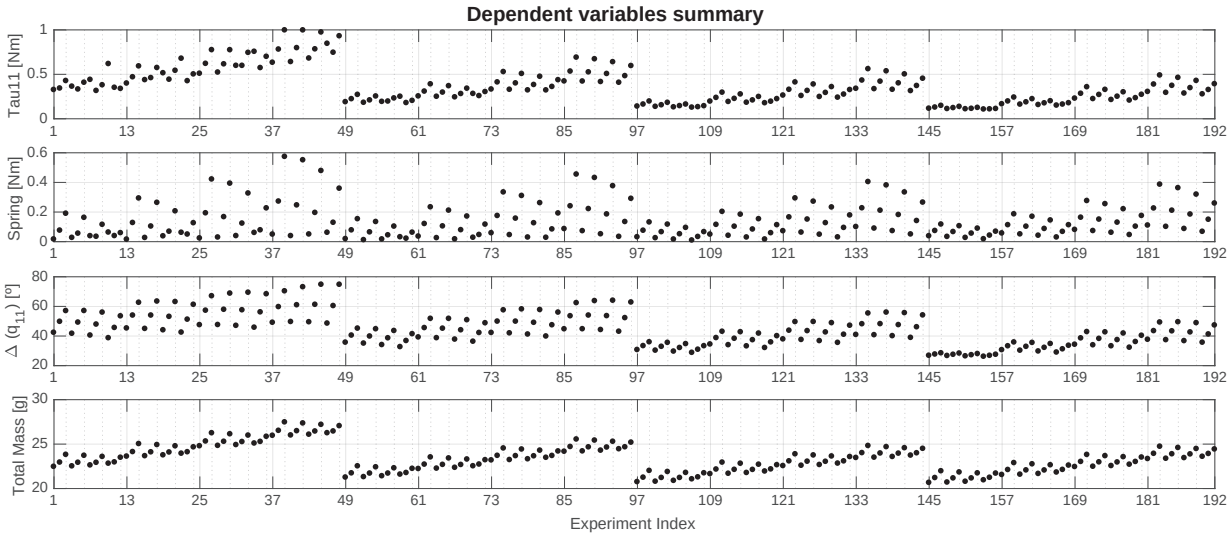

Figure A.13: Summary of the dependent variables along the experiments in relation to the independent ones.

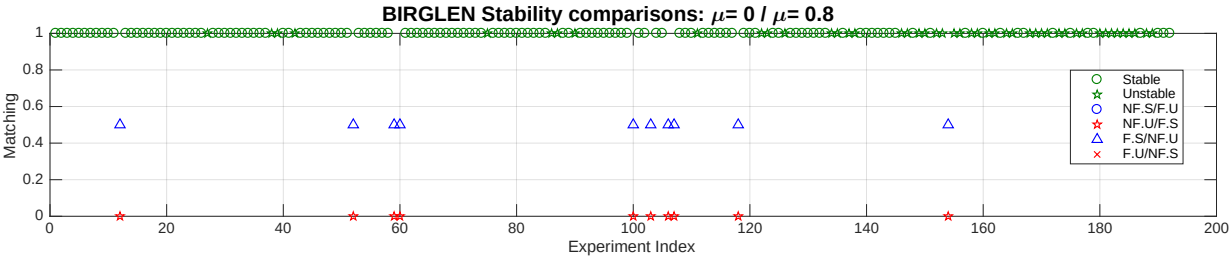

Figure A.14: Birglen stability checking with and without stability. (F: friction, NF: no friction, S: stable, U: unstable).

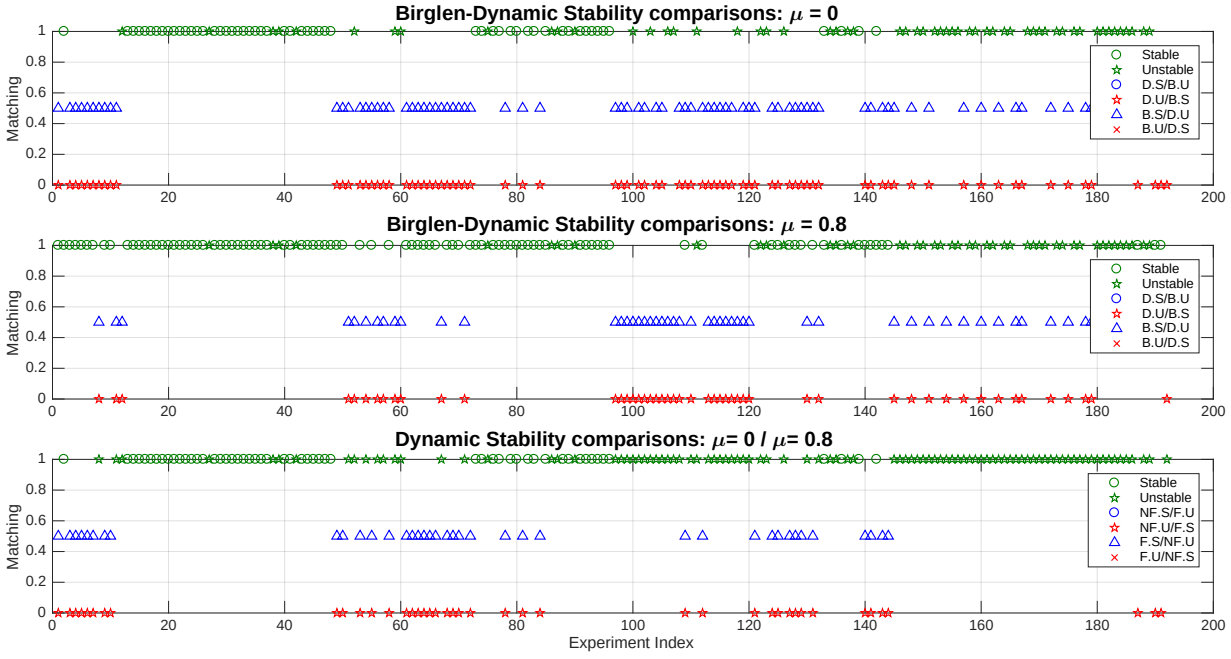

Figure A.15: Stability comparison between static/dynamic and with/without friction. (B: Birglen, D: dynamic, F: friction, NF: no friction, S: stable, U: unstable).

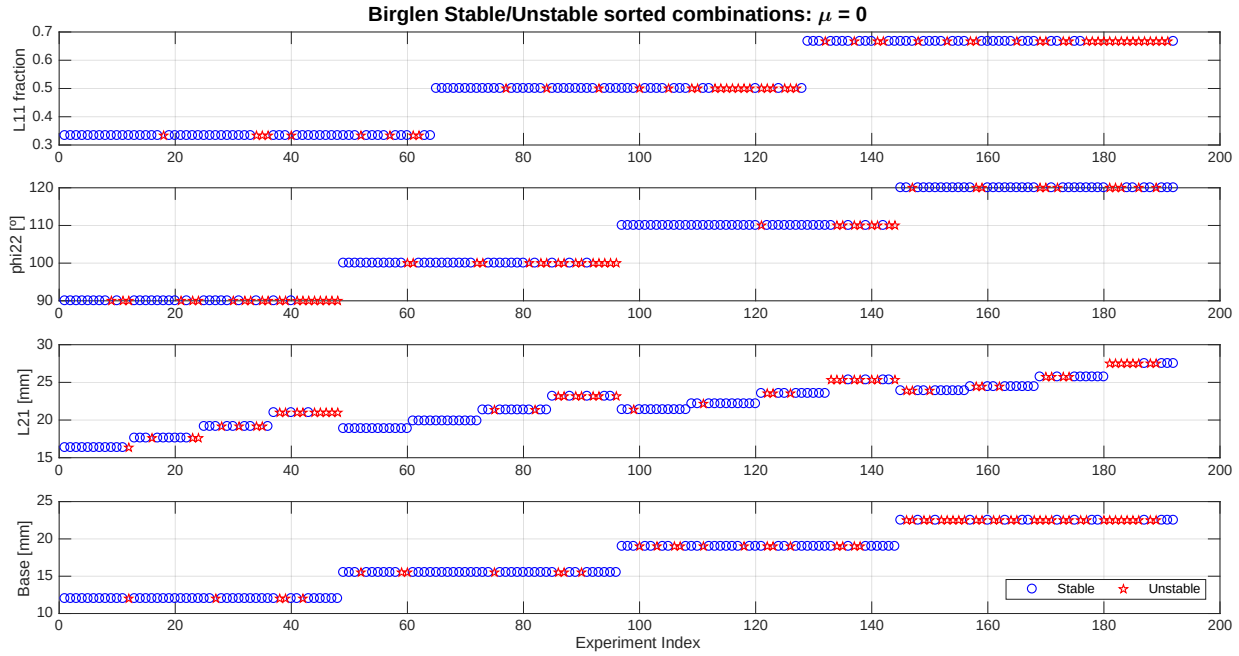

Figure A.16: Birglen stability analysis without friction in function of each one of the design variables.

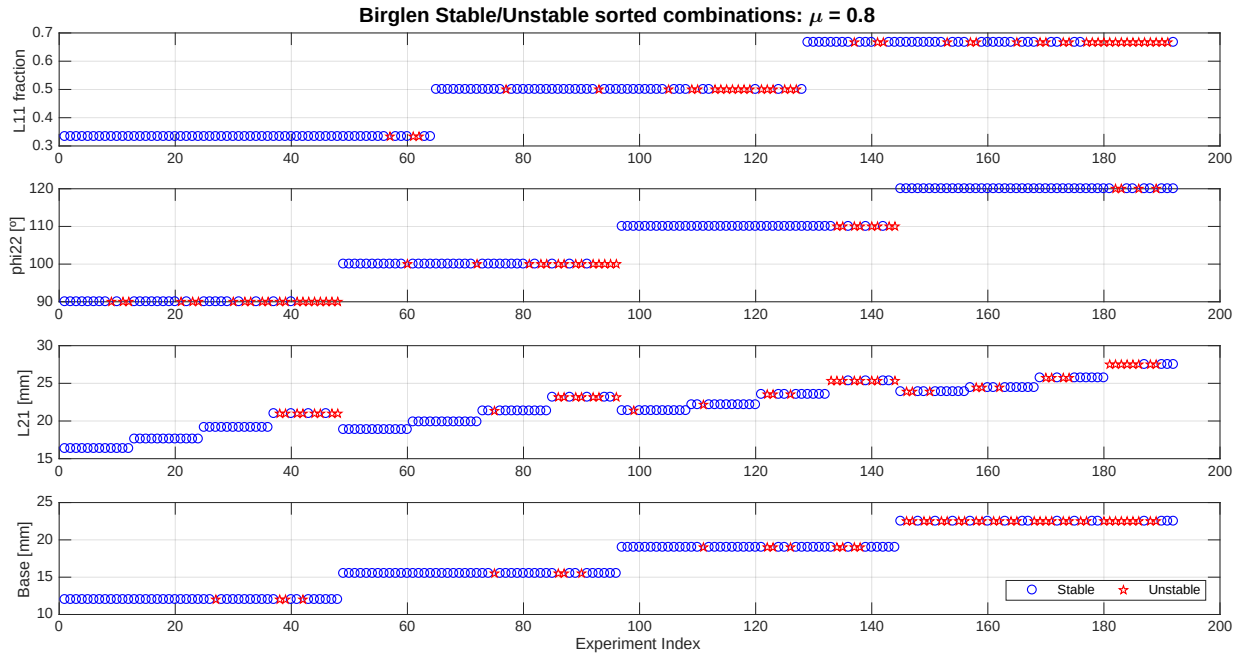

Figure A.17: Birglen stability analysis with friction in function of each one of the design variables.

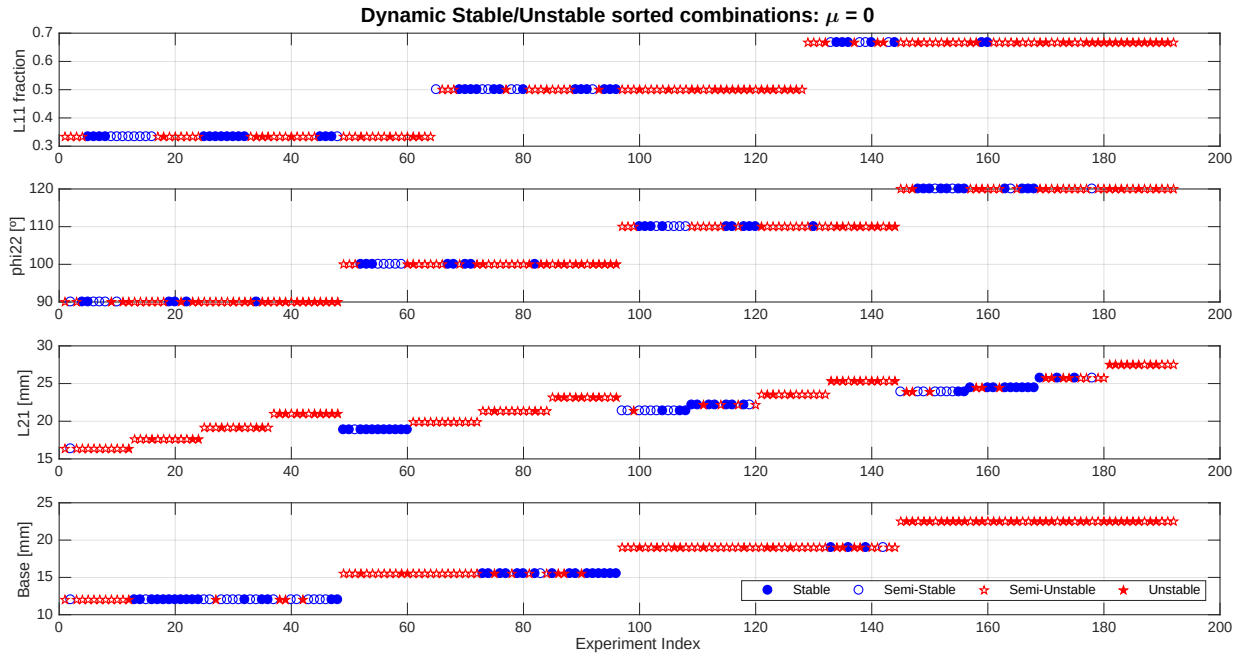

Figure A.18: Dynamic stability analysis without friction in function of each one of the design variables.

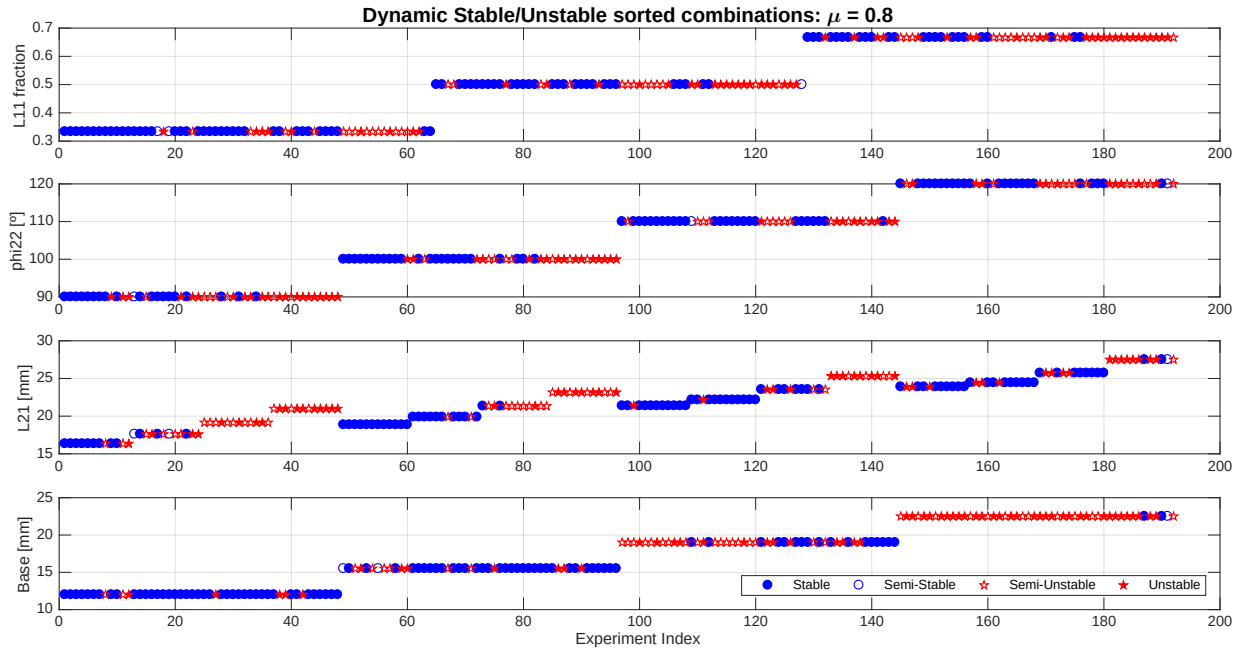

Figure A.19: Dynamic stability analysis with friction in function of each one of the design variables.

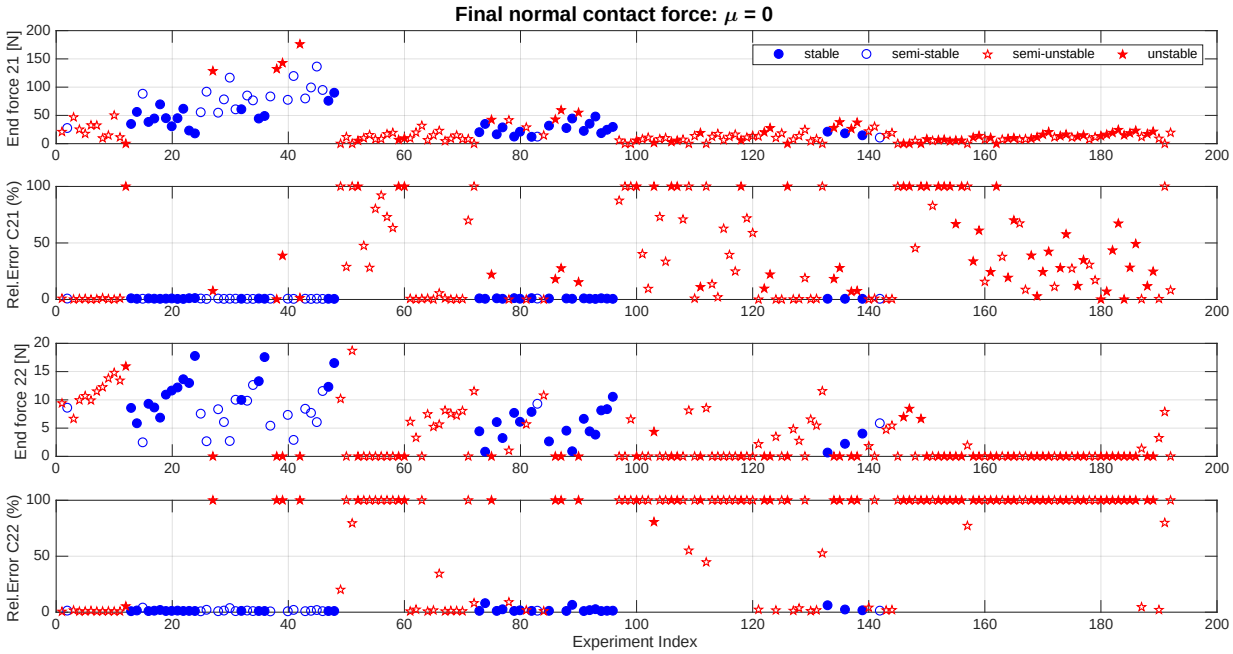

Figure A.20: Final normal contact force applied by the finger on to the object without friction.

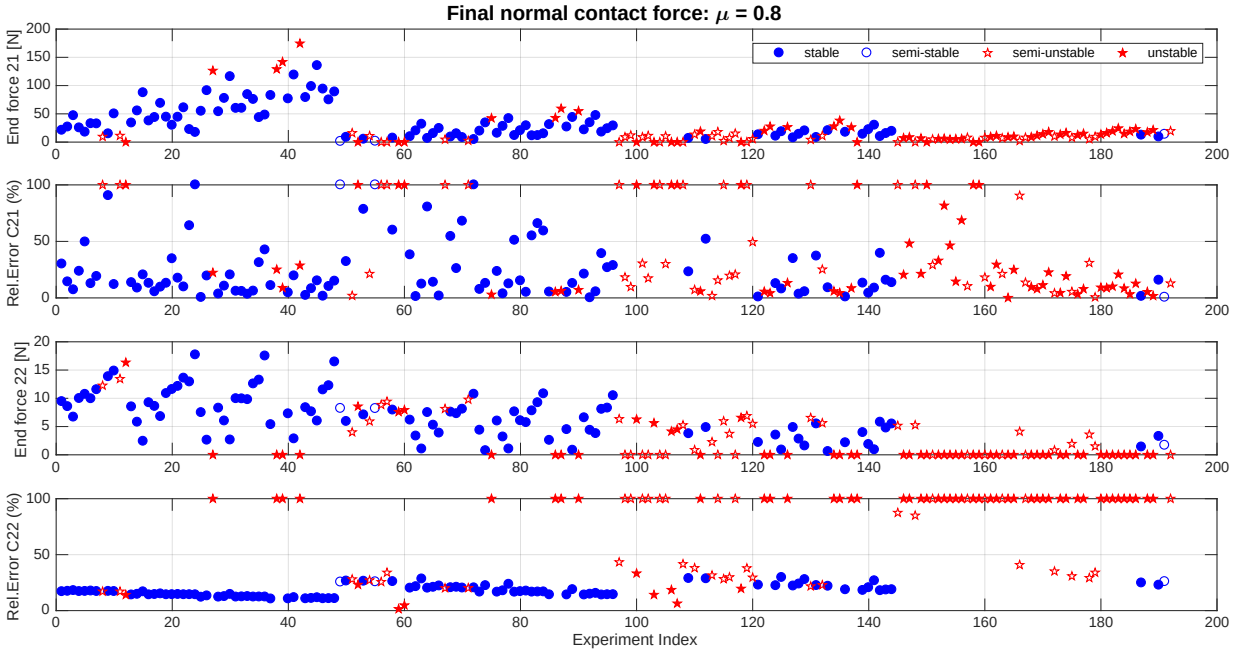

Figure A.21: Final normal contact force applied by the finger on to the object with friction.

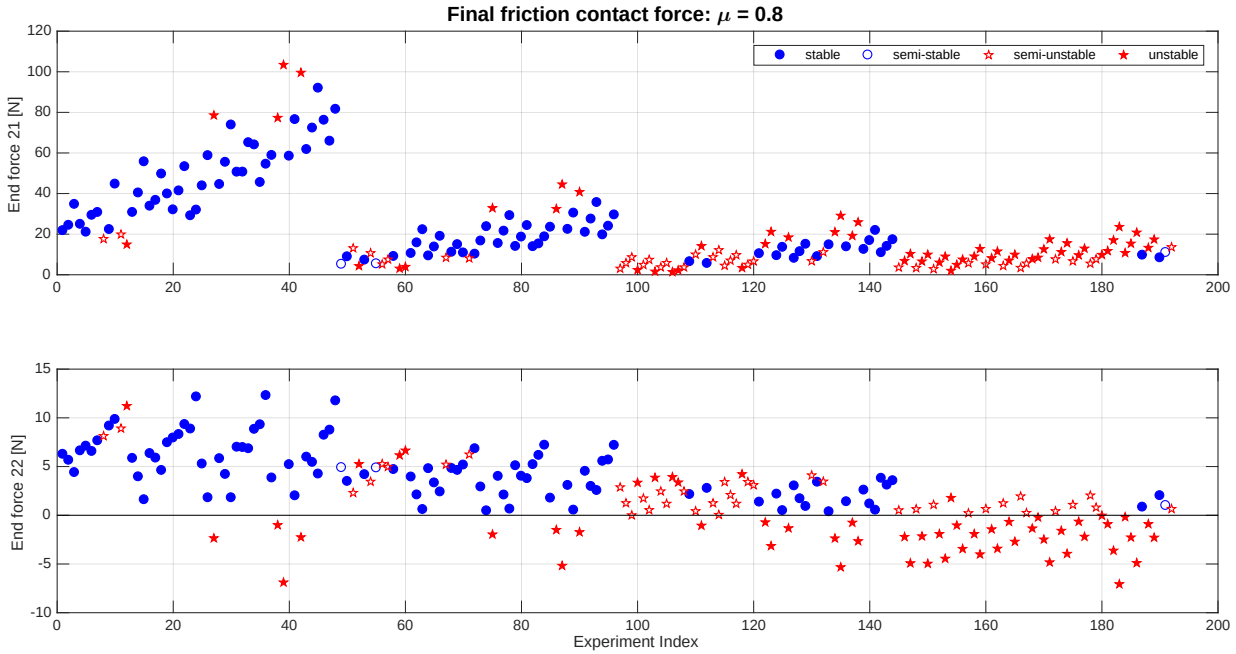

Figure A.22: Final friction contact force applied by the finger on to the object.

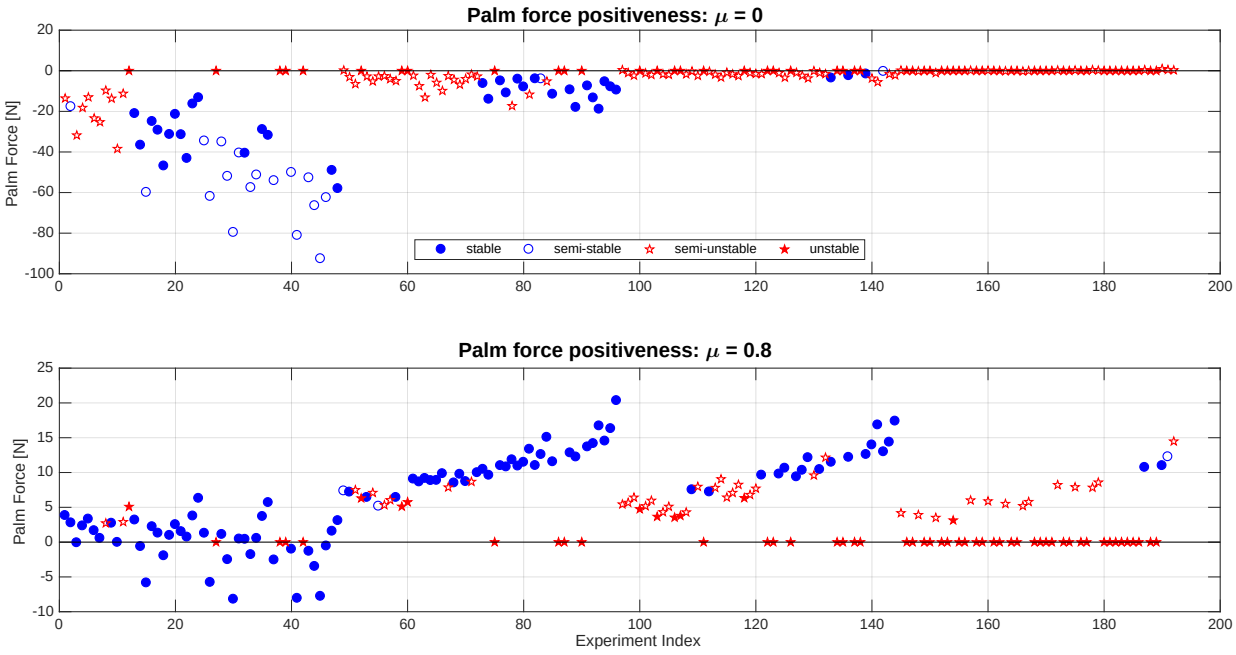

Figure A.23: Palm force positiveness with and without friction.

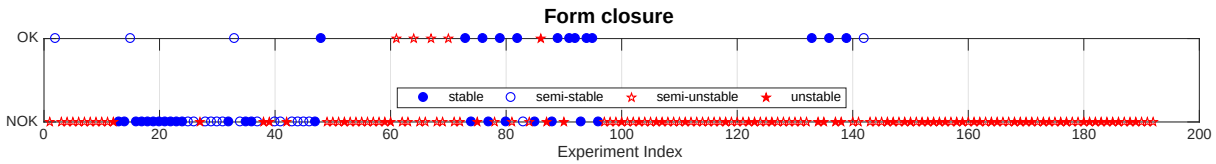

Figure A.24: Form Closure analysis over the experiments.

Appendix B

Models developments and cross-validations

B.1 Modeling contacts with ADAMS

How to create a contact force with ADAMS software is explained, the adequate settings are provided and the software is check in order to know if it respects the Herz contact theory hypotheses.

B.1.1 Create a contact between two solids

To create a contact between two bodies, go to "forces" on the ADAMS interface and in "special forces", click on the button "create a contact". First, must be chosen the contact type, regarding to what is desired to model (two-dimensional or three-dimensional contact) and the 3D model. The most intuitive contact type is "solid with solid", where one have to select the two solids between which the contact will be created; for this type of contact, the order of selection does not matter, as the phenomenon is bidirectional and symmetric. If desired, one can choose to display the contact forces and, finally, the parameters for contact and friction must be set (see *Fig. B.1*).

In a general context, where the contact won't be strictly elastic and friction will have some influence, one can select the *IMPACT* function in the Normal Force field and *COULOMB* function in the Friction Force field.

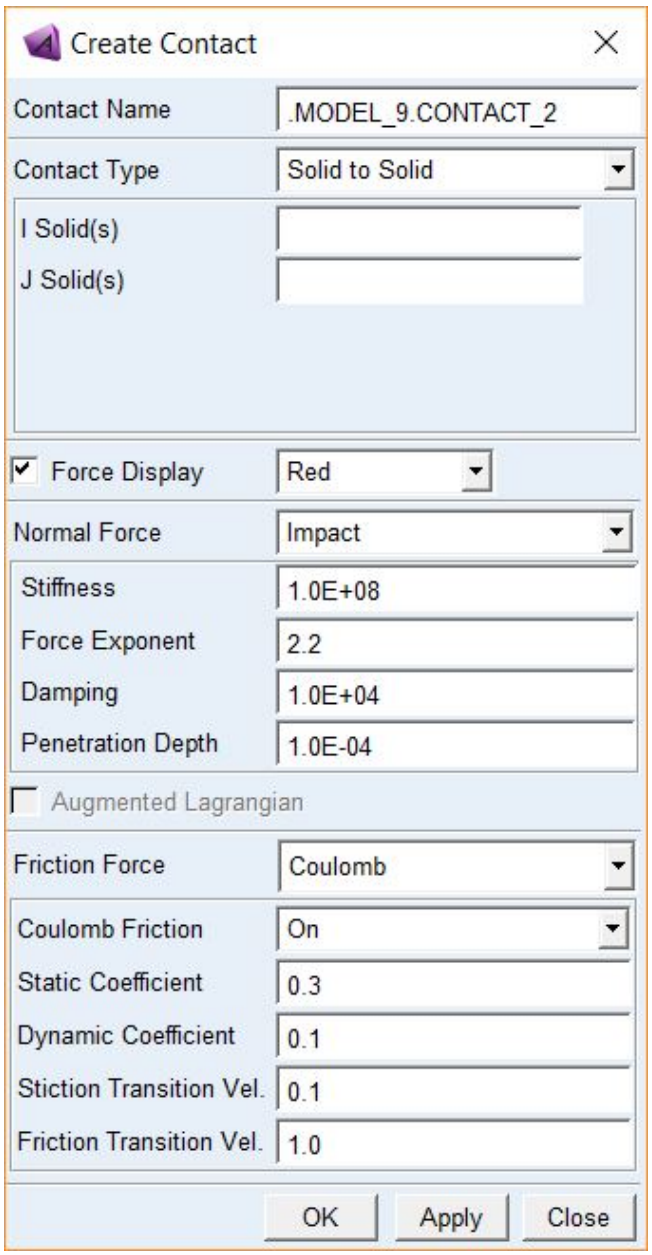

Figure B.1: Window in ADAMS for contact modeling

B.1.1.1 Normal Contact Settings

ADAMS software allows the user to set almost all the properties, from the design to the solver. Is in the latter where an important issue has been noticed: the choosing of the proper solver and the step size are a significant issue in the process to obtain a simulation with reliable results.

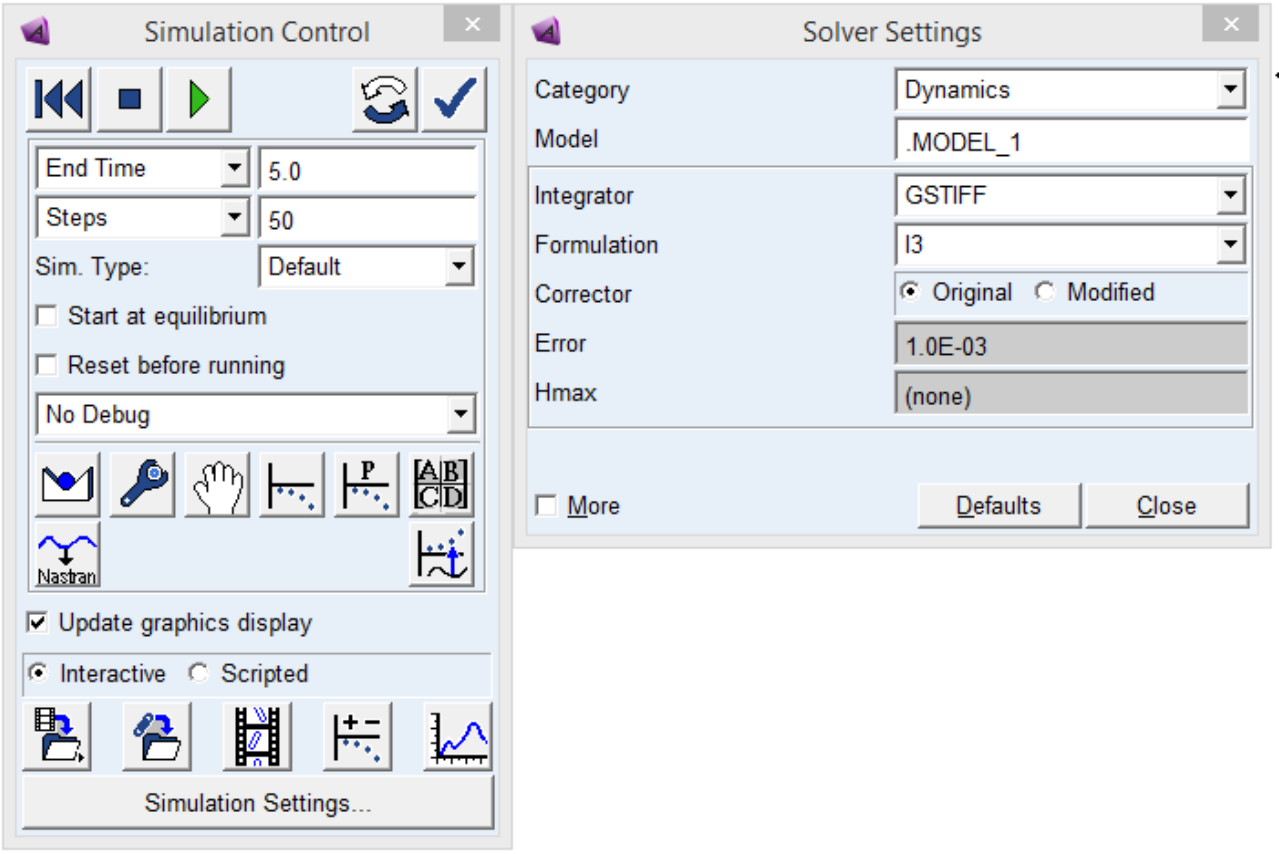

Figure B.2: ADAMS Simulation Control Window and Settings

In *Fig. B.2* are shown the Simulation Control window and the Solver Settings window (accessible through the button at the bottom of the Simulation Control window). The first thing that is worth changing is that, by default, the simulation is set to 50 steps independently of the simulation time. This can be changed in the *Steps* field to *Step Size*, which will ensure a better control on the simulation regardless of the simulation time. Second field worth checking is the *Sim. Type*. This field refers to the type of simulation that is desired to perform. As interaction between bodies are considered, instead of *Default*, we will choose *Dynamic*.

Moving to the Solver Settings, by default on the *Dynamics* Category, the solver is set to *GSTIFF Integrator* and *I3 Formulation* with an *Error* of 10^{-3}.

An important and interesting topic is the choosing of the good values for the *Step Size* and the *Error*, as they highly influence the outcome simulation in compromise with the computation time. Big *Step Size* will compute fast but is sensitive to miss important events (as the beginning of a collision) and if it is very small it will have a high computation cost. The same goes for the *Error*, where the iterations to converge are larger when smaller is the requirement.

For future research purposes explained later on this report, the simulation of a contact between two spheres (as Hertz model analyses) in ADAMS has been done and the Force has been plotted over the time (see *Fig. B.3*) using different of the above commented settings. If we take as a real reference, the modified setting that resulted on the purple curve, one can

observe that, taking a step size of a 1%, respect the plotted time, with the default settings (orange curve in *Fig. B.3*), the result is quite discontinuous and presents an error of a 60% in comparison with the purple curve. For the same solver but redefining the step size to 0.001% (clear blue curve), the number of computations have grown by 10^3 (the computation time is not scaled linearly) and the result approaches the real behavior of the collision, however, the time required is quite big for a non-smooth result. After some search into ADAMS documentation [1], one can find that if instead of using the default *I3 Formulation*, we can use *SI2 Formulation*, a more stable and reliable formulation of the integrator that achieves good results with much less computational cost, as can be appreciated with the red curve, in which the step size is of a 1% and the error decreased only by a tenth. Another positive point for this solver is that it has been noticed that if the step size is reasonable, the solver makes an interpolation when approaching the collision event and adjusts the step size to match the first contact.

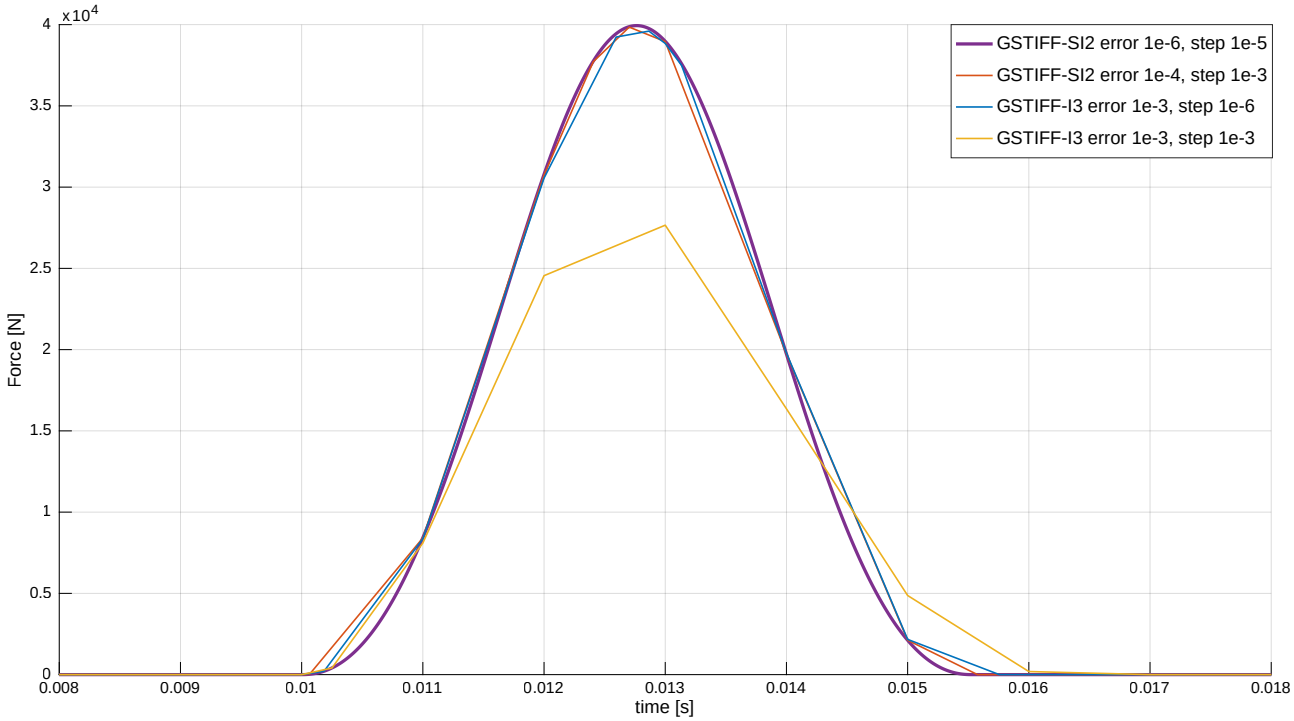

Figure B.3: Different Simulation/Solver settings comparison for a two spheres collision

B.1.1.2 Hertz contact hypotheses checking

The validity of the Hertz contact model has been checked. In the next sections, the model will be developed, but for now, the important point is to note that it is based in a spring. By the definition of the contact, no adhesion phenomena is modeled; the initial contact is a point (two spheres); because the collision is modeled by a spring, the interference between the bodies is elastic; no friction has been added. Hence, only one hypothesis is left to check: the contact area of the deformation is much more smaller than the objects' dimension/curvature radii.

The previous simulation has been reproduced colliding a fixed sphere of 10 cm radius against 3 different spheres of 0.05, 5 and 10 cm which are provided with the same mass and the same initial horizontal linear velocity (without gravity) as can be shown in *Fig. B.4*.

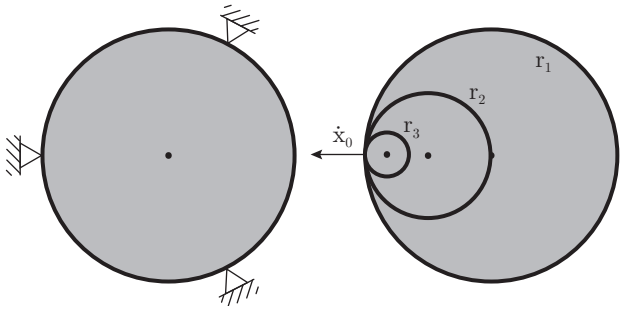

Figure B.4: Hertz dimension hypothesis experiment setting

The results of the simulation show that this hypothesis is not checked during a collision (as can be seen in *Fig. B.5* and *Fig. B.6*). The evolution of the position for the three spheres and the contact forces match exactly, meaning that the object shape is only taken into account to compute a normal penetration distance and that is in the hands of the user make sure that the contact parameters are set properly in order to simulate a real system. This output makes a little bit more tricky the setting, as some common knowledge of the system should be used as an input.

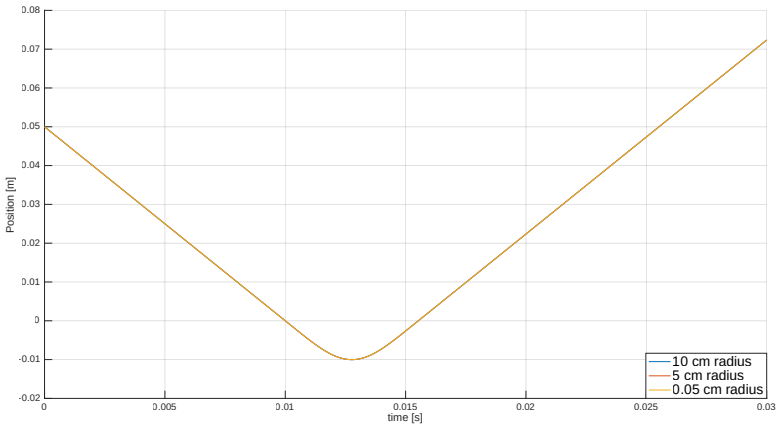

Figure B.5: Horizontal position of the 3 spheres over the time

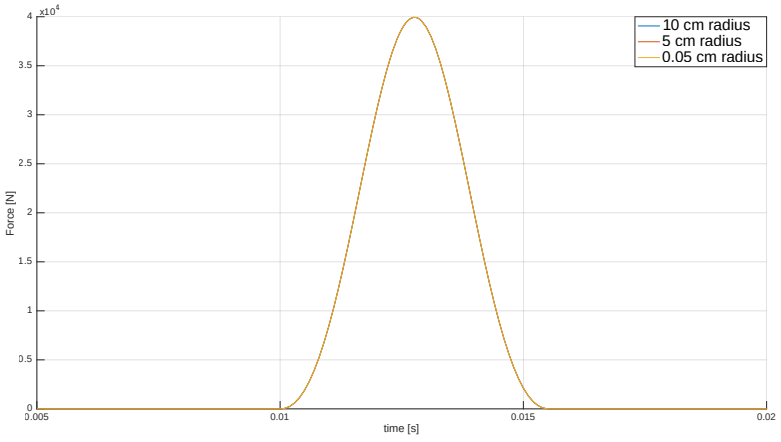

Figure B.6: Contact force of the 3 spheres over the time

B.1.1.3 Friction Settings

In the friction model there are some parameters that are user set. In the following paragraphs some hints are provided as how to tune them.

ADAMS provides a set of default proposed parameters. However, one must not forget that the software does not have any any material context unless the properties have been given before. In order to set the friction coefficient values, experimental data can be obtained, but if this is not easy to gather, ADAMS documentation gives a table with the static and dynamic coefficients for numerous couples of materials [2], from where one can at least approximate the values. Two notes, the first is that, unless the materials used are special, a standard value that can be used for performing first simulations can be $\mu_s = 0.6 - 0.8$ and $\mu_d = 0.4 - 0.6$. The second remark is that, independently of the pair of values for the friction coefficients, always must be respected $\mu_s \geq \mu_d$.

Regarding the transition velocities parameters, the best way to proceed is to simulate friction behavior a first time using $\mu_s = \mu_d = 0$, in this way, the values of the slipping velocity can be read but it does not have any dynamic effect into the simulation. Once the results are obtained, one can read the values of v_{slip} when the objects are slipping and also decide when the model is considered static and read then v_{slip} again. In this way a minimum and a maximum can be obtained. Remark that this transition effect is fictitious, hence, the interest relies on obtaining a compromise between small transition zones that respect the model and stable results / quick convergence of the model. It is difficult to set generic values for these parameters because they highly depend on the model.

B.1.2 Contact models crosschecking

B.1.2.1 Normal contact model crosschecking

In order to validate the two proposed models (the one for the spring and the one for the damper), a co-simulation between ADAMS and SIMULINK has been performed. The simulated system consists in the collision of two spheres, one is fixed and the other is given a constant velocity in order to eliminate other forces that can influence the system. With the proper setting of the parameters, two simulations have been performed:

1. A collision without damping. This behavior is achievable by setting $c_{max} = 0$. As can be observed in *Fig. B.7*, the model presents some discrepancy in high penetrations. However, 2 cm penetration for a collision with elastic effects around the contact point (Hertz hypothesis) is not a real effect. Nonetheless, the worst case scenario (even if it is not real) presents a relative error $< 1\%$.

2. A collision without spring, only the damping effect has been taken into account. This behavior is achievable by setting $k = 0$. As can be observed in *Fig. B.8*, the model presents some discrepancy in the transition zone but the maximum relative error is $<$ 2%.

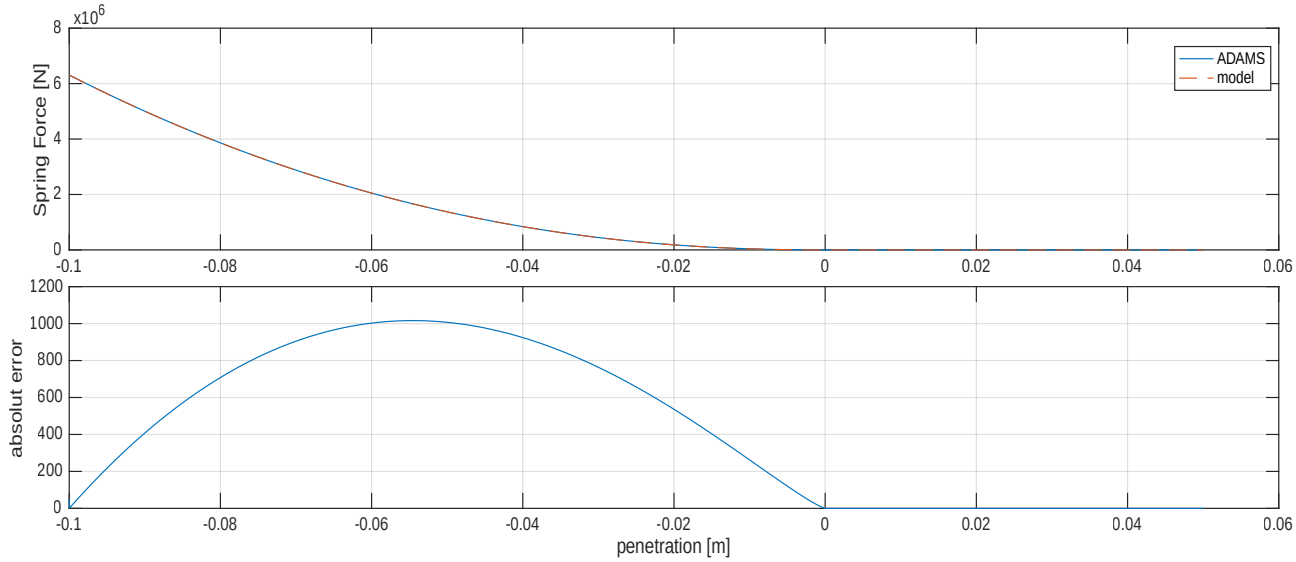

Figure B.7: Checking of the spring model in a collision.

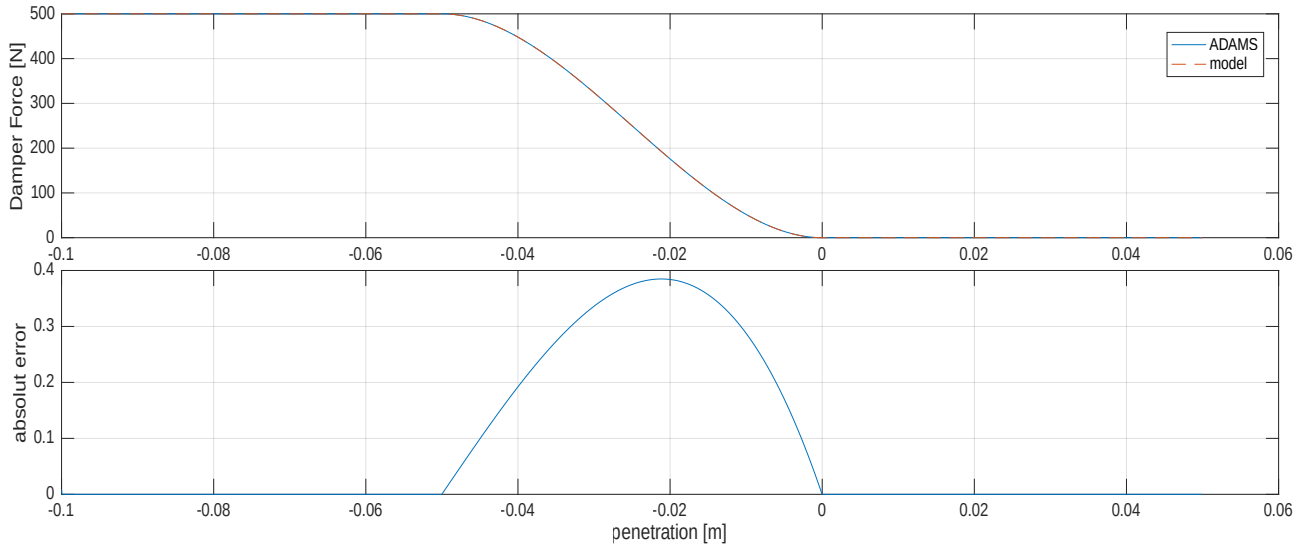

Figure B.8: Checking of the damper model in a collision

B.1.2.2 Friction model crosschecking

In order to validate the proposed model, a co-simulation between ADAMS and SIMULINK has been performed. The simulated system consists in a fix plane and a sphere. The sphere is provided with a small penetration with the plane and a constant velocity along the plane, in this way, the normal force is constant and the only tangential force is the one opposed to friction. As can be observed in *Fig. B.9*, the model is accurate, presenting relative errors $<$ 0.001%

taking into account that the friction force directly depends on the accuracy of the normal force computation.

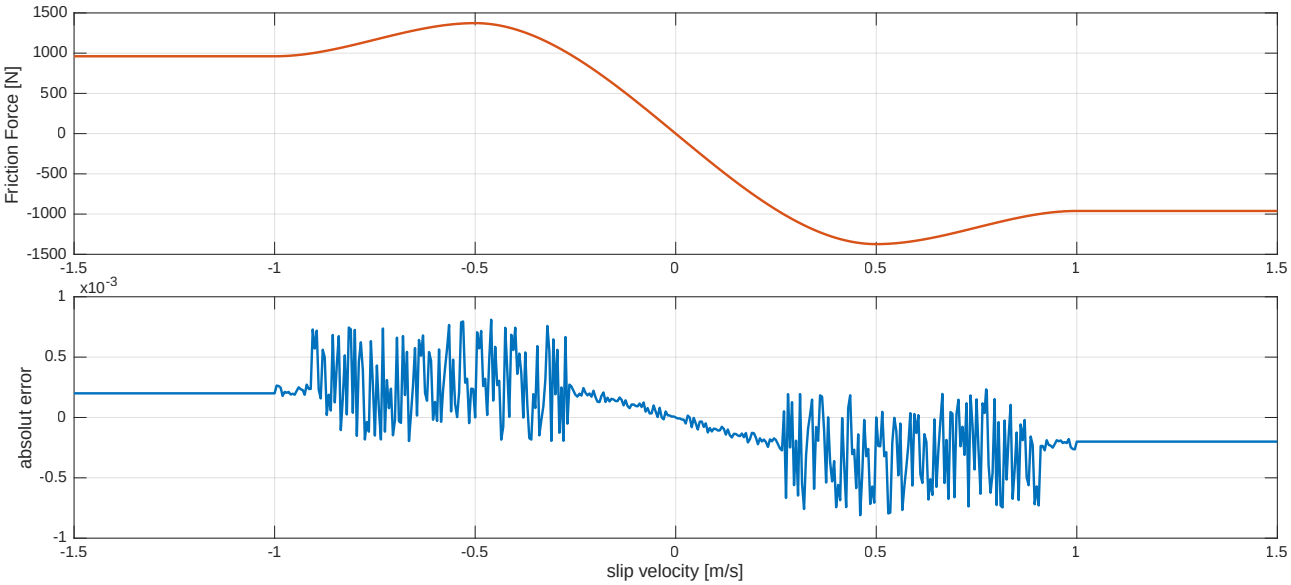

Figure B.9: Friction coefficient function checking with ADAMS.

B.2 Geometric relations computation

The next sections will have its on notation to do not add many intermediate variables to the main text. The main computed parameters: the penetration depth δ_n, the collision length l_c, and the slipping contact velocity v_{slip} for each contacting bar. Also, the geometric relation of l_{21min}, l_{21min}, l_{21}, q_{c2j}, l_{12} and t_{22} are developed.

B.2.1 Penetration depth (δ_n), collision length (l_c) and slipping velocity (v_{slip}) computation

[1]In order to compute the penetration distance respect a fix point, a conversion of the model to a virtual width (see *Fig. B.10*) eliminating the link width and adding it to the object's radius has been performed. Now, applying basic geometry to compute the distance between a line and a point, and substracting it from the virtual radius of the object, the penetration depth is obtained as (variables defined in *Table B.1*):

$$\delta_n = (r_c + w) - \frac{|a \cdot x_c + b \cdot y_c + c|}{\sqrt{a^2 + b^2}} \tag{B.1}$$

[1]To simplify the notation, symbols can change in the appendices in order to not create many intermidiate variables. Refer to figures of the section.

$$\begin{cases} \texttt{if } \delta_n \geq 0 & \texttt{contact} \\ \texttt{else} & \texttt{no contact} \end{cases}$$

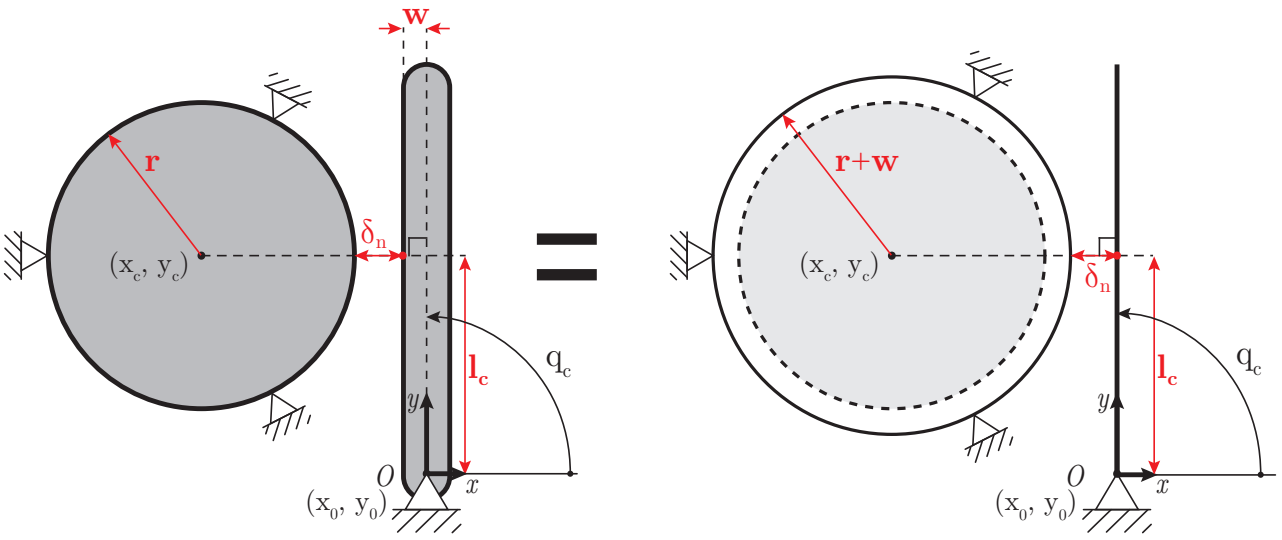

Figure B.10: Transform the system to a virtual length system.

Given the above equation, the point of the line where the contact is happening can be obtained, which will provide the collision length l_c by

$$\begin{aligned} x_r &= \frac{b(b \cdot x_c - a \cdot y_c) - a \cdot c}{a^2 + b^2} \\ y_r &= \frac{-a(b \cdot x_c - a \cdot y_c) - b \cdot c}{a^2 + b^2} \\ l_r &= \sqrt{x_r^2 + y_r^2} \end{aligned} \tag{B.2}$$

In order to compute the slipping velocity of the contact point, the angular velocity $\dot{q}_c$ of the analyzed link is needed. As can be seen in *Fig. B.11*, the slipping velocity corresponds to the tangential velocity on the contact point expressed on the reference base, thus for the second link, the velocity of the first link must be taken into account. Note that the tangential force opposes v_{slip} and that this one depends on the direction of $\dot{q}_c$. Also is interesting to remark that the slipping velocity on l_{21} (and by extension, the friction force) only exists if the contact point is not on the line defined by the link, *i.e.*, only exists if the link has width.

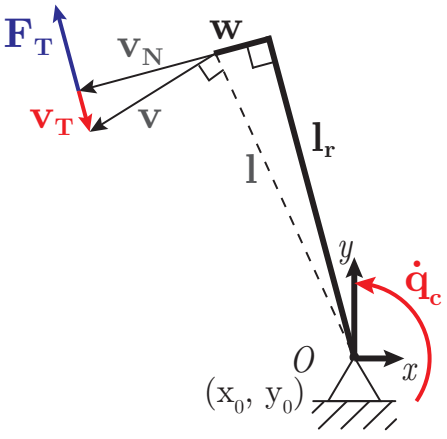

Figure B.11: Slipping velocity of the contact point.

The parameters for each link are summarized in the following table:

Variables	Link l_{21}	Link l_{22}
a	$\sin q_{21}$	$\sin(q_{21} + q_{22} + \varphi_{22})$
b	$-\cos q_{21}$	$-\cos(q_{21} + q_{22} + \varphi_{22})$
c	0	0
x_c	$-base$	$-base - l_{21}\cos q_{21}$
y_c	r_c	$r_c - l_{21}\sin q_{21}$
v_{slip}	$w\dot{q}_{21}$	$l_{21}\dot{q}_{21} + w(\dot{q}_{21} + \dot{q}_{22})$

Table B.1: Variables definition for the collision computation.

In the table above, can be noticed that in order to compute δ_n of l_{22}, the reference O has been moved to the end of l_{21} in order to have the same equations.

B.2.2 Variables reduction

[2]As introduced previously, the link l_{21} is bounded between a minimum and a maximum value. Hence, in order to obtain these bounds:

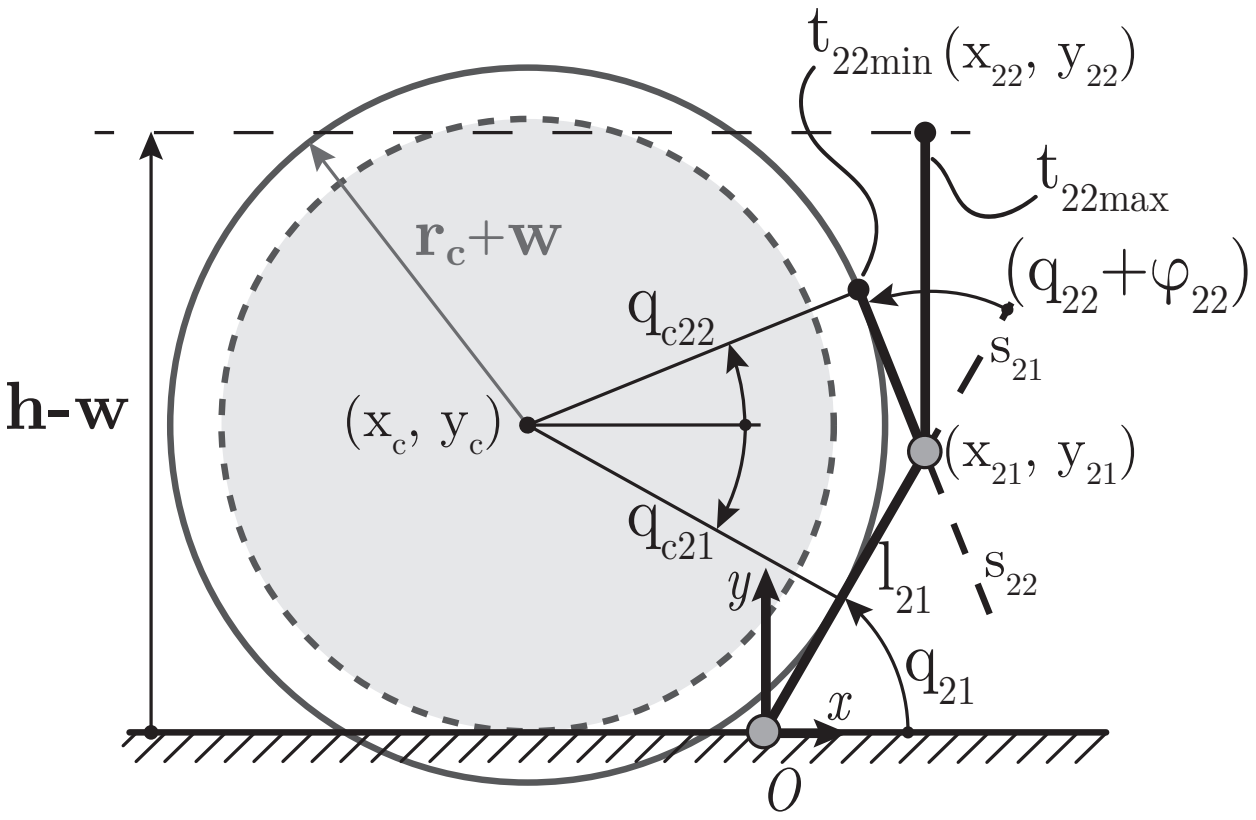

Figure B.12: Diagram for the computation of variables reduction.

[2]To simplify the notation, symbols can change in the appendices in order to not create many intermidiate variables. Refer to figures of the section.

where, s_{21} and s_{22} are the link generator line.These two lines are in the contact position, thus they are perpendicular to the object radius in the contact point.

Minimum l_{21}

The condition to compute l_{21min} is to find the intersection between s_{21} and s_{22} (see *Fig. B.12*) when $q_{c22} = q_{c22min}$.

Variables	**Link l_{21}**	**Variables**	**Link l_{22}**
a_{21}	$\sin q_{c21}$	m_{22}	$\tan(q_{c22min} - \pi/2)$
b_{21}	$-\cos q_{c21}$	c_{22}	$y_{22} - m_{22}x_{22}$
c_{21}	0	x_{22}	$-base + (r_c + w)\cos q_{c22min}$
		y_{22}	$r_c + (r_c + w)\sin q_{c22min}$

Table B.2: Variables definition to compute l_{21}.

$$l_{21min} = \sqrt{x_{21min}^2 + y_{21min}^2} \leftarrow \begin{cases} l_{c21} = \sqrt{x_c^2 + y_c^2 - (r_c + w)^2} \\ q_{c21} = 2\tan^{-1}\left(\dfrac{-(r_c + w) + \sqrt{(r_c + w)^2 + l_{c21}^2 - x_c^2}}{l_{c21} + x_c}\right) \\ x_{21min} = \dfrac{c_{21} + (c_{21}/b_{21})}{(-a_{21}/b_{21}) - m_{22}} \\ y_{21min} = \dfrac{(-c_{22}/m_{22}) + (c_{21}/a_{21})}{(-b_{21}/a_{21}) - (1/m_{22})} \end{cases} \tag{B.3}$$

Maximum l_{21}

The condition to compute l_{21max} is to find the intersection between s_{21} and s_{22} (see *Fig. B.12*) when $t_{22min} = t_{22max}$.

$$l_{21max} = solve(l_{21}, q_{c22}) \begin{cases} l_{21}\cos q_{c21} - t_{22max}\sin q_{c22} - (r_c + w)\cos q_{c22} - base \\ l_{21}\sin q_{c21} + t_{22max}\cos q_{c22} - (r_c + w)\sin q_{c22} - r_c \\ t_{22max} = h - w - l_{21}\sin q_{c21} \end{cases} \tag{B.4}$$

where, q_{c21} is computed in (B.3) and the other variables are defined in *Fig. B.12*.

Computation of t_{22}

Given a value of l_{21} inside the bounds,

$$t_{22} = 0.5(t_{22min} + t_{22max}) \tag{B.5}$$

$$\text{where} \begin{cases} t_{22max} = h - w - l_{21} \sin q_{c21} \\ t_{22min} = \sqrt{(l_{21} \cos q_{c21} - base)^2 + (r_c - l_{21} \sin q_{c21})^2 - (r_c + w)^2} \end{cases} \tag{B.6}$$

Computation of l_{12}

Given l_{11}, l_{21}, l_{12}, l_{22} and φ_{22}, l_{12} is computed based on a right trapezoid (see *Fig. B.13*). The initial angle considered between l_{11} and l_{21} is 90°, while φ_{22} can change. Finally, the relation:

$$l_{12} = \sqrt{(l_{11} - l_{22} \sin \varphi_{22})^2 + (l_{21} + l_{22} \cos \varphi_{22})^2} \tag{B.7}$$

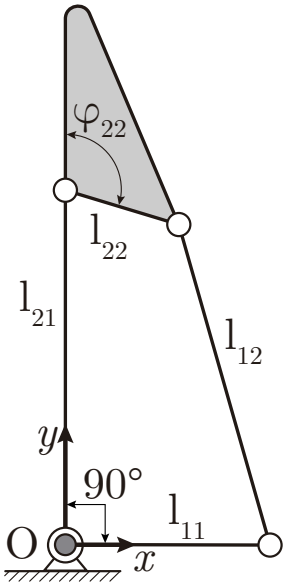

Figure B.13: Diagram for the computation of l_{12}.

Appendix C

CAD design

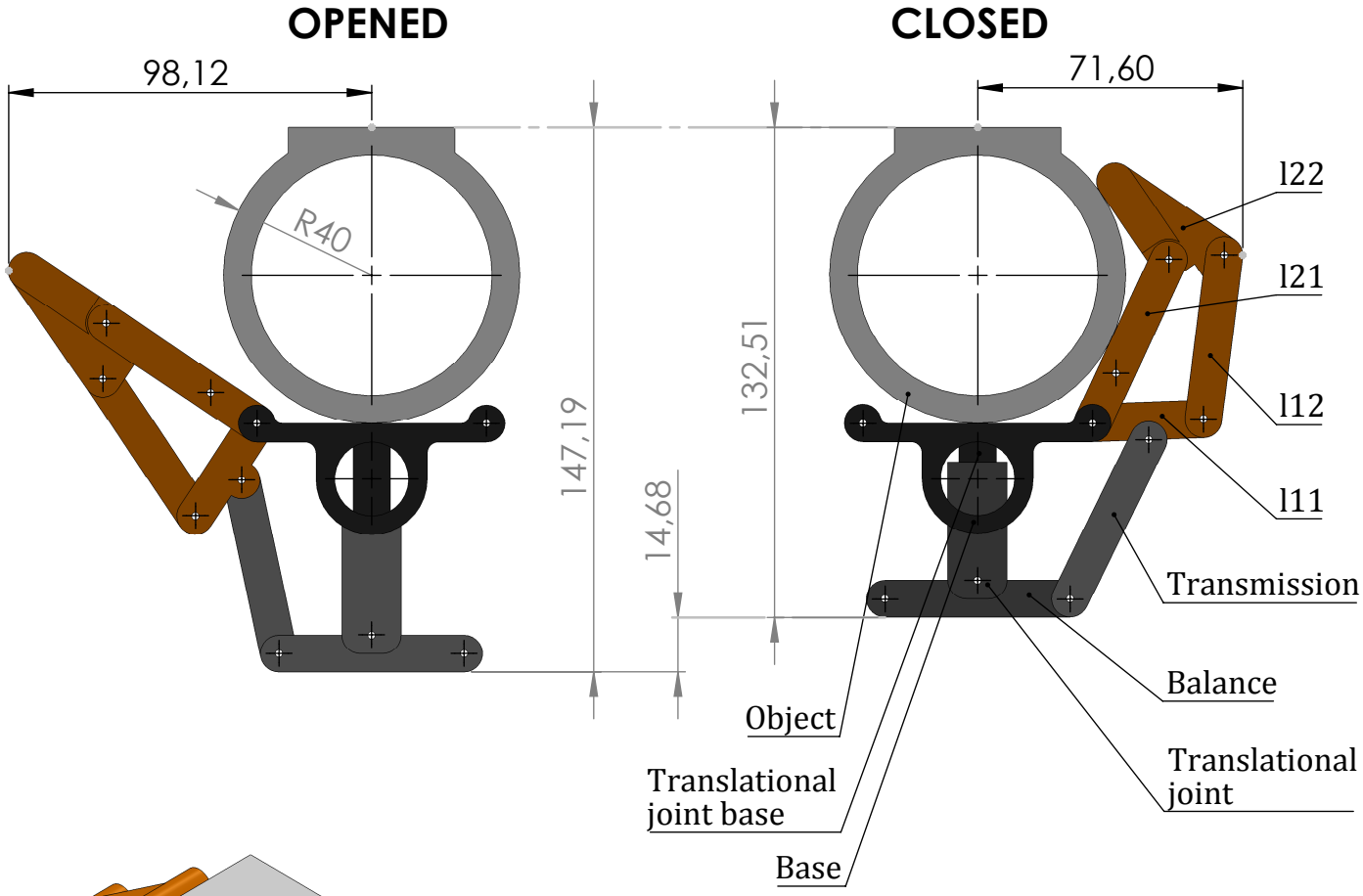

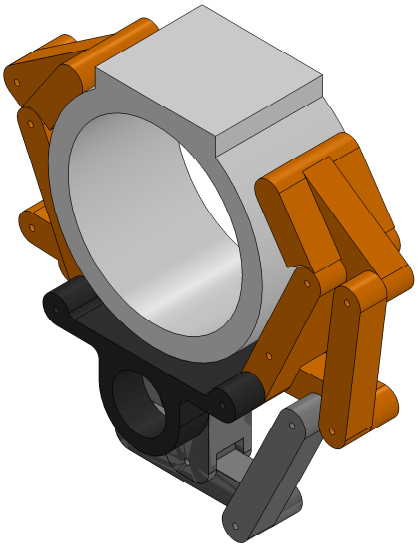

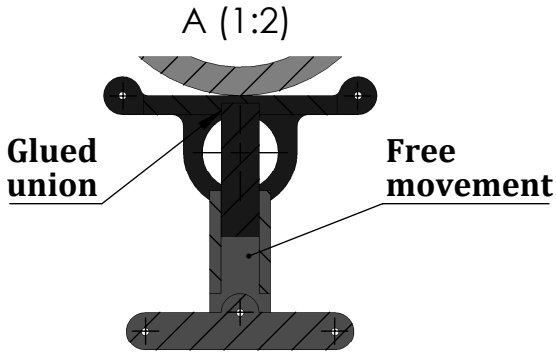

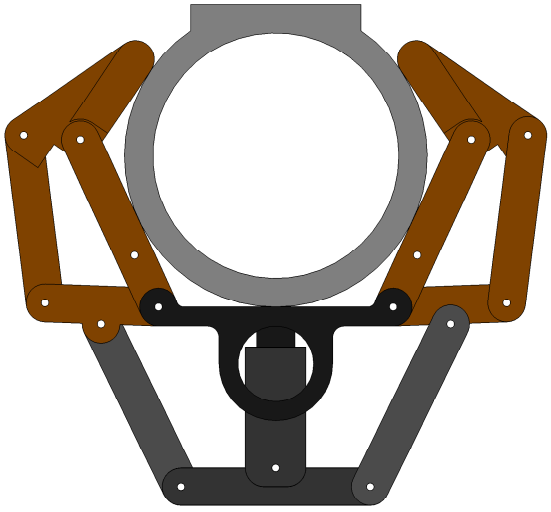

BOM	Quantity
Object	1
Base	1
Translational joint base	1
l11	2
l12	4
l21	2
l22	2
Translational joint	1
Balance	1
Transmission	4
Axis	21

Axes holes are at Ø2 mm. Post mecanization to: hold axis by friction or free rolling.

PART: Gripper Assembly	SCALE: 1:2	MATERIAL: ABS	DATE: 24/07/2017
ÉCOLE CENTRALE NANTES - LS2N	ARIA - ROBA	LLEVAT, David	

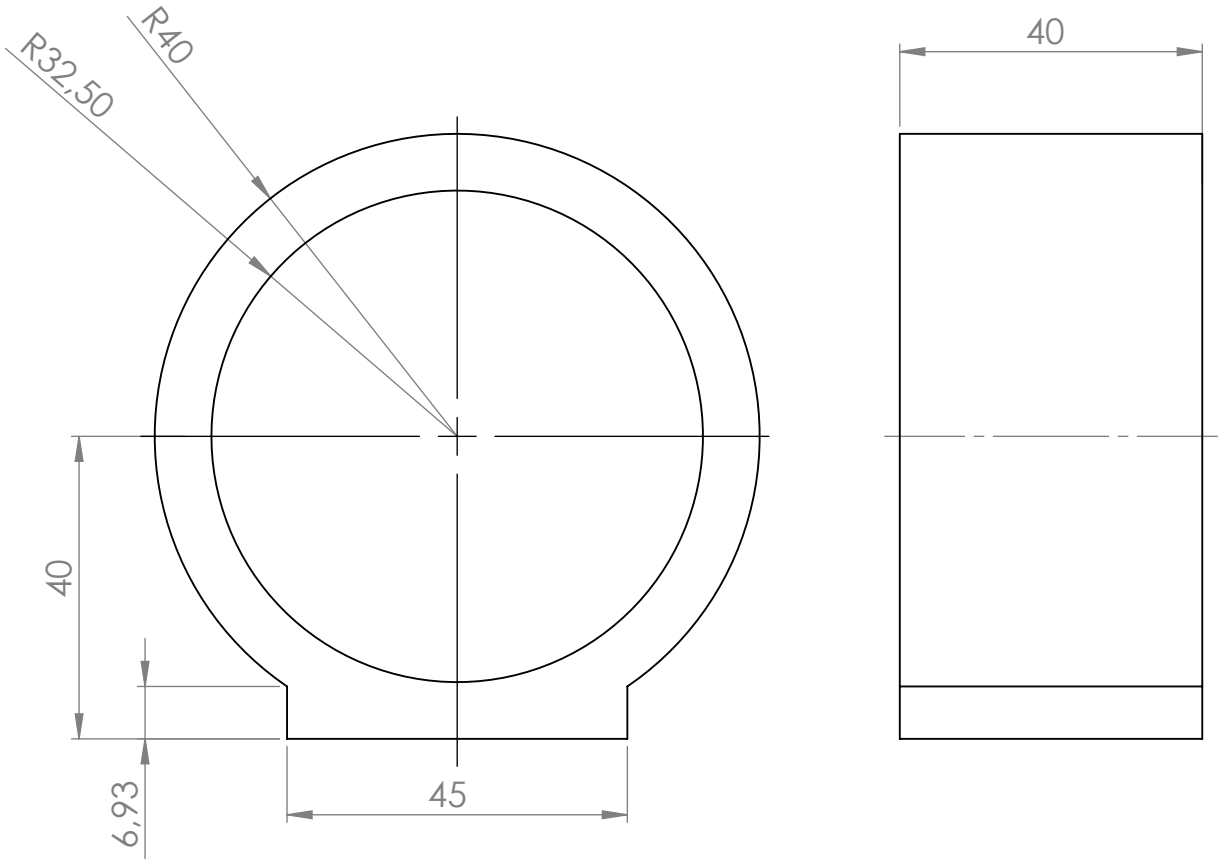

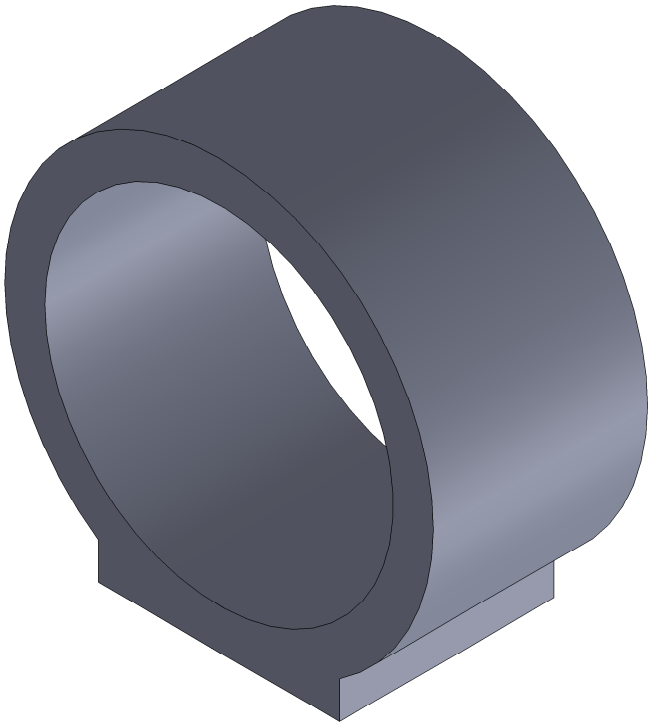

PART: Object	SCALE: 1:1	MATERIAL: ABS	DATE: 24/07/2017
ÉCOLE CENTRALE NANTES - LS2N	ARIA - ROBA	LLEVAT, David	

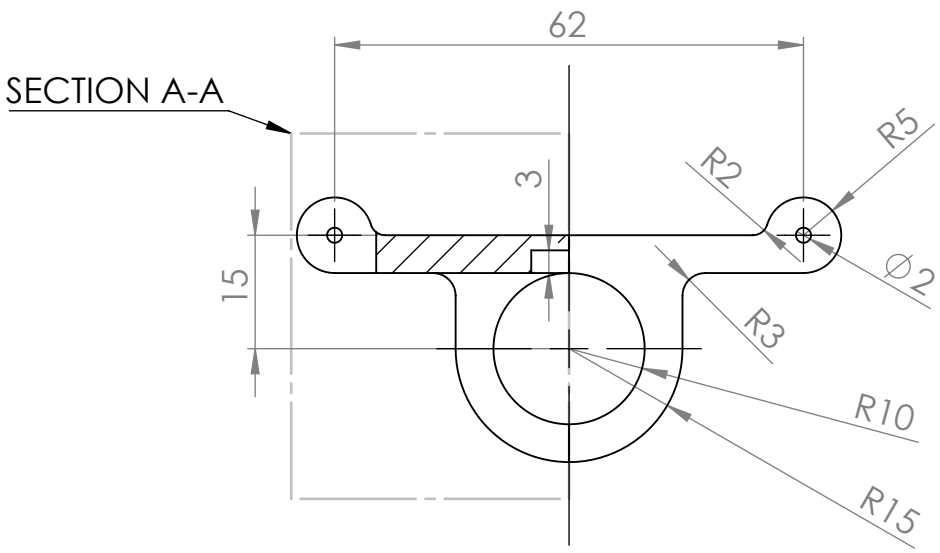

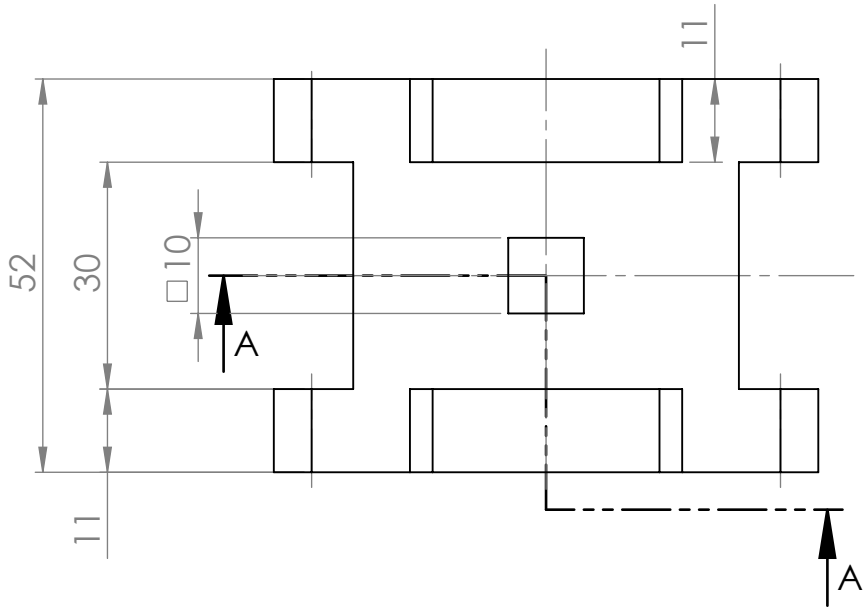

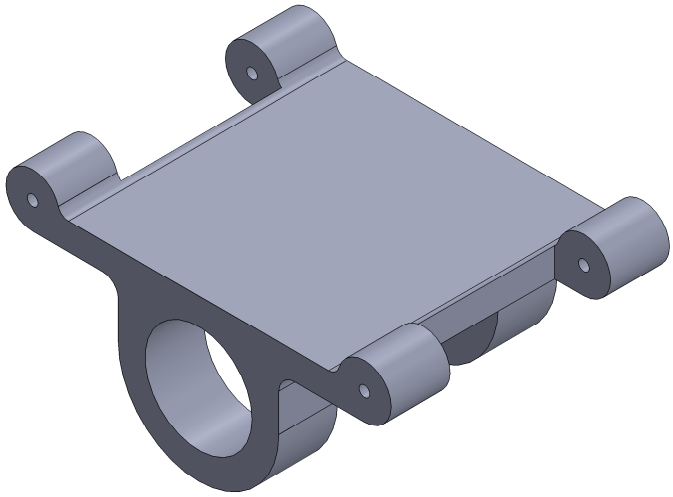

PART: Base	SCALE: 1:1	MATERIAL: ABS	DATE: 24/07/2017
ÉCOLE CENTRALE NANTES - LS2N	ARIA - ROBA	LLEVAT, David	

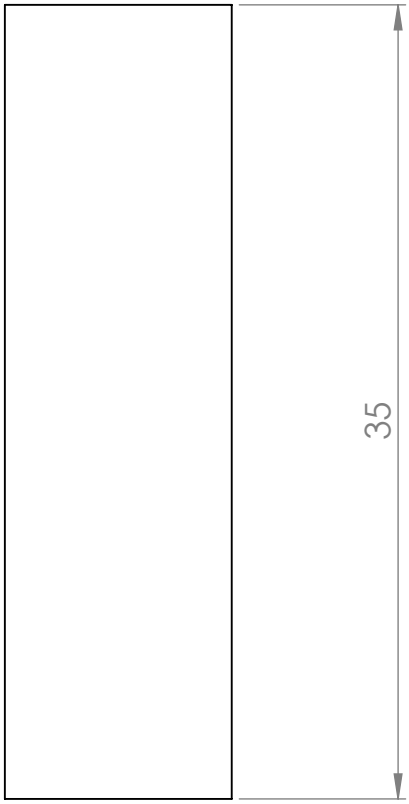

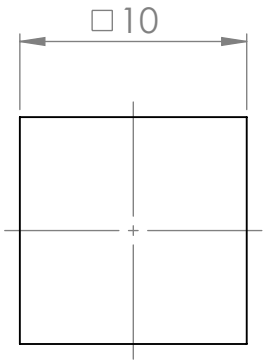

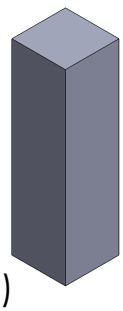

(1:1)

PART: Translational joint base	SCALE: 3:1	MATERIAL: ABS	DATE: 24/07/2017
ÉCOLE CENTRALE NANTES - LS2N	ARIA - ROBA	LLEVAT, David	

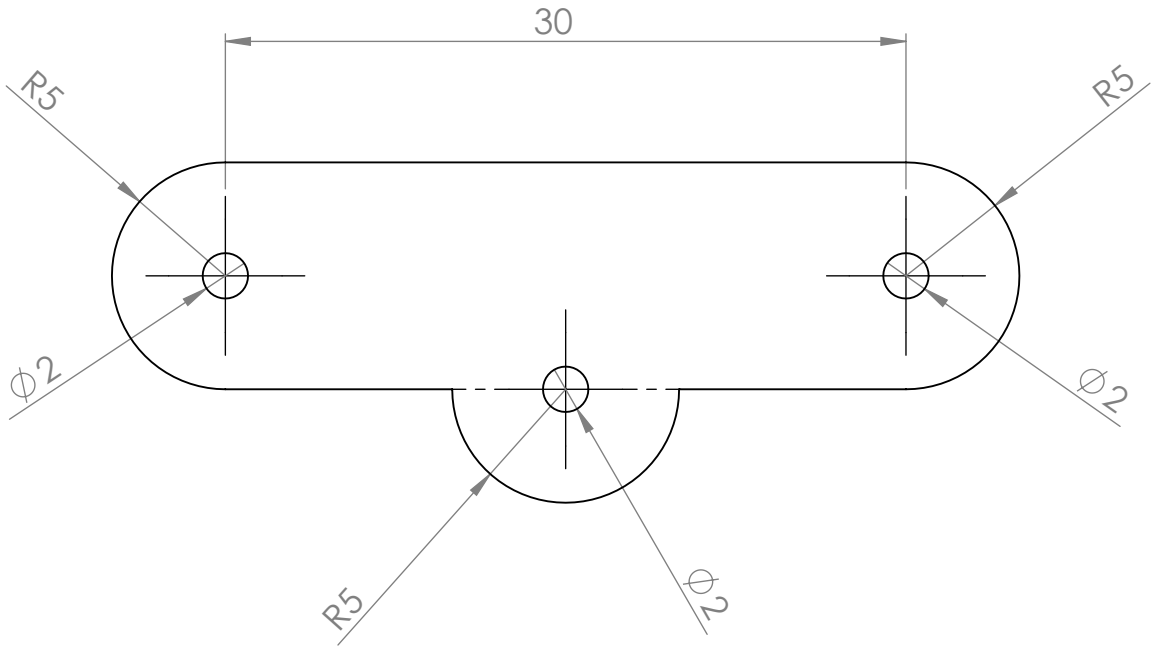

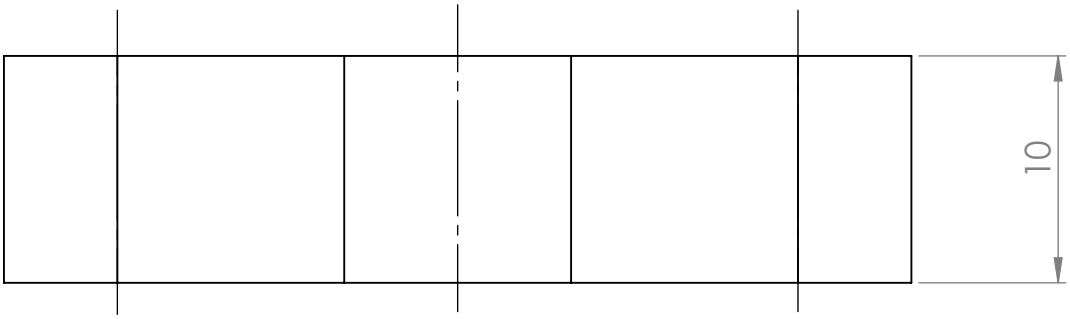

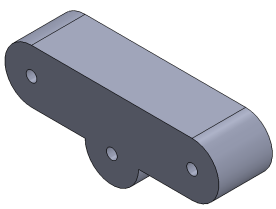

(1:1)

PART: Body L11	SCALE: 3:1	MATERIAL: ABS	DATE: 24/07/2017
ÉCOLE CENTRALE NANTES - LS2N		ARIA - ROBA	LLEVAT, David

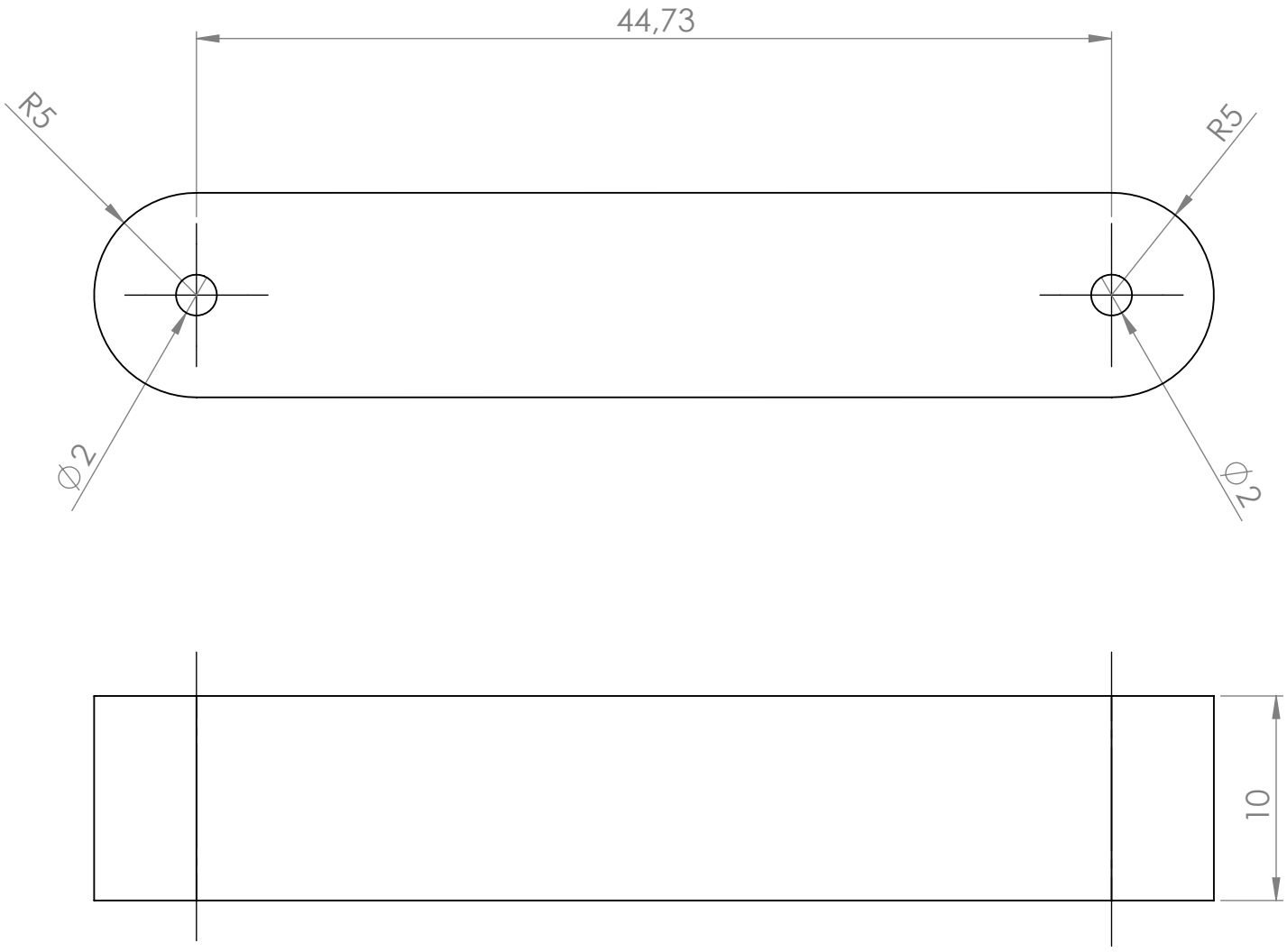

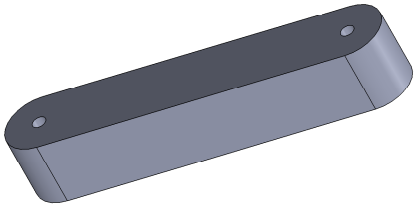

(1:1)

PART: Body L12	SCALE: 3:1	MATERIAL: ABS	DATE: 24/07/2017
ÉCOLE CENTRALE NANTES - LS2N	ARIA - ROBA	LLEVAT, David	

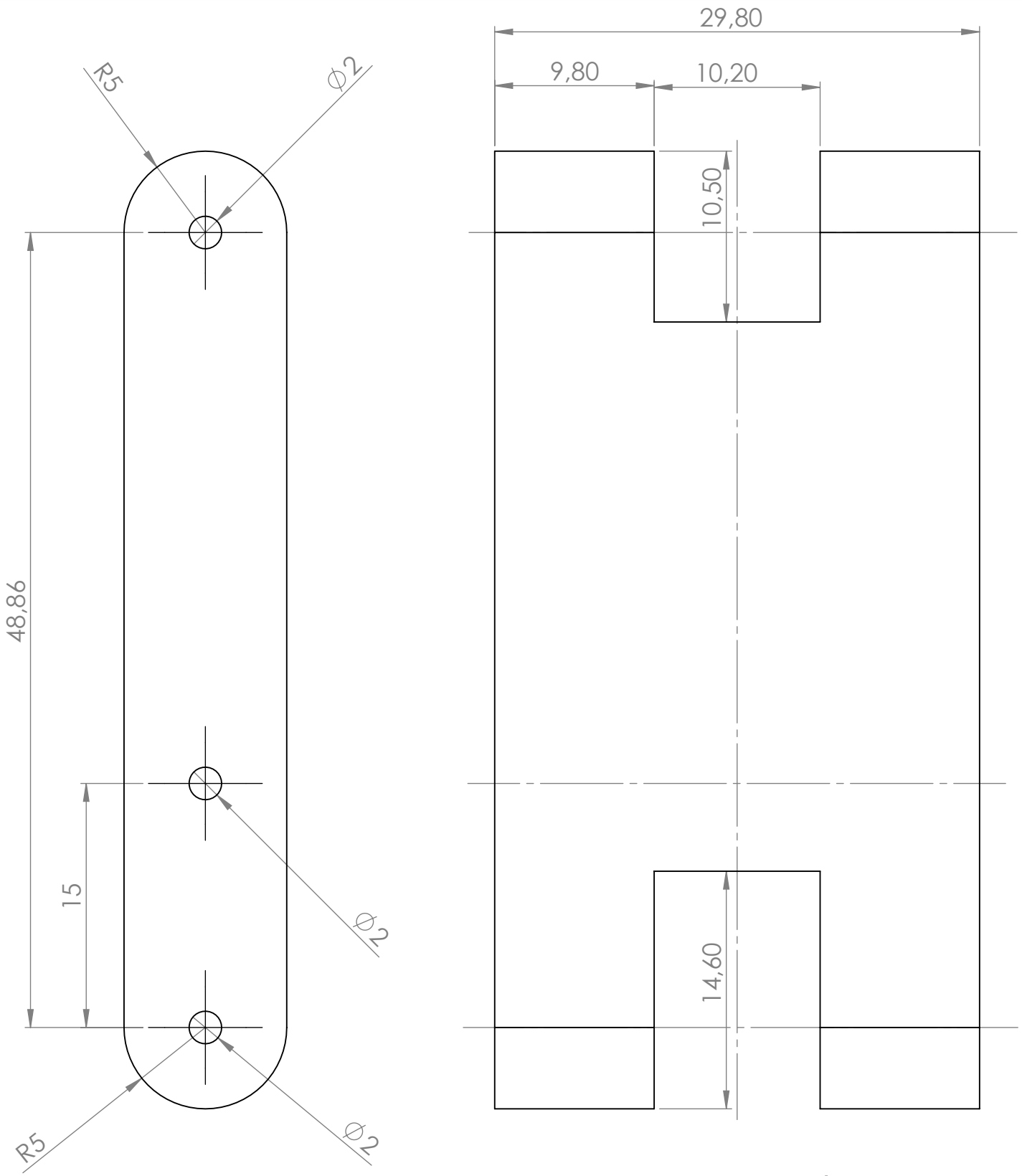

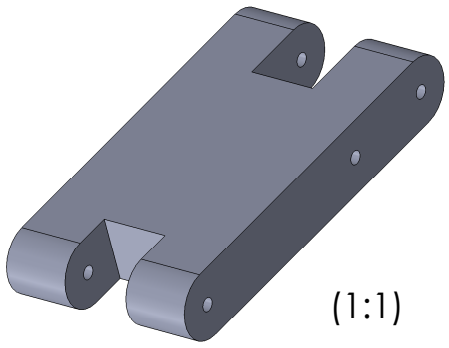

(1:1)

PART: Body L21	SCALE: 3:1	MATERIAL: ABS	DATE: 24/07/2017
CENTRALE NANTES LS2N ÉCOLE CENTRALE NANTES - LS2N	ARIA - ROBA	LLEVAT, David	

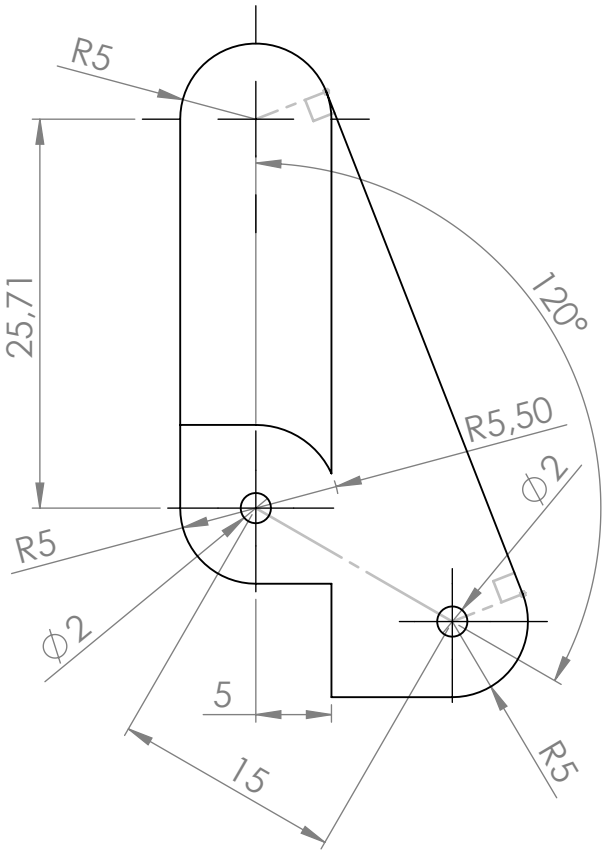

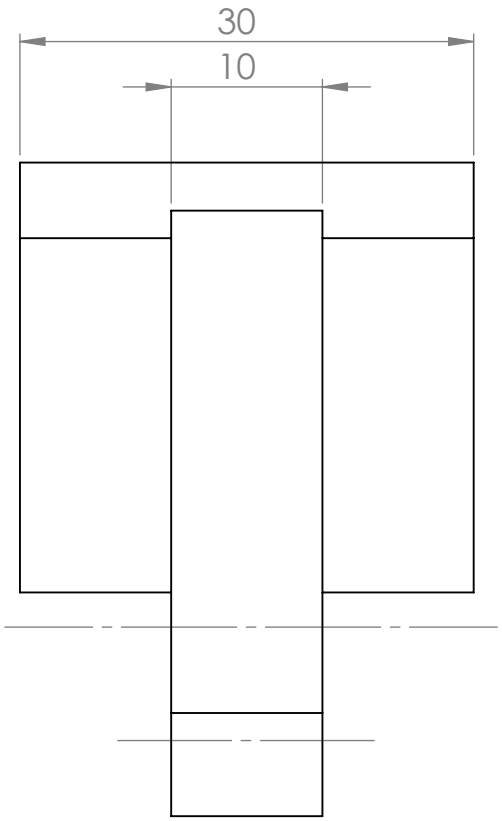

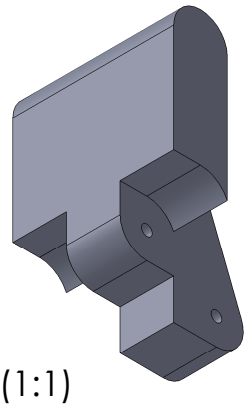

(1:1)

PART: Body L22	SCALE: 2:1	MATERIAL: ABS	DATE: 24/07/2017
ÉCOLE CENTRALE NANTES - LS2N	ARIA - ROBA	LLEVAT, David	

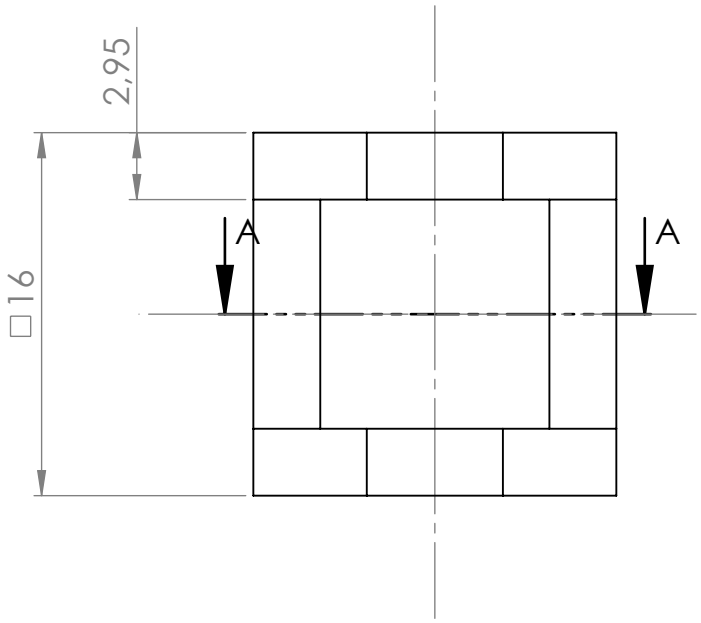

SECTION A-A

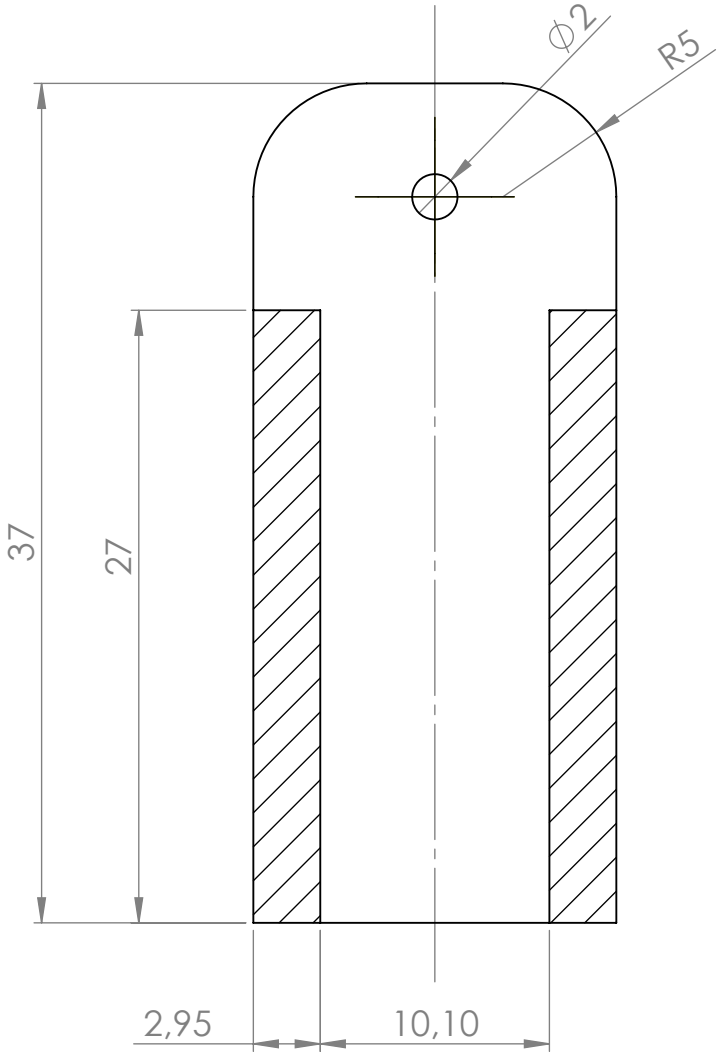

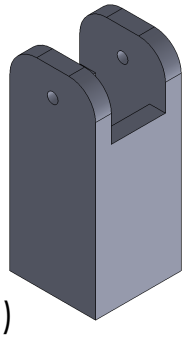

(1:1)

PART: Translational joint	SCALE: 3:1	MATERIAL: ABS	DATE: 24/07/2017
ÉCOLE CENTRALE NANTES - LS2N	ARIA - ROBA	LLEVAT, David	

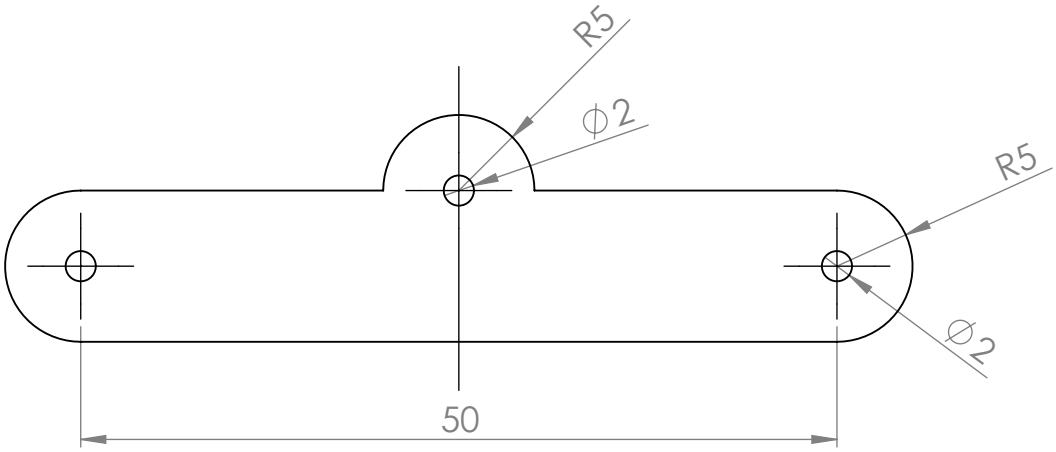

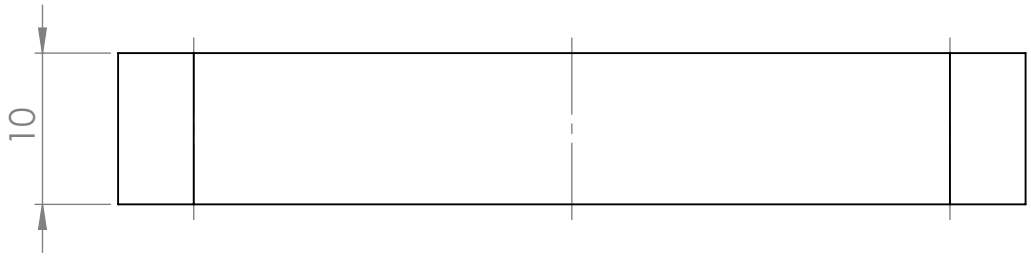

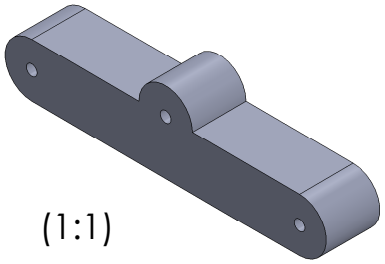

(1:1)

PART: Balance	SCALE: 2:1	MATERIAL: ABS	DATE: 24/07/2017
ÉCOLE CENTRALE NANTES - LS2N	ARIA - ROBA	LLEVAT, David	

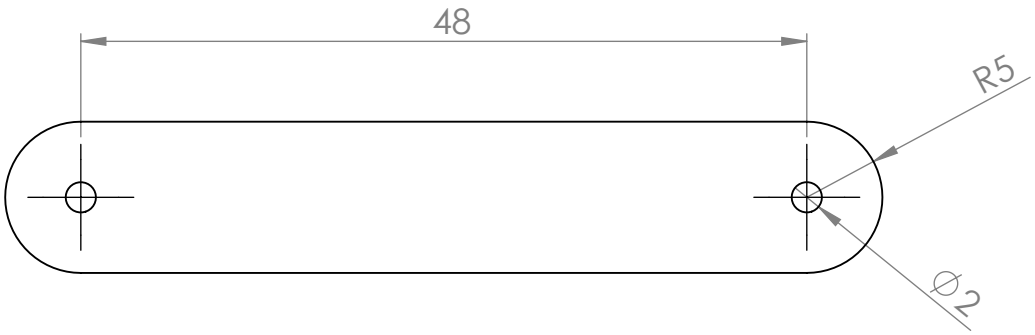

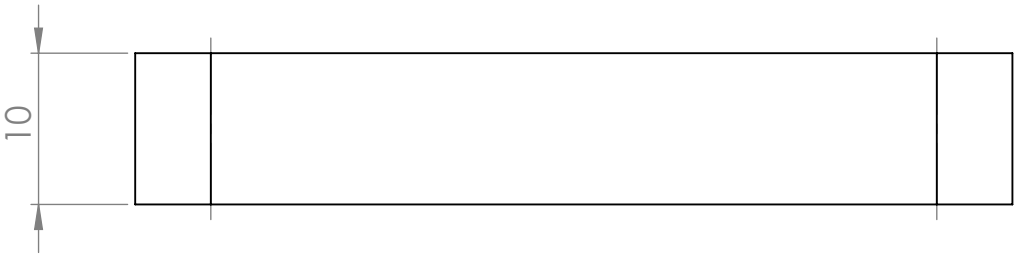

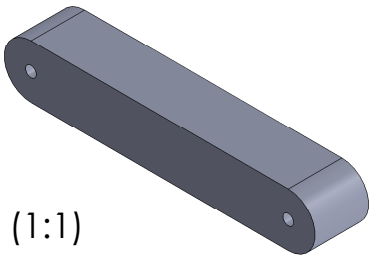

(1:1)

PART: Transmission	SCALE: 2:1	MATERIAL: ABS	DATE: 24/07/2017
ÉCOLE CENTRALE NANTES - LS2N	ARIA - ROBA	LLEVAT, David	

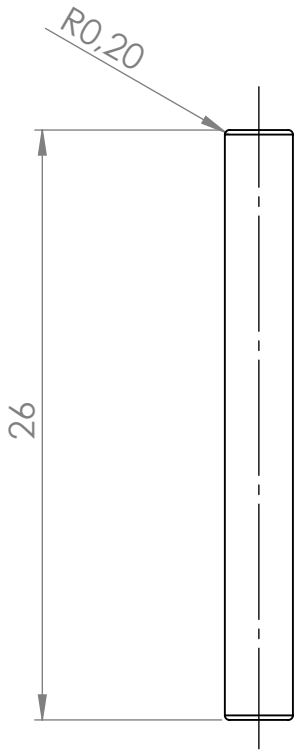

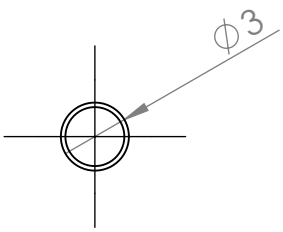

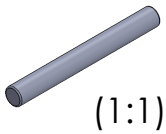

(1:1)

PART: Axis	SCALE: 3:1	MATERIAL: STEEL	DATE: 24/07/2017
ÉCOLE CENTRALE NANTES - LS2N	ARIA - ROBA	LLEVAT, David	